OPTIMIZING POLYMERS FOR USE IN ELECTRONIC ENVIRONMENTAL SENSORS

By

Jennifer Dailey

A dissertation submitted to Johns Hopkins University in conformity with the requirements for the degree of Doctor of Philosophy

Baltimore, Maryland
April 2018

A. Abstract

Electronic sensors are often an ideal choice for vapor and liquid environmental monitoring due to their highly adaptable structures, rapid testing time, and simplicity of use. Biomolecule sensors achieve selectivity to a particular analyte of interest through attachment of a specific antibody to a portion of the active device substrate. Sensors for gases such as ammonia do not have the option of a selective antibody, but must instead rely on monitored molecular interactions between the active surface and the atmosphere. In both of these cases, it is of utmost importance to design the recognition layer in such a way to allow for both high specificity and high sensor output response. We can modify these films in numerous ways to achieve optimum device performance. In the following projects, I investigated some chemical and physical attachment layer optimization methods that may be used to meet specific device requirements including flexibility, portability, and rapid speed.

This dissertation is broadly divided into two sections: **vapor sensing** (Chapter 2) and **biomolecule sensing** (Chapters 3 and 4).

For **vapor sensors**, many different methods allow for increased sensitivity to target gases. The addition of metal particles and controlled porosity to a conductive film provides for increased sensitivity to ethylene, which is typically poorly reactive due to its simple chemical structure. In a separate project, two electronic devices are used in tandem with an inverter geometry to increase selectivity for ammonia sensing. This device is fabricated entirely on a plastic, flexible substrate which can be conveniently worn by an individual at risk for ammonia exposure.

The **biomolecular sensors** presented in this work can detect the small electronic shift that occurs from protein binding to a corresponding antibody in the sensing layer. However, this attachment produces a limited voltage or current change alone. While it is common to use secondary labels and additives to increase this signal, in the case of measuring antibiotic-resistant bacteria in the field, the design is required to be as simple and portable as possible, thus limiting the possibility of complicated additives or processing. For this reason, I developed a binding polymer layer with acid-labile side chains that deprotect in the presence of pH changes. When measuring this film with electrochemical impedance spectroscopy, it is possible to see the decrease in impedance that occurs upon complementary protein binding, as the hydrophobic polymer layer degrades and allows infiltration with water.

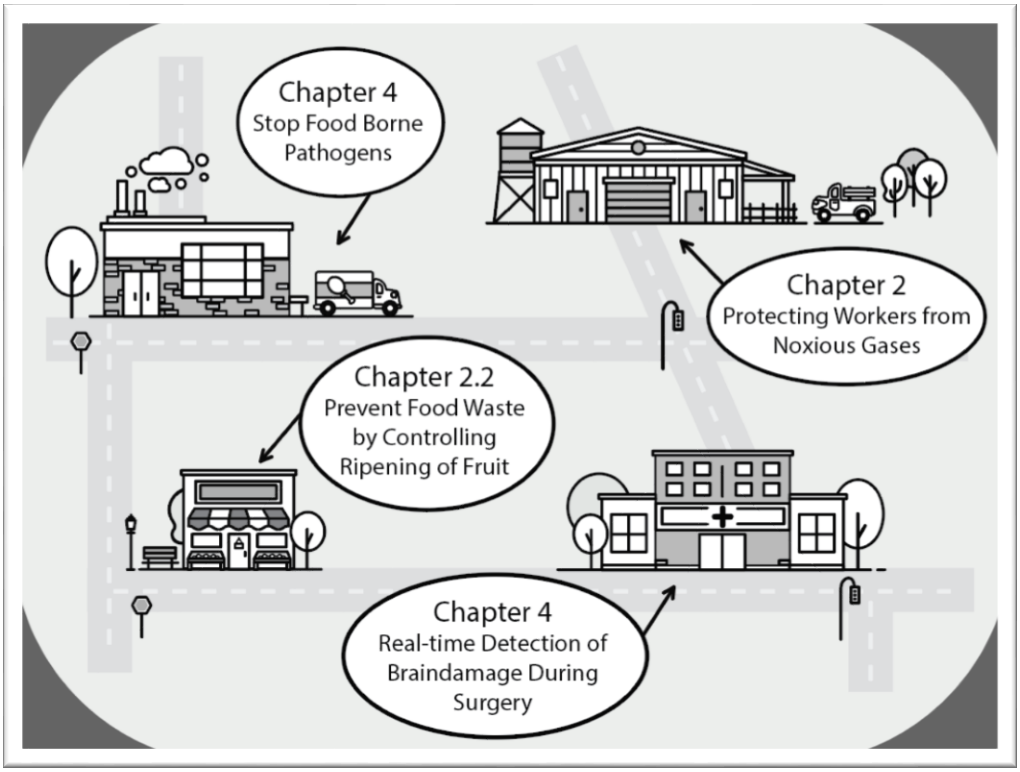

Readers:

Professor Howard Katz (Advisor)

Professor Ellen Silbergeld (Chair of the Defense Committee)

Dedicated to the memory of Poppops, from whom I inherited the "gift of gab";

I promise to use my power for good.

B. Acknowledgements

First and foremost I would like to thank my Ph.D. advisor, Prof Howard Katz, for his guidance and insight over the past five years. I feel truly blessed to have had a mentor who shares my public-spirited scientific beliefs and who gave me opportunities to discover my passions as student, researcher, and teacher during my time at Hopkins.

I would like to thank my committee chair and unofficial mentor Prof Ellen Silbergeld for her many talks over brunch that taught me first to cook my meat and wash my produce correctly, and also gave me to background necessary to tackle my next big project.

I thank my committee members Prof Jonah Erlebacher, who gave me incredibly useful advice that allowed me to balance my life at Hopkins, Prof James Spicer, who served as an excellent professor for my electronic properties class and gave valuable feedback on my thesis proposal, and Prof Susanna Thon who has graciously agreed to serve on the committee.

I would not have gotten into graduate school were it not for my first advisor, Prof Charlie Johnson at the University of Pennsylvania, who saved me from a summer bagging groceries and guided me through to my senior project and first publications. I thank Prof Dustin Brisson who showed me that I will frequently get a response when I go knocking on faculty doors looking for specific project guidance, and Dr. Mitchell Lerner who served as my graduate mentor and primary teacher throughout my undergraduate program.

I thank the late and much-missed Dr. Robert Nussenblatt from the National Institutes of Health, who showed me how valuable a caring clinician is to the research world. I also thank my supervisor Dr. Baoying Liu for giving me my first introduction to a clinical lab.

I acknowledge the help and support of the entire Katz lab over these five years, and am grateful for the opportunity to have worked with so many promising researchers including Dr. Weiguo Huang, Dr. Xin Guo, Dr. Kalpana Besar, Dr. Olivia Alley, Dr. Deepa Madan, Dr. Xingang Zhao, Dr. Hui Li, Dr. Jian Song, Dr. Wei Shi, Qingyang Zhang, Hyun-June Jang, and my officemate whom I sincerely thank for all enlightening conversations, scientifically relevant or not, Evan Plunkett. Thank you all

for introducing me to hot pot and black sugar and Korean tea, keeping me warm through the winter.

A special thanks to my undergraduate mentee of many years, Michelangelo Fichera, who helped in the gathering of some of the following data and assisted on many projects.

I am grateful for my experience mentoring students of all ages Michael, A.J., Kayla, Devyn, as well as all students whom I had the chance to instruct in the chocolate class. Your earnest desire to learn kept me going, even when my research hit a rough patch.

I am extraordinarily grateful for the support staff in the Department of Materials Science who helped keep the lab up and running by handling all things money related, academic, or machine break-downs including Ada Simari, Jeanine Majewski, and Bryan Crawford. Thanks to Anthony Lewis for assistance on the SEM.

I am grateful to the wonderful friends I have made in the department, and I can only hope to find as welcoming an atmosphere wherever I end up next.

I sincerely thank the mental health care providers at the JHU Counseling Center, who I strongly suspect to be the unsung heroes of many, many of our dissertations.

I thank Mr. James Harp, the choir director at St. Mark's Lutheran Church, for bringing music back into my life and being a source of positive inspiration.

I thank my parents for giving me molecular models to play with as a small child. I thank my dad for dinner table conversations about geometry and imaginary numbers, and for encouraging truancy for the sake of field trips to collect diatoms. I thank my mom for starting us on good literature at a young age with the Borrowers, and for still cutting my grilled cheese as a sailboat when needed. I thank my sister Kate for countless afternoons spent building K'nex racecars and learning the strength of the triangle by crashing them into each other.

Thanks to my fiancé Paul for picking me up from the train station with a fresh loaf of banana bread and single fork, solidifying my decision to stay in Baltimore. I'll never doubt that it was the right choice.

Contents

List of Tables

List of Figures

List of Schematics

List of Equations

I. Introduction

This dissertation will explore different sensing needs across the public health spectrum. For each type of analyte, I will demonstrate a method of organic device modification that will allow for more sensitive, stable, or realistic functionality in the given scenario. Chapter 2 will focus on vapor sensors (ammonia, ethylene, and NO2), while Chapters 3 and 4 will involve mechanisms to develop better biomolecule sensors (bacterial proteins and a brain injury marker).

A. General Sensor Development Considerations

There are many ways in which to alter the architecture of an environmental sensing device, but all such devices are based on the same two fundamental building blocks: sensing and transduction. "Sensing" refers to the method by which the device identifies an analyte of interest, whether through specific molecular binding or charge transfer or any other chemical or physical method. "Transduction" is any method by which we can read that recognition event, for example through a change in capacitance measured on a handheld multimode device or a fluorescent color change caused by some specifically binding particles.

This dissertation focuses on the following critical electronic transduction methods, as illustrated in this partial list which displays some of the range of device choices available.

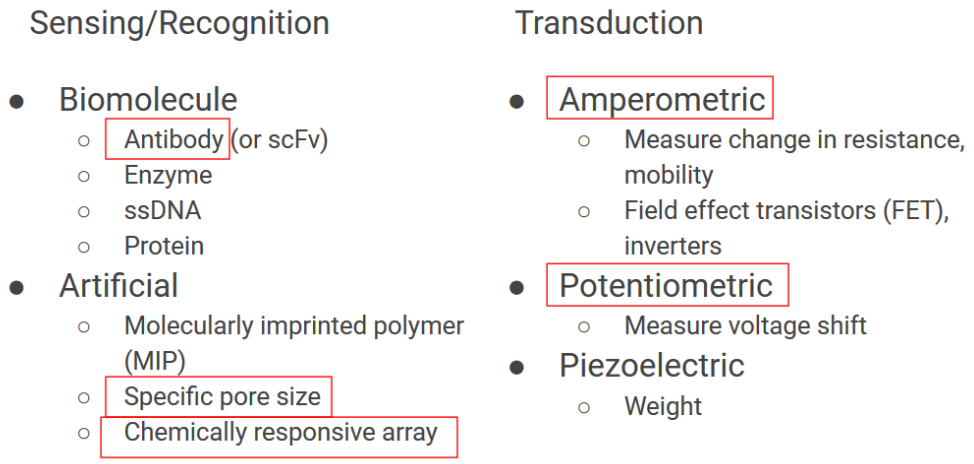

Figure 1 Examples of common sensing and transduction elements in a vapor or biosensor. Circled in red are topics explored in this dissertation.

Electronic sensors are the subject of study of many research groups and companies[1–4]. There are a variety of benefits universal in most successful electronic sensors, including exceptionally fast speed and a clear output reading. Additionally, typically no large equipment purchases (such as electron microscopes, usually only available to research institutes) are necessary to read the output. The following chart is extremely generalized for demonstration purposes, but broadly shows the niche currently occupied by electrochemical sensors. While many research groups have shown very promising advances in electronic biosensing technology that demonstrate more sensitive sensors than ELISA or Western Blot (the current medical gold standard) techniques, but most of these publications have yet to make it to market[5–7].

Throughout this dissertation, we bear in mind that while there is a ubiquitous competition for the "best" sensor (where "best" is defined as highest sensitivity), this generalized accolade is not necessarily the prime target. Instead, the aim is to show the reader some

technologies that improve organic electronic device functionality for a series of particular applications. In some sensing cases, there is merely minimal market demand for a more sensitive detection mechanism (this was the case with prostate-specific antigen (PSA) sensing techniques a few years ago, once technologies could detect 1 ng/ml)[8]. In commercial settings, frequently there is a cost-benefit analysis that severely limits which techniques may be considered, because a company may not be able or willing to invest in the necessary infrastructure for accurate readings. A medical technician may need to detect pathogens in a well-controlled clean room, but an explorer may want to immerse a pollution sensor in a flowing stream. In the fast-paced world of food production, improved detection schemes would be any that do not require shipping out a sample to an outside lab and waiting for results[9]. To the best of our knowledge, no device exists that is ideal for all of these cases. I have focused my work on specific areas of need, through both literature review of the current gold standards in vapor and biosensing technology and collaboration with experts from the worlds of medicine and public health. Armed with this invaluable feedback and guidance, I have thoughtfully designed new electronic sensing architectures and mechanisms that are each suited to their respective goals.

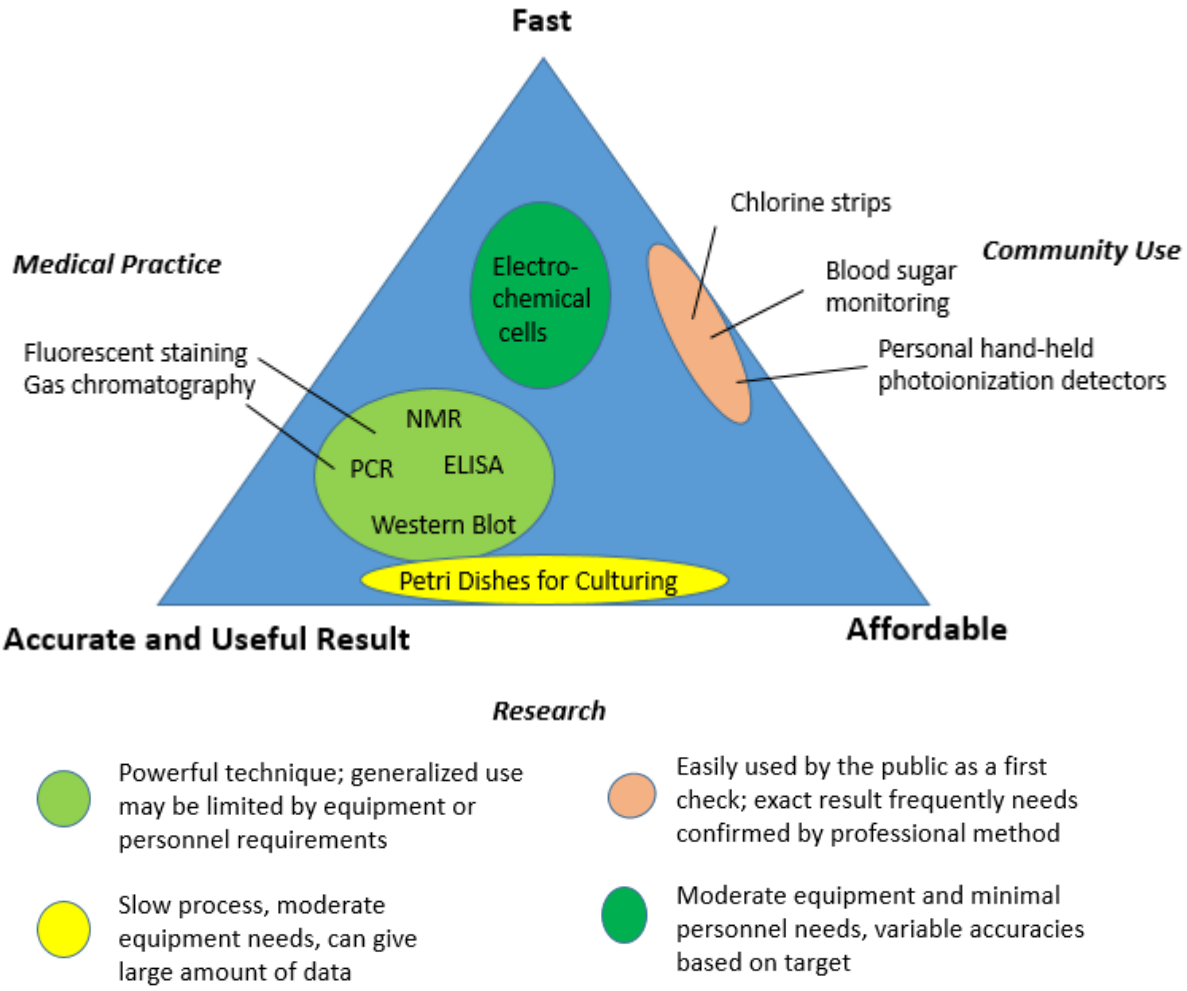

Figure 2 Triangle depicting the usual trade-off faced in sensing development and choice between speed, price, and accuracy, generalized for illustrative purposes rather than quantitative. There exist specific device requirements for each application, with no one device type fulfilling every biological or vapor sensing need.

B. Organic Electronic Materials

In this dissertation, an "organic" electronic sensing device is broadly defined as one which possesses a dielectric or semiconducting layer that is carbon-based.

1. Organic Semiconductors

A subset of electronic sensing devices is based on organic electronic materials. Organic semiconductors (OSCs) were considered impractical for most of the 20th century due to their poor stability and low current, leading to continued reliance on inorganic semiconductors like silicon and germanium. However, relatively recent advances have allowed OSCs to become prime candidates for use in electronic devices due to their flexibility, printability, and potentially lower cost, especially as inorganic minerals become scarcer and more countries turn to sustainable technologies.

Many OSCs are already on the market. Common uses include improved display technology with organic light emitting diodes (OLEDs), which can be seen in televisions and cell phones, and organic solar cells, which, despite issues with degradation, are inexpensive to fabricate and have achieved 13% efficiency[10].

Organic semiconducting is based on charge transport through conjugated π bonds with delocalized orbitals. Conduction can occur in small molecules such as pentacene or conjugated polymers and oligomers such as P3HT, PQT12, and DPPCN. These structures are shown in Figure 3. Based on charge carrier identity, organic semiconductors can be n- or

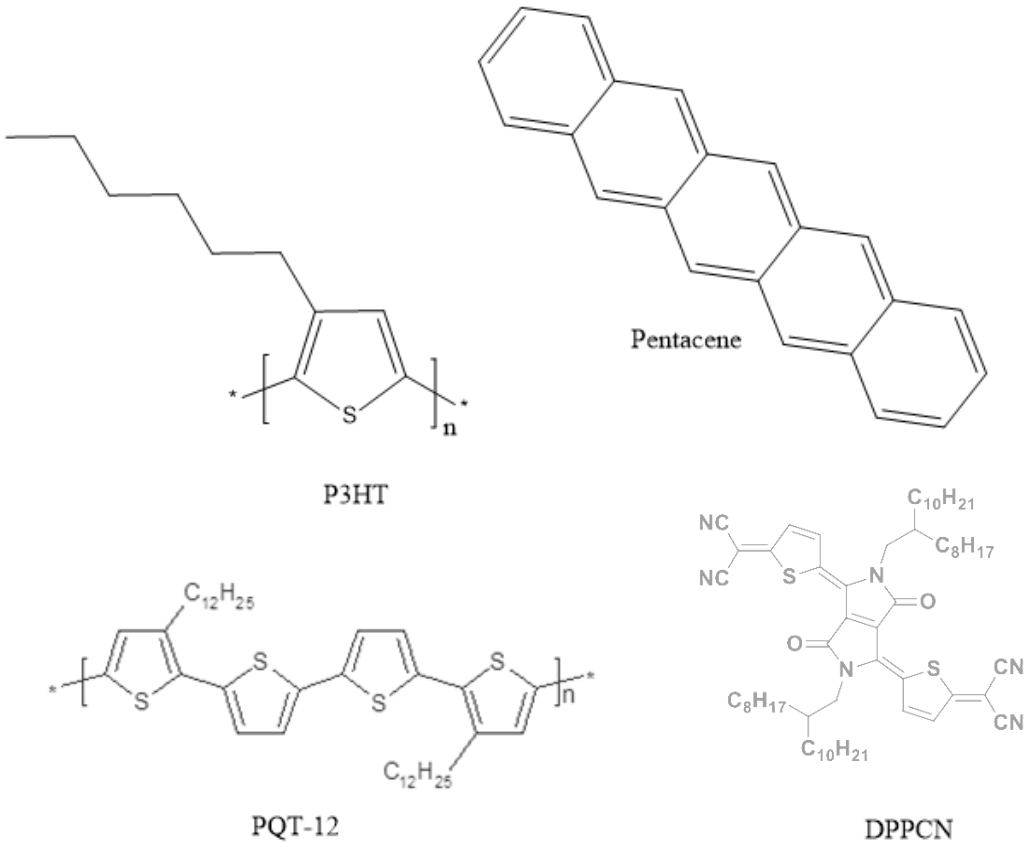

Figure 3 Structures of OSCs used in this dissertation: Pentacene, P3HT, PQT-12, DPPCN.

p-type, conducting electrons or holes respectively. A typical OSC has a band gap of around 2.5-4 eV, whereas inorganic semiconductors have a band gap of only 1-2 eV. Despite this higher conduction hurtle, OSCs can conduct current if they are injected with charge carriers through connected electrodes, excited optically, or chemically doped (whether accidentally from atmospheric contaminants like water, or purposefully in an attempt to create more conductive materials).

Organic semiconductors can be characterized by their charge carrier mobility, which will be of importance to our discussion in Chapter 2 when analytes will be detected based on related interactions. While the earliest OSCs had a mobility of less than 0.01 cm2V-1s-1, recent

progress has allowed for mobilities of over 10 cm^2/Vs, bringing this property within the range of inorganic counterparts. Charge carrier mobility can be largely modulated based on many non-covalent interactions with the environment: dipole-dipole interactions, hydrogen bonding, Van der Waals forces, doping, and charge trapping. Since these interactions are not highly specific, the mobility is likely to change similarly for different chemicals containing the same functional groups, which is not ideal for sensing purposes. Fortunately, there are some additional steps that can be taken to add selectivity to these semiconducting devices.

While there has been a marked improvement in the last decade, stability problems still exist with both n- and p-type polymers. Environmental conditions of humidity and oxygen may cause unwanted interactions in films, or raw fabrication materials may degrade within a short amount of time. The problem of stability becomes especially apparent when attempting to develop liquid phase sensors, as the water and electrolytes therein can often seep through the OSC layer and ruin the sensor by providing unwanted electrical current.

2. Organic Dielectric Layers

Non-conducting portions of electronic sensors come in a variety of compositions but are usually serving one of two purposes. All field-effect transistors (FETs) require a dielectric layer between the source/drain and gate electrodes capable of sufficiently high charge polarization to allow conduction of holes or electrons through the semiconductor layer. While this may merely be the oxide layer on silicon or layer of a conventional polymer such as PMMA, in many cases the dielectric layer is specially fabricated for the sensor. In some architectures, this layer or the semiconductor itself may also serve as the analyte receptor area, though frequently a secondary specialized receptor layer is needed to complete the sensor.

Martinez Hardigree et al. completed a study of the ability of the choice of dielectric material to change the threshold voltage of an organic FET. In a similar vein, Alley et al. examined various substituted polystyrene layers and their effects on a pentacene transistor[11, 12]. Porosity has been shown to have a potentially positive impact on the dielectric layer by increasing pore density[13]. However, it is necessary to ensure the dielectric layer retains enough structure not to allow excessive leakage current and thereby ruin the integrity and functionality of the transistor.

Dielectric layers not only serve an essential function in the formation of FETs but are also vital to the functioning of the simpler impedimetric sensor. Impedance characterization incorporates the resistance, capacitance, and inductance across a system. Due to the nature of adding capacitors in series, in impedance-based biosensors, it is frequently ideal to begin with a dielectric/binding layer that has a very high capacitance since any antibody of protein binding on top of the layer will usually have lower capacitance. Since the inverse of the resulting capacitance is equal to the sum of the inverse of these two values, a much more significant shift will be seen if the base layer as a high capacitance, due to either its dielectric constant or its thinness. The author highly recommends a thorough review by Jaffrezic-Renault for further discussion of this topic[14].

C. Organic Electronic Sensing Devices

1. Vapor Sensors

In this dissertation, all organic field effect transistor (OFET) based vapor sensors have their semiconducting layer in contact with the atmosphere. The electron withdrawing and donating interactions of the gas molecules with the surface are responsible for altering the

electronic properties of the OFET, and can manifest as a change in threshold voltage (if there is charge accumulation) or total bias current (if the interaction alters conductivity and number of electron or hole traps). The interface of the surface with vapor is less complicated than an aqueous solution, though these types of sensors must be stable enough such that high levels of humidity or oxygen will not cause excessive film degradation.

2. Biological Sensors

Biological sensors are usually meant to interact with an aqueous solution to detect a protein, DNA sequence, enzyme, etc. from a blood, urine, or water sample. Biosensors which rely on antibodies or antibody fragments as their binding identification mechanism, such as all described in this dissertation, are commonly referred to as immunosensors. Complex liquid samples can pose a problem to traditional OFET sensing architectures if the water manages to leak through the top sensing layer. This conductive liquid can cause an excessive amount of gate leakage current and would not make for a viable sensor. However, it is possible to physically relocate the sample input location to mitigate this problem, while maintaining the ability to see current changes caused by charge accumulation from protein binding.

Electrochemical impedance spectroscopy (EIS) is often frequently reported as the basis for enhanced immunosensors and involves measuring the total impedance from an electrode across a reacting film through some electrolyte solution and into a counter electrode. This makes it a potentially prime candidate for point-of-care sensor development since the liquid sample of interest can be placed into the measurement cell without further processing. However, the detection mechanism will rely entirely on the type of film interaction that occurs among the antibody-protein complex.

D. Outline of this Dissertation

In this Introduction, Chapter 1, I gave a brief overview of vocabulary and fundamental concepts present in the field of electronic environmental vapor and biomolecule sensors. I also discussed the motivation for choosing to use electronic sensors due to their portability, adaptability, and ease of use as compared to many standard biological laboratory methods.

In Chapter 2, I will discuss the specific functional requirements necessary to vapor sensors. First I will review the operations of field effect devices, which have already introduced. The first major project will focus on a field-effect transistor structure with a functional organic semiconductor layer that was strategically modified to detect ethylene, a generally non-reactive molecule. The second project will examine the concept of using two electronic devices with complementary sensing outputs to produce a strong detection signal. Using two FETs in an inverter architecture, we were able to achieve a very low limit of detection for ammonia gas. I will discuss other unique multiplex arrays that can offer increased sensitivity compared to a single electronic device.

Chapter 3 will focus on polymer design for biomolecule sensors and sensor application. Since changing the dielectric or attachment layer of an electronic device can have such a drastic impact on performance, it is useful to design specific polymers to suit their necessary roles. In the primary case of creating a MRSA sensor, it is desirable to have a degradable attachment layer. I will detail the design and testing of impedance devices since impedance spectroscopy will be used to analyze these samples. I will discuss the choice of chemical components and polymer design, as well as the electronic properties thereof.

In Chapter 4 I will detail the specific requirements that must be met for useful sensor design from a public health perspective. I will then use the novel degradable polymer to fabricate a biomolecule electrochemical impedance sensor to detect MRSA protein. I will discuss further amplification methods that may be used in EIS sensing involving secondary labeled particles.

I will then offer a few concluding ideas regarding the path forward for electronic sensors, and where I believe they will have a considerable place in the market.

II. Design of Vapor Sensors

A. Introduction to Field Effect Transistors

Organic field effect transistors (OFETs) are very useful to the sensing world because they can act as a transducer and amplifier in one package. A schematic of one type of OFET with back gate geometry is shown in Figure 5 and is used in much of this dissertation. There are many potential electrode geometries for OFETs depending on usage requirements, but all function by the same mechanism. A voltage difference is set between a source and drain electrode, and a gate voltage is applied to produce a transverse electric field that will allow sufficient charge carrier mobility and density to generate a current between source and drain. This current will vary between its on and off state based on the sign and value of the applied gate voltage with increased gate voltage beyond a threshold value resulting in increased current. The current will increase with larger amounts of drain voltage, until saturation is reached when drain voltage exceeds the gate voltage, resulting in a variable "on" state current. Typically we gather both output curves and transfer curves to characterize these OFETs, as shown in Figure 6.

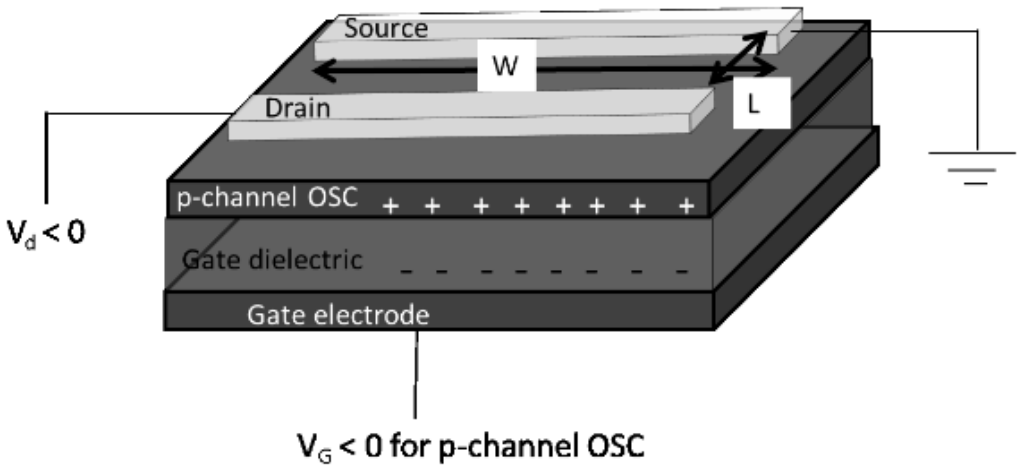

Figure 4 Schematic of p-type OFET [12]

In the saturation region when the drain voltage is larger than the difference between gate and threshold voltages, the characteristic equation relating mobility and current is:

Equation 1 Drain current equation in saturation regime

$$I_{D,sat} = \frac{W}{2L} C_i * \mu_{sat} * (V_g - V_{th})^2$$

Where W and L describe the width and length of the channel, respectively, and Ci is the capacitance of the dielectric film.

If we fit a line to a graph of the square root of drain current versus gate voltage, mobility can be calculated according to:

Equation 2 Calculation of mobility from OFET device measurement.

$$\frac{\sqrt{I_{D,sat}}}{\sqrt{\frac{W}{2L} C_i * \mu_{sat}}} = V_g - V_{th}$$

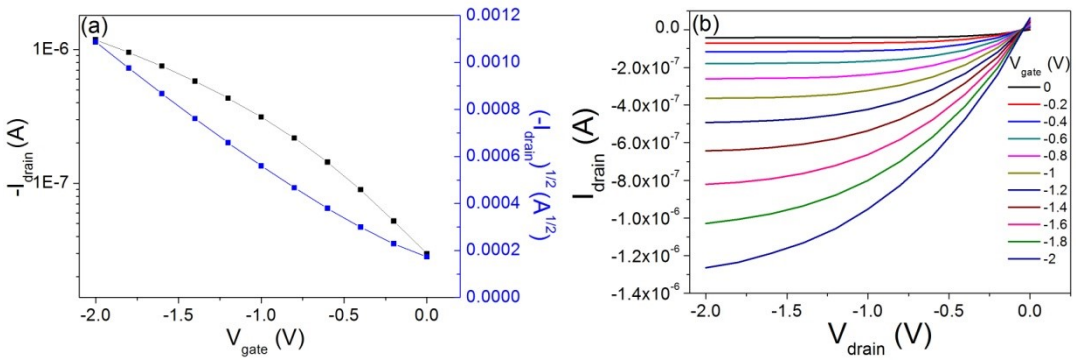

Figure 5 Typical (a) transfer curve and where the drain voltage is set at 2 V (saturation region) (b) output curve of a pentacene OFET tested in air at different gate voltages.[15]

Figure 5 shows an example of OFET geometry using a p-type OSC. If there is an analyte interaction on this top layer, there will be some alteration of the measured drain current (if this were n-type, all interaction signs would be reversed). Environmental interaction can change the charge carrier mobility as previously described, and result in an altered on-state current. Also, the additional detected charge may alter the threshold voltage, which is the gate voltage corresponding to "turn-on" of the device[16].

Many factors will alter the overall sensitivity of the device since detection is dependent on the entirety of the environment-device interaction. The more surface area of the detection layer that is exposed, the more significant the overall sensing effect will be. Additionally, if analytes can be drawn and held at the surface preferentially through charge interactions, this will improve the chances of analyte detection. The choice of analyte will have a large effect on sensing design: a highly charged analyte is likely to cause a much more obvious voltage effect to an OFET, but a small neutral molecule will likely have less of an impact on mobility for each binding event. In the following sections, we will discuss some methods and

demonstrations of using polymer modifications to improve specific analyte interactions and device performance.

B. Embedded Additives to Improve Sensitivity

1. Porosity

The addition of pores to an otherwise flat sensing layer offers two primary benefits. Firstly, pores can drastically increase the overall free surface area for analyte interaction while maintaining the same dimensions. Pore size and density can be calculated using atomic force microscopy or scanning eletron microscopy. Assuming correlation of electrical response with the quantity of bound analyte, this corresponds to a higher signal change per concentration than a standard flat surface. As an additional benefit, sufficient pores of suitable size can act as a protective screening layer to prevent more massive objects such as dust particles from overwhelming the sensing platform.

Pores may be created in a variety of ways for organic or polymeric incorporation. Al-Hardan et al. crafted a highly sensitive pH sensor using porous silicon in the gate geometry, thereby achieving a "super Nernstian" value and overcoming a common drawback found in this orientation[17]. Wu et al. produced similarly increased response in a humidity sensor by using a phase-separation phenomenon to create a macroscopic porous structure[18]. An enhanced ammonia sensor had a similarly improved gas response and created a porous structure through the use of a simple vacuum freeze-drying template method[7]. The type of porous structure can be well-regulated by control of processing methods and chemical additives to provide the optimal density and pore size necessary for the desired outcome.

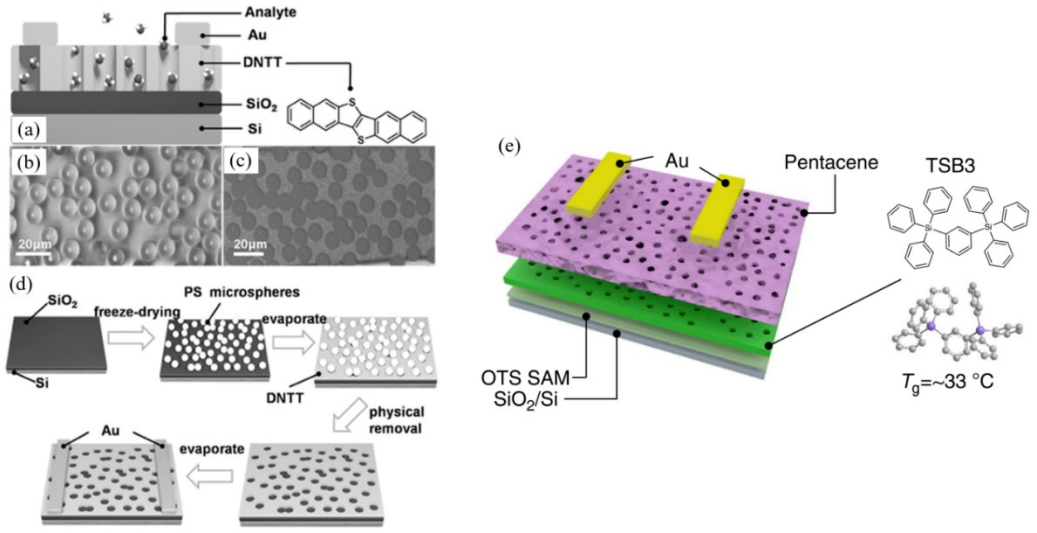

Figure 6 Schematic illustration of the porous OFET-based sensors.

(a) The device structure of the porous OFET-based sensors and the molecular structure of DNTT. Optical images of a porous DNTT film (b) with polystyrene microspheres and (c) after removing polystyrene microspheres. (d) The fabrication procedure of the porous OFET-based sensors.. (e) Device schematic and the molecular structure of TSB3.

In 2014, Cho et al. developed an approach of evaporating pentacene on top of m-bis(triphenylsilyl)benzene (TSB3), resulting in unusual morphology with far fewer grain boundaries and myriad nanometre-sized pores in pentacene, as shown in Figure 8 [19]. These peculiar structures were formed by differences in molecular interactions between the organic layers and the substrate surface. The pore-rich structure improved the sensitivity of the OFET to methanol gas. While not precisely 'pores,' Yu et al. clearly demonstrated the positive sensing impact of increased surface area by altering the morphological characteristics of the ammonia sensing semiconductors[20].

2. Metal Particles

The addition of specific metallic nanoparticles or nanowires to semiconducting layers has shown similar promise in increasing electronic response, though for very different mechanistic

reasons. Surya et al. developed a hydrogen sulfide detection system by incorporating tin oxide nanoparticles into the sensing area[21]. Zheng et al. used ultrafine platinum nanoparticles in their work with a similar drastic response increase to DNT vapor[22]. Zheng discusses that this improvement is thanks to the particles' charge transfer interactions with the vapor, compared to a film with no particles. A different mechanism was demonstrated by Han et al. when they incorporated zinc oxide particles into a pentacene layer, thereby decreasing the average grain size. This encouraged increased diffusion of CuPc molecules to the interface. The combination of particles and CuPc also increased possible overall interaction with the environment[23].

These types of additives can also act in synergy, as I will demonstrate in the following section, development of an ethylene vapor sensor, completed with colleague Kalpana Besar. This design uses both palladium particles and chemically-induced porosity to achieve a substantially higher specific sensing response[24].

3. Ethylene Sensor Development with Additives

The following data also appeared in:

Besar, Kalpana; **Dailey, Jennifer**; Katz, Howard. 2017. "Ethylene Detection Based on Organic Field-Effect Transistors with Porogen and Palladium Particle Receptor Enhancements." ACS Applied Materials & Interfaces. 9(2), pp. 1173-1177

Ethylene is a small hydrocarbon with no odor or color. It occurs naturally as a plant hormone[25] or in natural gas, it regulates various physiologically important events like germination[26], development or growth of the plant[25, 27, 28], flowering[29] and most

importantly the ripening and subsequently senescence of the fruits post harvesting, especially climacteric fruits[25].

Specific pathways and the role of ethylene in a plant's life cycle have been thoroughly investigated[30–32] considering the enormous losses to the horticulture industry (millions of dollars) due to premature deterioration or overripening of fruits and flowers during transportation and storage[33]. Ethylene is produced as a product of biosynthesis in plants; it permeates cells and triggers the fruit-ripening gene resulting in a change in texture, color, and taste of the fruits. Ripened fruit produces more ethylene which in turn induces more ripening and ultimately rotting of the fruits. By measuring the concentration of ethylene in the vicinity of the fruits at a particular time, we can figure the approximate stage of ripeness of the fruit. We can theoretically control the whole process by monitoring the ambient condition maintained in the storage units and thus increase the shelf life of the fruits. By retaining the storage unit temperature close to 0 ℃, oxygen levels to 1 to 2%, high humidity nearing 92% and carbon dioxide levels to 200 ppm, fruits and vegetables can be successfully stored for weeks or potentially months[34]. While monitoring these conditions is relatively straightforward, developing a suitable sensing platform for ethylene is still a challenge owing to the small molecular size and very limited physiochemical reactivity.

Existing technologies for sensing ethylene include photoacoustic spectroscopy, gas chromatography, metal-oxide semiconductor-based sensors, electrochemical sensors, electro-catalytic sensors, and non-dispersive spectroscopy[34–37]. All current techniques are either too expensive at present to meet universal need, too bulky, require high temperature or do not have high sensitivity. Very recently, Swager et al. developed a reversible chemiresistive sensor based on single-walled carbon nanotubes modified by copper(I)

complex to enhance selectivity. The sensor could detect ethylene concentrations ranging from 0.5 to 50 ppm[38]. Following this work, Kathirvelam et al. published a multiwalled carbon nanotube sensor for ethylene on a flexible substrate. They report a sensitivity of 20 ppm and the response to be ten times higher than the earlier single-wall carbon nanotube sensor report[38]. However, no selectivity studies were reported[39]. Selectivity is a significant concern for the carbon nanotube-based sensor devices due to various Van der-Waals interactions on carbon nanotube surface. Although Swager et al. included a selectivity study, several gases like acetonitrile (100 ppm), tetrahydrofuran (200 ppm) and acetaldehyde (75ppm) had much higher response than the reported lower limit of 1 ppm for ethylene and almost equal response to 20 ppm ethylene, which can be a significant problem for practical application of these devices where a high selectivity is of utmost importance. Another hindrance for the commercialization of the carbon nanotube-based sensor is the cost of scaled-up production of separation of purely semiconducting nanotubes. Nanotubes purified to 98% semiconducting cost on the order of $500 per gram, and further purification would probably be necessary [40, 41].

Over the past few years, organic field effect transistors have received much attention for their potential in sensing application due to their easy processibility, which makes them both time and cost efficient. Dongyoon Khim et al. recently reported the very first organic field effect ethylene sensor[42]. Using a precise bar-coating method, 1000 ppm ethylene was detected. This is nearly 10 times the ripening room concentration, and is too high for most purposes.

Here we report a much more sensitive OFET based sensing platform (Figure 8) for ethylene using poly(3-hexylthiophene-2,5-diyl) (P3HT) as active semiconductor and palladium

particles as ethylene receptor. P3HT alone is not specifically designed to sense ethylene. Instead our main goal herein is the introduction of both pores and specific metal particles to markedly increase the detection abilities of this sensing matrix. A related interaction between transition metals and the hydrogen atom has been studied extensively in the context of hydrogen storage, to be used as an alternative and renewable fuel[43–48]. Reports indicate that hydrocarbons like ethylene[43–45] have an affinity to bind with transition metals and form complexes, likely through coordinate bonding, which then can be used to store hydrogen successfully. Palladium, platinum, zirconium, and titanium have been proposed for this application[43]. In a report by Durgun et al., binding between titanium and ethylene had been studied thoroughly[43]. The paper stated that a single Ti-atom could bond to an ethylene molecule to form C2 H4 Ti complex without any input energy. However, considering the practical limitations like stability under ambient condition and handling, we chose palladium as the potential receptor metal for ethylene. It is expected that increasing the concentration of ethylene near the surface of the sensor by having it bind preferentially to the Pd particles will result in an increased sensing response.

Materials and Methods:

Materials

Highly doped n-type silicon used for device fabrication was bought from Si Tech. Palladium particles, tert-butyl phenyl carbonate (S1) and N-(*tert*-butoxy-carbonyloxy)-phthalimide (S1) were purchased from Sigma Aldrich. (P_3HT) was purchased from Solaris. Ethylene gas with a defined concentration of 25 ppm and 500 ppm in dry nitrogen was purchased from PRAXAIR.

Device Preparation

Highly doped n-type <100> silicon wafers with 300 nm silicon dioxide were diced into 1 inch by 1-inch pieces. The wafers were then cleaned using piranha solution (3:1 of sulfuric acid: hydrogen peroxide) followed by sonication in acetone and then in isopropanol for 30 minutes. The wafers were dried using nitrogen gas flow. Gold electrodes (50 nm) were deposited through a shadow mask (channel width/length ratio approximately 308 (77000 μm /250 μm)) at a rate of 0.3 Å/s using physical vapor deposition. The pressure of the deposition chamber was maintained at $<5\times10^{-6}$ Torr. P3HT is deposited from a 4mg/ml solution in chlorobenzene. 50 weight% palladium particles were added to a 4mg/ml solution of P3HT in chlorobenzene in order to introduce transition metal traps for ethylene in the active semiconductor layer. To further enhance the ethylene sensing performance tert-butyl phenyl carbonate (25 volume%) and N-(*tert*-butoxy-carbonyloxy)-phthalimide (25 weight%) were added as porogen to P3HT/Palladium solution. The P3HT/Palladium/porogen mixture is spin coated on silicon/SiO_2 substrate (with the predeposited gold electrodes) at 1000 rpm. The devices are baked at 170-degree Celsius under vacuum for 2 hours.

Measurements

Organic field effect transistor devices with P3HT/Palladium/porogen spin-coated film as the active semiconductor films were used as a sensing platform for ethylene sensing. Typical OFET transfer curves are shown in Fig. S1 OFETs were evaluated under Vds=-60V and Vg from 5 to -60 V.

Mobilities were calculated using Equation 1.

All the OFETs were measured using an Agilent 4155C semiconductor analyzer. A home-built, well-sealed chamber with a volume of 1770 ml was used for exposure experiments. Devices were allowed to come to an equilibrium state before all measurements. P_3HT is not extremely air-stable in this type of device, but after a short amount of time, it develops a small (1-4%) and consistent current decrease when measured in 5-minute increments. This was analyzed and corrected for in data analysis as shown above.

Results and Discussion:

Ethylene is not a very strongly interactive analyte and can only affect the sensing membrane via weak interactions with delocalized double bond electrons in the semiconductor. We chose P3HT as the primary organic semiconductor layer for this study because P3HT and related thiophene polymers have been well established for sensing ammonia[49–51]. The lone pairs on ammonia molecules trap the hole carriers in the p-type semiconductor, effectively decreasing the mobility and/or mobile charge density. We hypothesize, and experiments confirm, that ethylene should have similar interaction (electron donating tendency, although less strong) with the semiconductor layer because of its slightly nucleophilic double bond. Properties of unexposed devices are shown in Table 1.

Table 1 Threshold voltage, mobility, and on/off ratio of P3HT device combinations.

	P3HT	P3HT + Porogen	P3HT + Porogen + Palladium
Vt (volts)			
Average	-4.25E+01	-5.30E+01	-2.21E+01
St dev	7.57E-01	5.49E+00	2.90E+00
Mobility (cm2/Vs)			
Average	2.68E-04	4.78E-05	2.93E-05
St dev	4.91E-05	2.69E-05	1.93E-05
On/off ratio			
Average	8.13E+00	3.94E+00	5.36E+00
St dev	6.86E-01	1.57E+00	9.59E-01

Ethylene response was monitored by investigating the percentage change in drain current of the P3HT based transistors (with and without palladium particles) upon exposure to 25-ppm ethylene. An average decrease of 14.6% in drain current was observed on exposure to 25-ppm ethylene gas for 5 minutes (Figures 8b and 8c), consistent with the expected mechanism. Three or four independent devices were measured for each data point shown, and the error bars represent one standard deviation from the calculated average. The response was reversible under ambient conditions.

P3HT-only devices were also exposed to nitrogen (used as the balance gas for the ethylene mixture) as a control; only a 4% drain current decrease was observed. The current decrease on exposure to nitrogen is considerably smaller than ethylene exposure, and it can be attributed to the displacement of oxygen molecules from the P3HT film due to nitrogen flow.

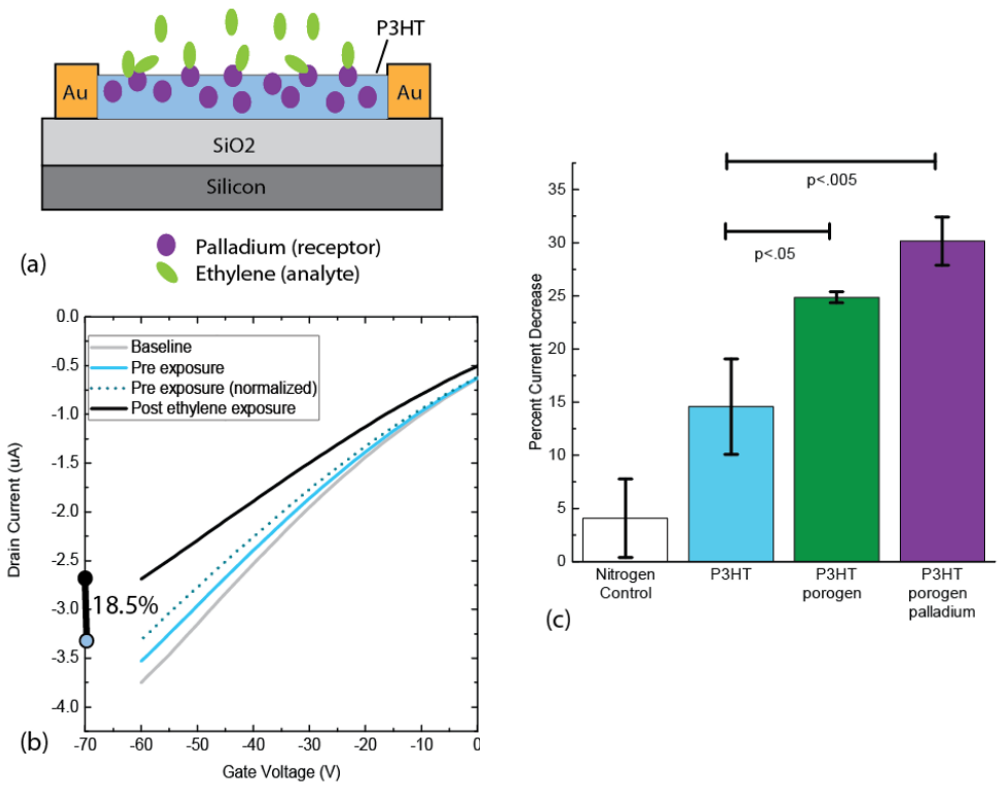

Figure 7 (a) Schematic of OFET device sensing ethylene gas indicating ethylene gas binding preferentially to palladium particles. (b) Typical transfer curve and analysis of standard P3HT device before and after exposure to ethylene. "Normalized" means corrected for projected drift (Figure S3). An 18.5% current change is seen after exposure to ethylene. (c) Average percent decreases in current for each type of sensor (P3HT, with the addition of porogen, and with the addition of both porogen and palladium particles) when exposed to 25 ppm ethylene for five minutes, measured immediately (before recovery occurred).

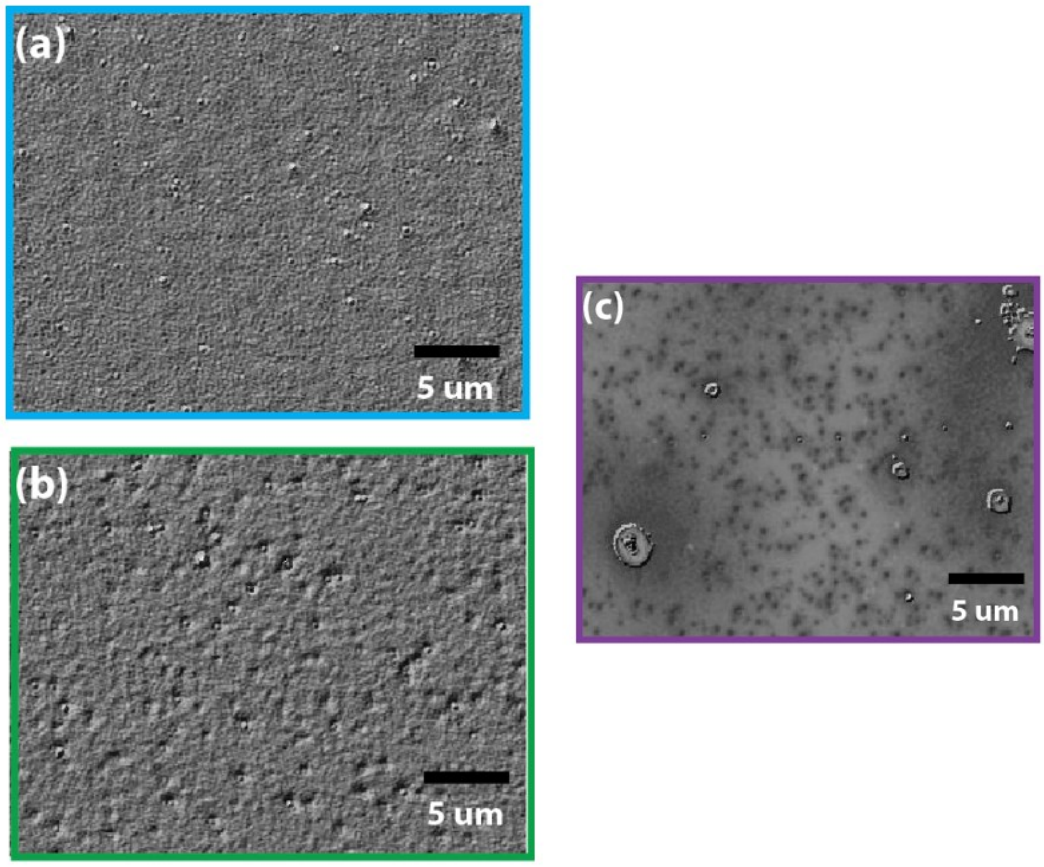

Figure 8 DIC images taken on laser scanning microscope at 100X magnification of (a) plain P3HT surface with minimal roughness and binding sites, (b) P3HT surface with porogens with visible pitting that increases overall surface area and binding sites, and (c) P3HT surface with porogens and palladium particles, showing increased roughness.

Figure 8b shows a typical example of sensing data based on a simple P3HT sensor without added porogen or palladium particles. The difference between the baseline and pre-exposure curves allow us to normalize the data based on the reproducible slight changes of this type of OFET in air. The final curve is taken immediately following exposure to ethylene. The percentage decrease in current is calculated based on the drain current measured when the gate voltage is at -60V.

A simple approach to increase the response of any gas sensor is to increase the interaction area of the sensitive film, which will increase the permeation of the gas molecules into the films and add sites for chemical interaction. There are reports stating that adding polystyrene beads increases the surface area and the adsorption of ethylene molecules in a carbon nanotube-based sensor and thus results in an overall increase in response to ethylene[38]. To investigate the influence of the film porosity for P3HT film, we added tert-butyl phenyl carbonate (25V/V %) and N-(tert-butoxy-carbonyloxy)-phthalimide (25 wt%) to the P3HT coating solution. Both tert-butyl phenyl carbonate and N-(tert-butoxy-carbonyloxy)-phthalimide decompose above 150 degrees Celsius to form pores in the thin film. Optical laser microscopy images of the P3HT films with tert-butyl phenyl carbonate and N-(tert-butoxy-carbonyloxy)-phthalimide films baked at 170 degrees Celsius were taken. Pores in the film with N-(tert-butoxy-carbonyloxy)-phthalimide are visible under the 3D laser scanning microscope VK –X100 (Figure 9) compared to plain P3HT, while the pore formation is not as obvious for tert-butyl phenyl carbonate. P3HT devices with N-(tert-butoxy-carbonyloxy)-phthalimide added as porogen gave a response of 24.9% current decrease on exposure to 25 ppm ethylene for 5 minutes (Figure 8c.). Thus we observed a 70% increase in response by increasing the interaction area of the sensor layer via introducing higher porosity in the active semiconductor layer.

To further enhance the response, we chose a strong receptor additive to trap the ethylene molecules without compromising the porosity of the thin film. Palladium particles (<1-micron diameter) were added to the semiconductor solution in a nitrogen-filled glove box. The mixture was then spin coated on the silicon substrates (with gold source and drain electrodes already patterned). By adding 50 wt% of palladium particles to P3HT + N-(tert-butoxy-carbonyloxy)-phthalimide, a response of 30.2% drain current decrease was obtained,

equivalent to a 107% increase in the response, was observed(Figure 8c). Increasing the wt% of palladium particles beyond 50% led to a very high density of palladium particles resulting in the formation of conductive pathways in the film. On further increasing the wt% of palladium particles to 70%, the semiconductor characteristics were lost completely.

We conducted a student T-test to determine the significance of the increase in sensitivity from the addition of porogen ($p<.05$) and the further addition of Pd particles ($p<.005$). This increase was anticipated due to the pores increasing site availability for gas molecules and due to the well-documented binding interactions between Pd and ethylene gas. Thus we have demonstrated a method by which non-specific P3HT can be made to have statistically significant increases in sensitivity of the ethylene analyte.

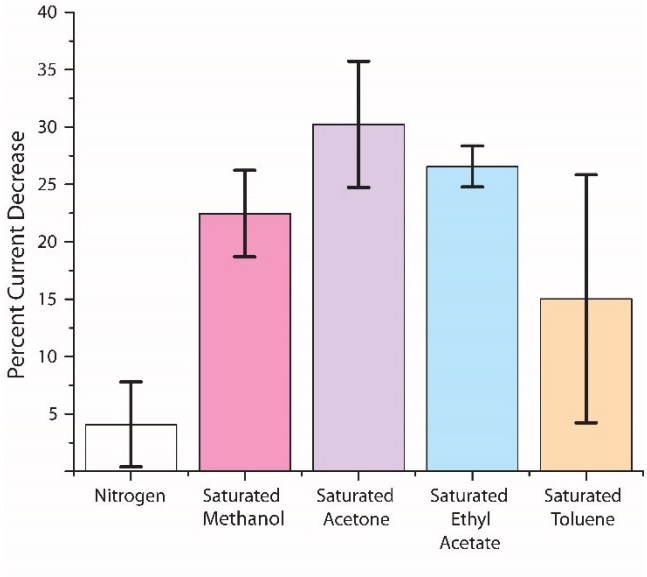

Figure 9 Selectivity data from saturated solvent conditions indicating relatively large current decreases upon exposure to extremely high levels of solvents. While these responses are higher than ideal for a specific device, these tested gases are not levels that would be seen under standard operating conditions for this sensor. Further experiments indicated changes within error for a more reasonable solvent concentration of 1% saturation.

A selectivity study was conducted for this ethylene-sensing platform for common solvents vapors like ethyl acetate, methanol, and acetone at saturation concentration. The study was conducted under saturated solvent vapor, with concentrations from one hundred to nearly five hundred times that of ethylene. Additional experiments of each solvent were conducted with concentrations of vapor at only 1% saturation, which has approximate concentrations of 180-2000 ppm, well above the amount of ethylene sensed. While results at extraordinarily high saturation concentrations show a significant sensing response, at more reasonable concentrations (as would be expected in fruit-related applications), the response ranged from only 5-9%, which is within the error bar of the nitrogen control. As a check to see the interaction of the sensor with another alkene, styrene vapor at a concentration of approximately 315 ppm was also exposed for 5 minutes and resulted in a response of about 12%. The interaction of palladium is expected to be highly specific for ethylene molecules, so while it is reasonable that a more similar molecule would have a higher response than the dissimilar solvents, it is not surprising that this platform is highly selective for ethylene at a much lower concentration than common solvents (Figure 10). While significant responses were found with all solvents, saturated conditions of any of them would not be expected in an environment where ethylene is being sensed. Additionally, the calculated per-100ppm response of the solvents is less than .5 %, far less than the simple variance caused by exposure to flowing nitrogen gas, and of course much less than the responses to ethylene. We have successfully demonstrated a sensitive and selective OFET sensor suitable for effective detection of ethylene at a concentration at or below 25 ppm, far more sensitive than the previously reported OFET ethylene detection. More importantly, we showed that the addition of pores to increase overall sensing area of the thin film and palladium nanoparticles to increase ethylene binding are highly constructive for increasing ethylene

sensitivity. The numerous possibilities for further tuning this system, such as adjustments in polymer orbital energy levels, pore sizes, and palladium particle diameters, offer promising paths to reaching the sub-ppm sensing level needed for monitoring produce during storage.

C. Devices with more than one element

Multiple organic electronic devices may be used in tandem to achieve higher analyte specificity. While any film layer may respond similarly to a certain type of functional group (positive or negative charges, polarity, etc.), these similarities are unlikely to be identical over a wide variety of films due to the opportunities for other chemical or physical interactions. Therefore, it is possible to align multiple types of detector films in different geometries to gain additional information than one film may give individually.

In the following two sections, there are examples of two different multi-element structures. To detect ammonia, we take advantage of the lone pair of electrons on ammonia's nitrogen atom and its opposite effects on p- and n-type semiconductor films. When these effects coincide, it results in a complete on/off response of the device in an inverter geometry, which is an easily interpreted signal. In the next section, we show that even two similar films can have drastically different responses to an analyte of interest with some minor polymeric adjustments. This system requires the user to compare the measurement ratio between two devices to determine whether a sensing event has occurred, with that ratio giving a much better indicator of selective detection than a single OFET could be alone.

1. Ammonia Sensing

The following data appeared in Besar, Kalpana*; **Dailey, Jennifer***; Zhao, Xingang; Katz, Howard. 2017. "Flexible Organic Inverter Made from Printable Materials with Synergistic Ammonia Sensing." Journal of Materials Chemistry C. 26(5) pp 6506-6511

***Equal Contribution**

The necessity for effective ammonia sensing has attracted substantial interest in the research community as the impacts of ammonia on public health have been elucidated[50, 52–59]. Ammonia-related particulate matter measuring under 2.5 microns in diameter is now considered a severe air pollutant worldwide and can contribute to chronic diseases such as asthma, respiratory inflammation, and pneumonia[60, 61]. Effective sensing of ammonia is necessary to improve the high health costs and morbidity associated with excess ammonia pollution, which is considered by the World Health Organization recommendations to be above 25-50 ppm depending on job type, with a recent no-observable-adverse-effects level (NOAEL) of 6.5 ppm for chronically exposed workers [62, 63]. In this work, we focus on unbound ammonia gas sensing as a proof-of-concept for sensor design. However, an effective sensor should be able to detect ammonia which is bound in particles, and may present additional challenges that are not seen in this work.

In recent years, much progress has been made in the development of sensors based on chemiresistors (CRs) and inorganic field effect transistors (FETs)[64–71]. However, many of these types of sensors are associated with low sensitivity, high operational temperature, lack of flexibility, or difficult readout methods. Use of organic semiconductors (OSCs) can alleviate many of these problems due to their low cost, ability to be printed on flexible substrates[72–74], and the ease with which we can tune their properties to make them

sensitive to the appropriate chemical agent. Organic FETs for sensing ammonia have previously been reported with good sensitivities of up to 0.1 ppm: a level more than sufficient for pollution monitoring purposes. However, OFET geometries lack good stability or an easily recognizable signal.

The complementary inverter structure is generally accepted as an ideal method for simply converting the analog signal achieved from traditional FET devices to a binary signal[65]. Briefly, an inverter is composed of two FETs joined in one circuit to form a logic gate. One of the FETs is p-type while the other is n-type. The devices are connected as shown in Figure 1a. At low gate voltage, the output ("bulk") voltage reads as the drain, and at high gate voltage, the output will read as ground. This results in an input-output curve as shown (Figure 11b).

For a complementary circuit to act as a sensor, it is essential that both p and n arms of the circuit give an equal and opposite response to the analyte of interest. In this paper, the organic semiconductors chosen were DPPCN (n-type) and P3HT (p-type), which were found to have approximately equal and opposite responses to the presence of ammonia when deposited using our concentrations and procedures. This circuit can give a binary response in terms of the output voltage by measuring at one standard gate voltage. We additionally discuss a dual layer dielectric which we developed to minimize gate current leakage and maximize layer integrity during semiconductor deposition. This flexible device made from printable materials has, to the best of our knowledge, the lowest sensitivity of any inverter-based ammonia sensor, at 1 ppm for five minutes exposure, or 0.5 ppm for longer exposures.

Materials and Methods.

Materials:

Indium tin oxide (ITO) coated polyethylene terephthalate (PET) with a surface resistivity of 60Ω/sq used as the substrate for all devices was purchased from Aldrich. P3HT was purchased from Solaris. The DPPCN was synthesized by Xingang Zhao according to a procedure in the reference[75], NMR of which is consistent with that reported in the reference[76]. Ammonia gas was received from Praxair with a concentration of 4.98 ppm ammonia and a balance of nitrogen. All other materials were purchased from Sigma and used as received.

Deposition and Measurement of Dielectric Films:

Polystyrene (PS) was dissolved in chlorobenzene at a concentration of 80 mg/mL, and poly(N-(2-hydroxypropyl)methacrylamide) (PHPMA) was dissolved in ethanol at a concentration of 100 mg/mL. Both solutions were heated to 55°C for one hour with occasional agitation to ensure complete dissolution. The solutions were then passed through a syringe filter of pore size 2.2 μm. Each layer was spin cast on a 1X1 inch square of ITO substrate at a rate of 1000 RPM for 60 seconds, then allowed to anneal in air for 30 minutes at 90°C to ensure complete solvent evaporation. Double layers of polystyrene and PHPMA were allowed to anneal before the addition of the second layer. One corner was left clear during deposition to allow for easy placement of the gate voltage electrode.

10 μm^2 gold electrodes were deposited on top of the dielectric layered devices to measure capacitance using a metal-insulator-metal sandwich configuration. Capacitance and dissipation factor were measured from 20 Hz to 1 MHz using an Agilent 4284A Precision

LCR Meter. Roughness and height measurements were taken in differential interference contrast (DIC) mode using a Keyence VK-X100 3D laser scanning microscope.

Semiconductor Device Fabrication:

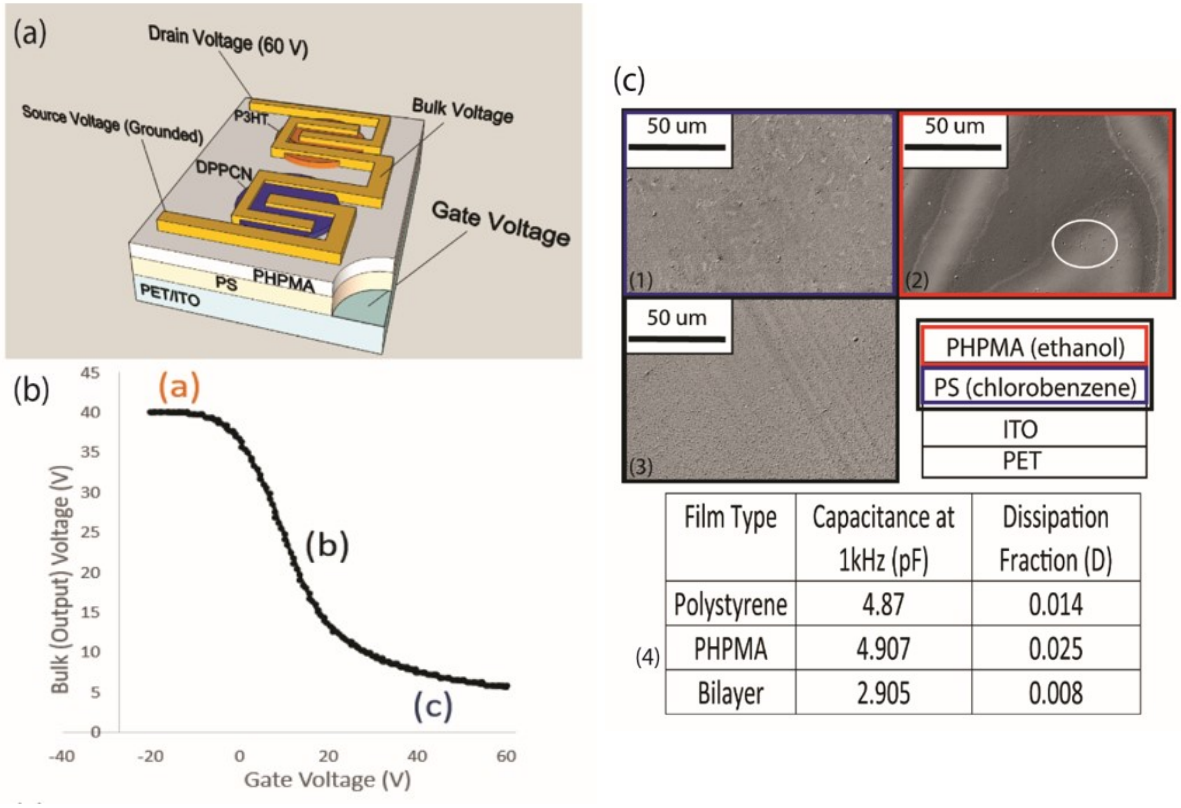

Film Type	Capacitance at 1kHz (pF)	Dissipation Fraction (D)
Polystyrene	4.87	0.014
PHPMA	4.907	0.025
Bilayer	2.905	0.008

Figure 10 (a) Schematic of inverter structure composed of two intersecting transistors. (b) Explanatory graphic of inverter bulk (output) voltage curve where a.) indicates that P3HT is conductive, b.) indicates the switching voltage and c.) indicates that DPPCN is conductive and thus the bulk voltage reads near ground. (c) DIC images comparing film morphology of (1) PS, (2) PHPMA with the white circle indicating large holes, and (3) bilayer of higher quality. (4) Capacitance and dissipation table for the films.

A dual dielectric layer of PHPMA on top of polystyrene was made as described above on ITO-covered PET substrates. 40nm gold contact electrodes were deposited using physical

vapor deposition. P3HT was dissolved at a concentration of 1.1 mg for 1.5 mL of chlorobenzene and spin cast by dropping solution only on the p side of the inverter at 1000 RPM for 60 s. The device was annealed for 1 min at 90°C. DPPCN was dissolved at a concentration of 1.2 mg DPPCN to 0.25 mL of chlorobenzene. It was then mixed at a 1:2 ratio with a 10mg/mL solution of polystyrene in chlorobenzene. This combined solution was drop cast on the n side of the inverter and immediately wicked away with a soft paper tissue. Solutions were made fresh and used the same day due to avoid degradation of the semiconducting properties upon exposure of the solution to light and contaminants.

Transistor and Inverter Measurements:

It was necessary to take transistor measurements to ensure complimentary responses from the p and n sides of the inverter structure. Transistor devices were obtained by splitting the inverter structure in half and depositing each semiconducting material as described above on one of the two halves. Drops of indium gallium were used between the probes and electrodes on the devices to ensure gentle contact between the sharp probe tips and sample, in order to prevent damage to the film that would lead to gate leakage. Measurements were made using an Agilent 4155C Semiconductor Parameter Analyzer. Inverter measurements were taken by setting the drain current to 40V and sweeping the gate voltage from -40 up to a maximum of 100 V. The bulk voltage was read as output.

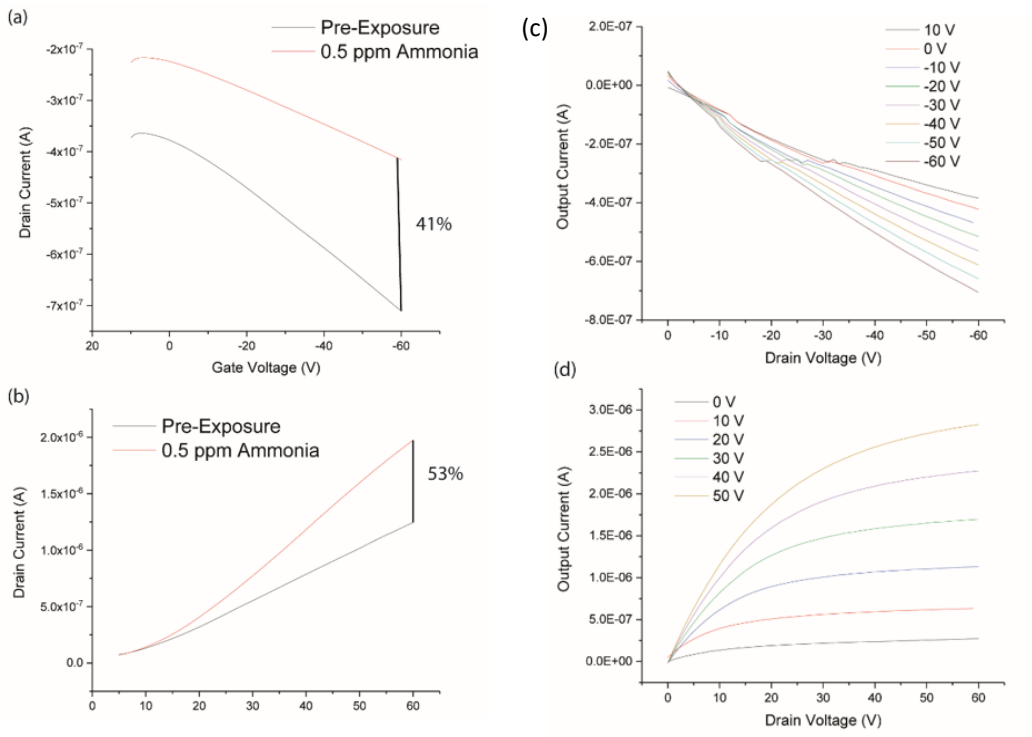

Figure 12 (a,b) Response curves of individual OFETs. (c,d) Output curves of P3HT and DPPCN

Ammonia Exposure:

Ammonia was diluted in an Environics Gas Dilution System series 4040 with house air (humidity measured as ~45%). The ammonia dilution was fed through Teflon™ tubing into a covered beaker with an outlet to ensure air flow through the container. The device was positioned under the gas flow for the duration of the experiment, then immediately taken in a covered container to be characterized electronically (<1 minute)

Selectivity Measurements:

Selectivity measurement exposures took place in a 125 mL corked flask into which the device was placed. A 20 mL syringe of saturated vapor of interest was plunged into the flask to expose the inverter to a high concentration of solvent vapors. Inverter measurements were taken immediately as described. House air tests were taken the same way as those for ammonia, but with cleaned tubing connected to house air supplying the inlet gas.

Statistical Analysis of Data

In the sensor design process, it is useful to determine a quantitative description of a sensor's accuracy and tendency to false positives and negatives. In the biosensor field, this is frequently described in terms of "limit of blank" and "limit of detection". The limit of blank refers to a calculation of how much voltage shift we can reasonably expect from a sample not containing any analyte, which can be similar to detecting noise of a system. Assuming a Gaussian distribution of signal, this number will encompass 95% of all tested blanks. The limit of detection describes how low of a concentration of analyte can be reliably detected, for an arbitrarily chosen degree of reliability (in our case, $p<0.05$).

Though we may see some small voltage shift at incredibly low atmospheric concentrations of ammonia, this raw data should be treated cautiously so that environmental noise (as seen in blank samples) is not mistaken for a detection signal.

The limit of blank is determined by the calculation over many samples of:

Equation 3 Limit of blank calculation from mean and standard deviation.

$$LoB = mean_{blank} + 1.645(SD_{blank})$$

Where we are inputting the values of voltage shift to calculate mean and standard deviation. The calculated limit of blank is on the order of 1 V.

The limit of detection is 5 ppm, and is calculated by:

Equation 4 Limit of detection calculated from limit of blank and data from low concentration samples.

$$LoD = LoB + 1.645(SD_{low\ concentration\ sample})$$

Dual Dielectric Layers

While polystyrene is frequently used alone as a dielectric layer, this was not a viable choice due to the use of chlorobenzene as solvent for both polystyrene and the two semiconducting polymers. It was necessary to identify an orthogonally soluble dielectric capable of allowing semiconducting film deposition without sacrificing the integrity of the underlying dielectric layer. PHPMA was chosen as the second dielectric layer due to its solubility in ethanol and insolubility in chlorobenzene. However, through a series of sandwich electrode capacitance measurements, it was observed that a PHPMA layer had a higher than ideal dissipation factor (D) of 0.025 at 1 kHz, with obvious defects when viewed with a microscope. Typically a D value of less than 0.01 is considered suitable for transistor use.

In Figure 11c, pockmarks and large hills are visible in the PHPMA film. The polystyrene film is significantly more uniform, as is the bilayer of PHPMA on polystyrene. Additionally, the bilayer had a measured D of only 0.008, with good stability and reliability across many samples. The bilayer indicated no dissolution when chlorobenzene was spin coated on top of the devices. The capacitance of the bilayer was measured as 2.9 pF, compared to ~4.9 pF for both PS and PHPMA. This decrease is consistent with the large increase of height caused by the addition of another film layer. While the additional step is not ideal for a simple fabrication process, this bilayer was necessary in order to produce a sturdy, insoluble structure with sufficient dielectric characteristics to operate the inverter with minimal gate leakage.

Transistor measurements:

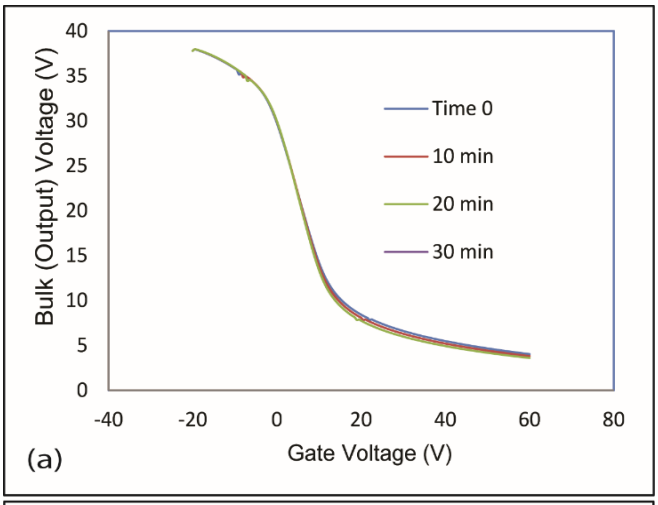

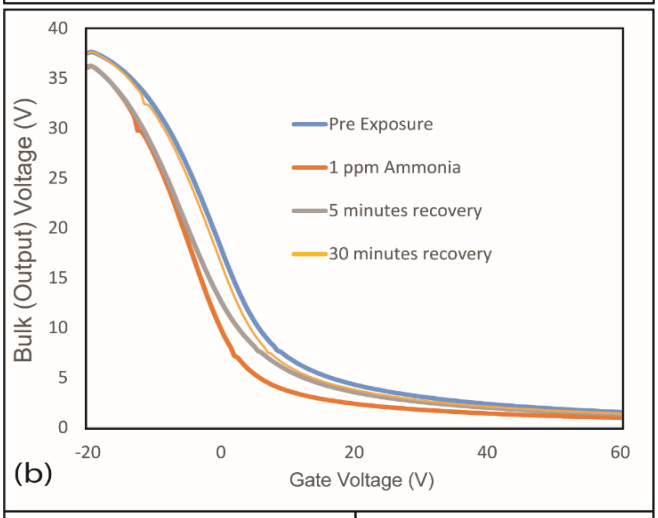

Analyte (5 min exposure)	% Signal Recovery
1 ppm ammonia	92.3
5 ppm ammonia	73.8
Saturated acetone	70.5

Figure 13 (a) Stability of one inverter over 30 minutes. There is only a 1 volt output voltage shift, which is not observable on the graph. (b) Example of device recovery in air over 30 minutes and table of average recovery rates after 30 minutes.

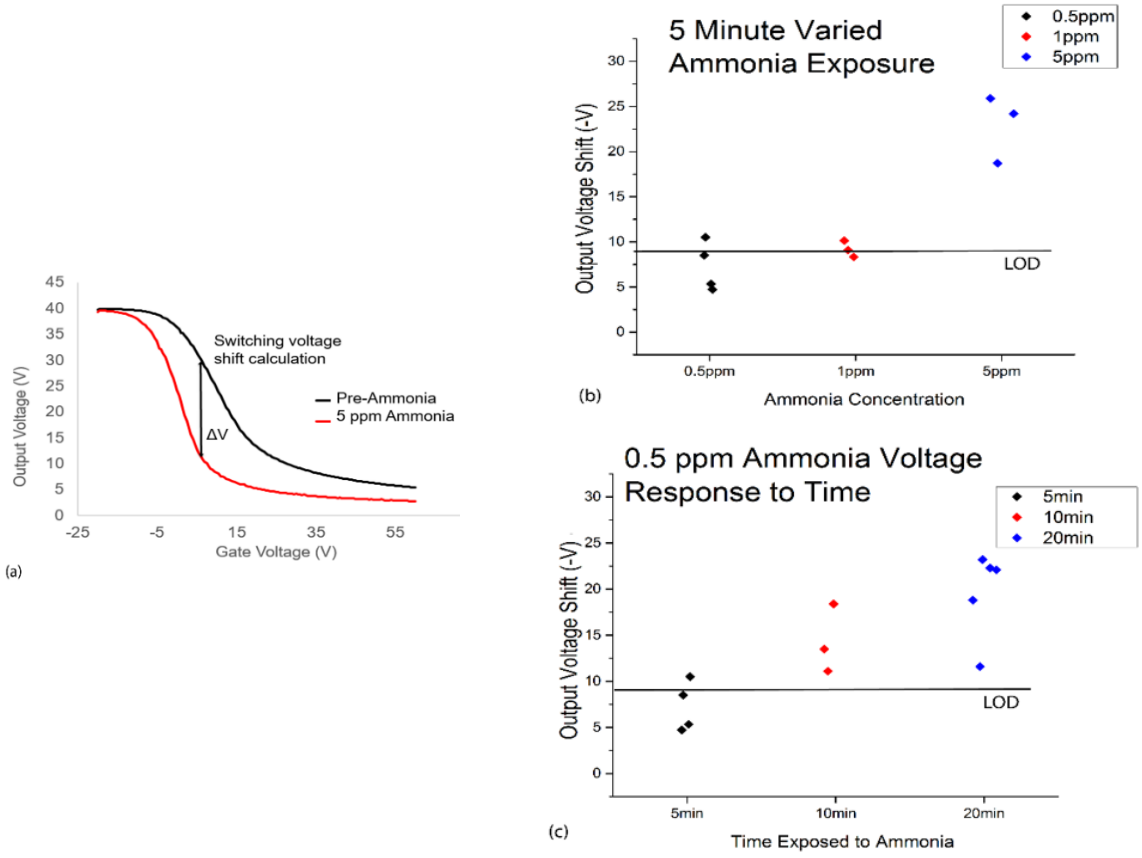

Figure 11 a) An example of calculation of output voltage shift pre- and post- ammonia exposure. (b) Graph depicting shift in voltage as a function of ammonia concentration with limit of detection at 1 ppm ammonia and (c) Graph depicting change in voltage shift with change in exposure time for 0.5 ppm ammonia.

In order for the inverter to function reliably as an ammonia sensor, complementary n- and p-type semiconductors that react proportionately and inversely to ammonia were necessary. To achieve this balance, a series of transistor measurements for each individual semiconductor were conducted in order to find the optimum solution concentrations and deposition methods.

At higher concentrations of P3HT, such as 2 mg/mL, the p arm of the inverter became overly conductive compared to the DPPCN, and the resulting input-output curve maintained a consistently high voltage, without turning off. Transistor sensitivity measurements were taken using devices made with a concentration of 1.1 mg P3HT/0.5 mL chlorobenzene and 1.2 mg DPPCN/0.25 mL chlorobenzene, further diluted with .5 mL 10 mg/mL polystyrene in chlorobenzene to increase mobility and conductivity, as previously reported for semiconducting polymers[79–84]. After 5 minutes in 0.5 ppm ammonia, the P3HT devices had an average reduction in the current of 41%; the DPPCN transistors had an increase of 35% (example calculations shown in Figure 2). These were determined to be the optimum conditions for the creation of the inverter.

Inverter measurements:

Inverter input-output curves were found to vary in approximately the first hour after device fabrication (Figure 4a). To ensure reproducible results, measurements with gas exposure were only taken after the voltage curves had stabilized. This shifting is likely a result of many factors, such as final solvent evaporation and semiconductor doping with oxygen and water vapor, known contaminants[85]. Further support of this assumption lies in the fact that a small reverse shift was observed after this stabilization when devices were measured using house air as a control (a slightly lower humidity than the room, ~45% versus ~50%,

representing a change of about 1000 ppm of water). This shift was seen to reverse back to the previous stable level after a few minutes left in the general atmosphere, where water is the main contaminant. Once devices became stable in a given atmosphere, they remained so for many hours of testing.

The ammonia-induced change in output voltage was measured by comparing the pre- and post-exposure voltage curves and finding the input voltage where there was the largest difference between the two outputs (which corresponds to the location of the highest slope, as shown in Figure 12a). This change was measured for three samples that were exposed to .5 ppm, 1 ppm, and 5 ppm ammonia for 5 minutes each and measured directly after. We see a significant increase ($p=0.01$) in output voltage shift in the presence of 5 ppm ammonia, as determined by the student's t-test comparing low (0.5 and 1 ppm) concentrations to high (5 ppm) concentrations of ammonia (Figure 12b).

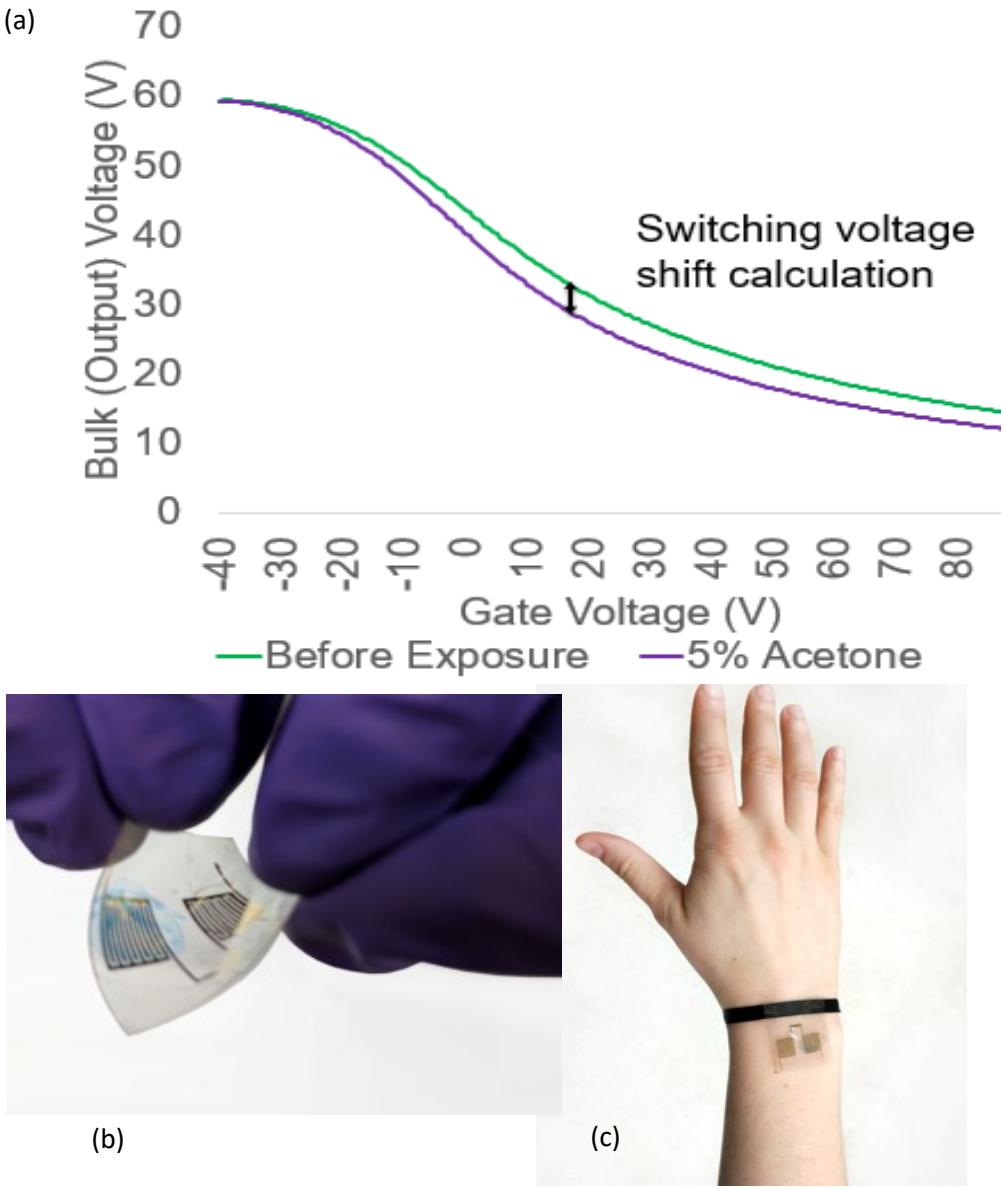

Figure 12 (a) Inverter graph showing minimal shift upon exposure to acetone at 5% saturation concentration. (b) Bending the device back and forth results in no visible deformation of significant voltage shifts. (c) The device is easily wearable and does not degrade.

Additionally, as a measure of the evolution of the responses over time, 0.5 ppm ammonia was applied to at minimum three devices for 5, 10, or 20 minutes. We see a gradual increase over time in the output voltage change, as more ammonia molecules interact with the films

(Figure 12c). Recovery of devices is still nearly complete within 30 minutes following these exposures (Figure 13b). There is little shift in output voltage with further time, so it is likely that within 20 minutes the film has become saturated to the ammonia and will not have a further increased response. This supports our conclusion that the increase in amine groups from additional ammonia molecules is causing further doping since similar increases are seen both in the presence of additional ammonia, as well as when the device is left in ammonia for a longer period of time. The calculated limit of detection[86] (LOD) based on our blank sample measurements and other data is 1 ppm ammonia for 5 minutes or more exposure.

Stability and Wearability:

One of the primary focuses of this work was to create a proof-of-concept device with sufficient flexibility to become the base architecture for a sensor capable of being worn by individuals. To this end, a standard device was made wearable by cutting slits through the substrate and weaving a ribbon through the back of the device, such that the skin did not come in direct contact with the semiconducting materials. The sensing side of the device was exposed to the outside environment, while the PET and ribbon were pressed against the wrist. This bracelet was worn by a lab member for one hour while she continued with her standard work. Thus the sensor was exposed to body heat, movement and minor bending, and a variety of low concentration solvent vapors (dichloromethane, ethyl acetate, hexane, and acetone) that were found in the chemical lab at this time. As an additional test to replicate potential user misuse, the sensor was then bent strongly back and forth three times with no visible alterations occurring to the polymer layers or electrodes. The device showed excellent stability following this experiment, shifting switching voltage by only 1.7 volts (Figure 14) after all of these exposures and bends.

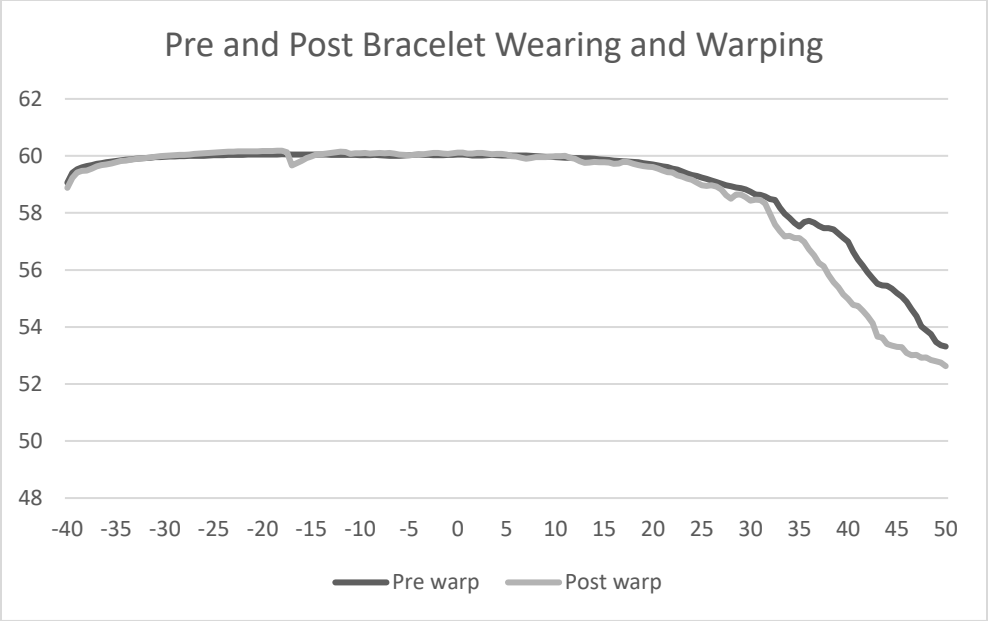

Figure 13 Inverter graphs before and after wearing sensor for one hour in laboratory and deforming through bending.

Table 2 Average voltage shifts caused by saturation solvent vapor conditions on inverter.

(-V) Shift				
Solvent	Run 1	Run 2	Run 3	Average
Toluene	28.4	18.06	20.36	22.27
Acetone	22.56	19.9	16.06	19.51
Ethyl Acetate	12	12.7	15.9	13.53
Methanol	28.9	33.6	8.6	23.70

While exposure to saturated solvent conditions (thousands of ppm) also produced large effects (Table 2) in the output voltage, exposure to 5% of saturated acetone concentration (which we would expect to be the most reactive among the solvents tested and weakly Lewis basic, and still at a much higher concentration than would be expected for an interferent)

resulted in only a minimal shifting of the output voltage by 2 V, which is below the limit of blank calculation and is considered to be small. It was considered that saturated conditions of solvent result in morphological changes to the film, which could impact the overall conductivity of each arm of the inverter. However, due to the similar recovery percentages of these devices compared to ammonia-exposed devices, it seems likely that the complete saturation of the films resulted in increased doping. As these sensors are not expected to be used in any condition near interferent saturation levels, and due to the very high stability when exposed to a variety of chemicals (when worn in the chemical lab), this level of selectivity is determined to be appropriate for environmental ammonia sensing applications.

Conclusions

We have developed a robust and potentially printable architecture that is able to function as an inverter with specific sensing layers to detect ammonia. To the best of our knowledge, this is the first time a flexible inverter sensor for ammonia has been tested for wearability. This type of device could achieve a digital signal by measuring at one specific gate voltage and labeling an output voltage as "on" or "off" if some cutoff exposure is reached. The LOD of 1 ppm in a five-minute detection window is already well below the necessary realm of interest for workplace measurements. Due to this range of detection, this device may be suited additionally to measuring breath samples of individuals with various mouth, liver, or kidney ailments that cause them to produce up to the 10s of ppm of ammonia upon exhalation[87, 88].

2. NO2 Sensing Using Multiple Semiconducting Polymers

The following project appeared in: Li, Hui; **Dailey, Jennifer**; Kale, Teju; Besar, Kalpana; Koehler, K; Katz, Howard. 2017. "Sensitive and Selective NO2 Sensing Based on Alkyl- and Alkylthio-Thiophene Polymer Conductance and Conductance Ratio Changes from Differential Chemical Doping." ACS Applied Materials & Interfaces. 9 (24), pp 20501–20507

My contribution to this project lay in optimizing a method for testing vapor selectivity and response which is described thoroughly below, as well as final data analysis and presentation. See citation for complete methodology and discussion.

Project Abstract:

NO_2-responsive polymer-based organic field-effect transistors (OFETs) are described, and room-temperature detection with high sensitivity entirely from the semiconductor was achieved. Two thiophene polymers, poly(bisdodecylquaterthiophene) and poly(bisdodecylthioquaterthiophene) (PQT12 and PQTS12, respectively), were used as active layers to detect a concentration at least as low as 1 ppm of NO_2. The proportional on-current change of OFETs using these polymers reached over 400% for PQTS12, which is among the highest sensitivities reported for a NO_2-responsive device based on an organic semiconducting film. From measurements of cyclic voltammetry and the electronic characteristics, we found that the introduction of sulfurs into the side chains induces traps in films of the PQTS12 and also decreases domain sizes, both of which could contribute to the higher sensitivity of PQTS12 to NO_2 gas compared with PQT12. The ratio of responses of

PQTS12 and PQT12 is higher for exposures to lower concentrations, making this parameter a means of distinguishing responses to low concentrations for extended times from exposures to high concentrations from shorter times. The responses to nonoxidizing vapors were much lower, indicating good selectivity to NO_2 of two polymers. This work demonstrates the capability of increasing selectivity and calibration of OFET sensors by modulating redox and aggregation properties of polymer semiconductors.

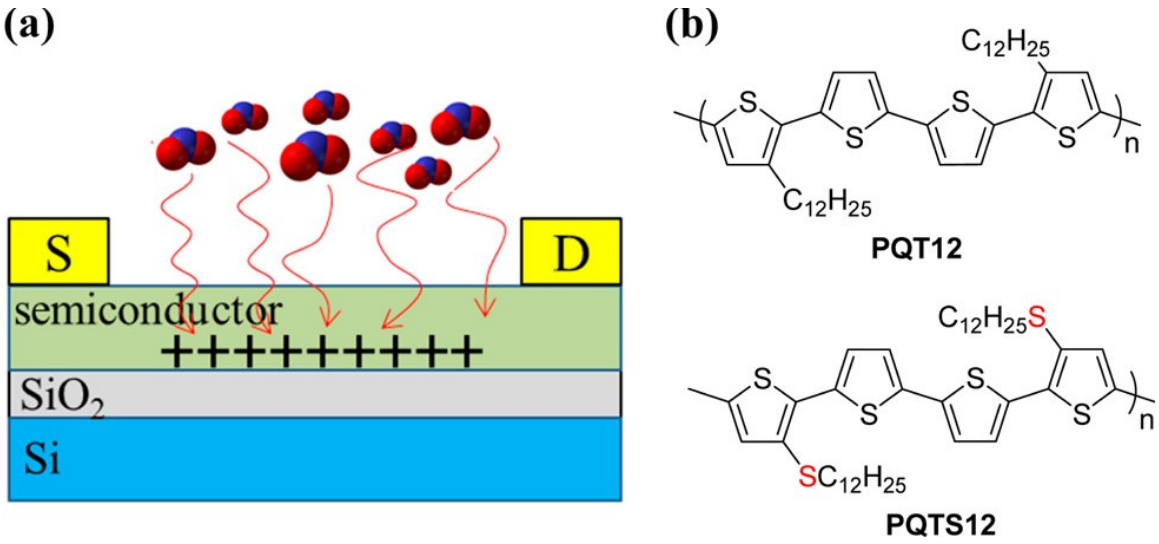

Figure 14 (a) Schematic diagram of the device structure. (b) Chemical structures of polymer semiconductors.

Top-contact, bottom-gate architecture OFETs were fabricated as sensor devices. The polymer semiconductors were spin coated with a 4 mg mL^{-1} chlorobenzene solution at 2000 rpm and then were annealed at 120 °C for 10 min in the glovebox. Au source/drain electrodes (W = 8000 μm, L = 250 μm) were used to measure the electrical performances of PQT12 and PQTS12-based devices. The field-effect mobilities were calculated from the transfer characteristics of more than seven devices in the saturation region (V_{DS} = −60 V).

The original devices without gas exposure show typical p-type transport. The transistors of PQT12 show hole mobility of 0.027 ± 0.004 $cm^2 V^{-1} s^{-1}$, while PQTS12 films exhibit hole mobility of 0.010 ± 0.002 $cm^2 V^{-1} s^{-1}$. The lower mobility of PQTS12 indicates that the sulfurs in side chains impact the carrier transport in films. We calculate the trap densities using $N_{trap} = C_i \times |V_T - V_0|/e$, where C_i is the capacitance per unit area (11.5 nF cm^{-2}), V_T is the threshold voltage, and V_0 is the turn-on voltage. For a pure PQT12 film with a thickness of 100 nm, the surface trap density is about 7.1×10^{15} cm^{-2}. For the pure PQTS12 film, the value (1.2×10^{16} cm^{-2}) is higher than that of PQT12 film. This further confirms that more traps exist in the PQTS12 film which is consistent with the result of CV. Tapping mode atomic force microscopy (AFM) was employed to analyze the morphology of PQT12 and PQTS12 thin film. Continuous thin film formation with large domains was observed in the PQT12 thin film, which provided efficient channels for the carrier transport. Smaller grains and numerous grain boundaries were observed in the PQTS12 thin film, which presumably promoted the trap activity and decreased the mobility.

Selectivity studies of PQT12 and PQTS12 films were carried out by exposure to common solvent vapors like acetone, chlorobenzene, hexane, ethyl acetate, methanol, 2-propanol, triethylamine, and chloroform, as shown in the following figure. The solvent vapor pressures were much higher than the NO_2 vapor pressures used in this study. Acetone could be considered a more Lewis basic carbonyl compound than atmospheric CO_2, while methanol is a carrier of OH groups at higher vapor pressure than atmospheric humidity[19, 89, 90]. The data were obtained using a gate voltage of −30 V. For PQTS12 films, a large increase of I_{DS} is observed after exposure to chlorobenzene and chloroform, which could possibly be attributed to the rearrangement of morphology analogous to saturated solvent vapor annealing treatment or to HCl impurity in the film, which could be pre-filtered using a

weakly basic powder in a real application. Only chloroform vapor significantly increases the conductivity of the PQT12 film, and this may have been because of the HCl contaminant ubiquitously present in chloroform. Triethylamine gives a large decrease of I_{DS} because of its electron-rich, trapping character as we and others have reported for amines in the past[91, 92]. PQTS12 is a bit more sensitive to the alcohols methanol and 2-propanol compared with PQT12. Only minor changes to I_{DS} are observed after exposure of this OFET to acetone, ethyl acetate, and hexane. Except for chloroform and triethylamine, we found that current decreases with high concentrations of other solvents and that current increases with low concentrations using PQT12 film. This indicates two possible mechanisms. At low concentrations, there is a synergistic interaction with oxygen or other impurities that slightly dope the semiconductor or decreases grain boundary barriers. At higher (fully saturated) concentrations, the dipole quenching effect is more important, as many of the vapors caused current decreases.

Selectivity Measurement Specifications:

It is vital to ensure good selectivity of vapor devices, especially since their underlying detection mechanisms can be subject to interference from similar compounds. Without good selectivity, false positives may give a consistent overestimation of the analyte of interest, making the sensor useless in complex environments.

Due to the nature of these semiconducting films, extremely saturated vapors of almost any sort will cause some sort of response. As this sensor is meant to sense levels of toxic gas in a working environment that is not saturated by any given solvent, we are not concerned with the effects of complete solvent saturation. We, therefore, choose to examine the selectivity response at one-tenth saturation concentration, as determined by the below equation:

Equation 5 Calculation of PPM of solvent in air.

$$\frac{\text{Vapor pressure of the liquid}}{\text{Total atmospheric barometric pressure}} * 1{,}000{,}000 = \text{PPM of solvent in air}$$

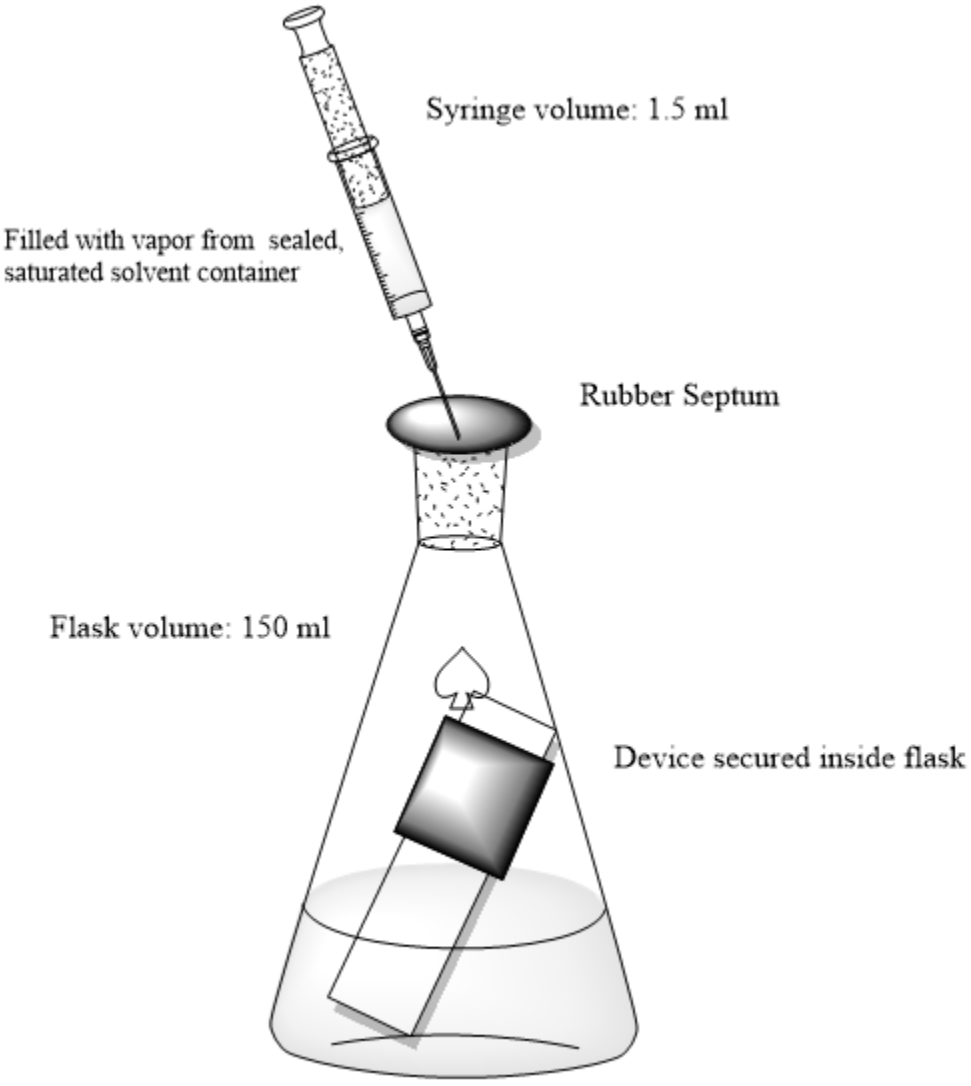

Figure 15 Method of determining solvent vapor concentration exactly for device selectivity testing

Saturated vapor was collected from a covered solvent container, where the internal vapor was allowed to come to equilibrium. This concentration is known for each common solvent at room temperature. This volume was measured in a syringe as shown in the above Figure 16 and plunged into a sealed container of known volume. The new PPM concentration was calculated based on this volume change. This method of selectivity determination resulted in very consistent detection results, with changes far less than those that occur at saturation, as expected. The percentage changes in measured current are shown in Figure 17.

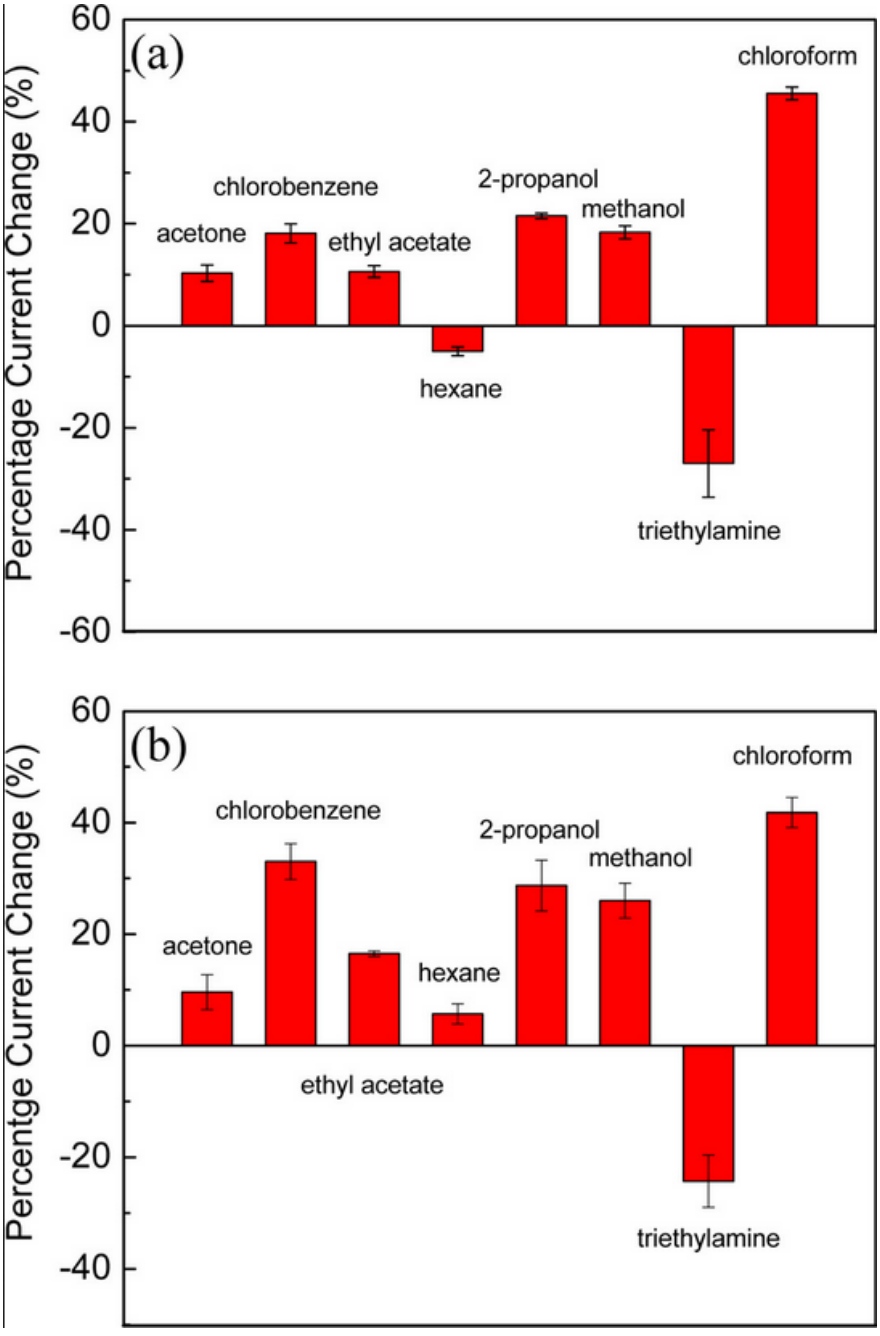

Figure 16 Responses of I_{DS} after exposure to common solvent vapors on (a) PQT12- and (b) PQTS12-based sensor. (V_G = −30 V) acetone (16 200 ppm); chlorobenzene (1050 ppm); ethyl acetate (8300 ppm); hexane (10 400 ppm); 2-propanol (3800 ppm); methanol (11 100 ppm); triethylamine (4500 ppm); chloroform (14 000 ppm). None of these solvents have a similar effect as

our target, making this combination of polymers selective even at very high concentrations of other gases.

D. Summary

In Chapter 2 we have discussed a variety of methods by which vapor sensors can be modified to suit various needs. Particles and pores can be added to an OSC layer in order to attract or hold an analyte of interest. In the ethylene project, we showed evidence that each of these types of additions can add more sensitivity to the device through different mechanisms. Additionally, multiple films can be used simultaneously, and a combined reading may give more information than any single device could individually. The ammonia sensor acts as an inverter and gives a simple "on" or "off" response when held at a certain gate voltage, but the NO2 sensor must compare the output current of two different devices.

Advances in machine learning are encouraging, since they may be able to design algorithms to determine a chemical "fingerprint" based on multiple inputs from different sensing layers. In this case, it is not necessary to determine precise effects of an analyte on each material, but rather the neural network can be trained to differentiate the resultant signal much like artificial intelligence in photograph identification.

These vapor sensors are very promising for point-of-care use in a variety of conditions. However, long-term stability is still unclear, and it may be necessary to examine potential encapsulation methods until the sensor is ready to be used.

III. Design of Polymers for Biosensors

A. Previous work tuning dielectric materials

The dielectric layer of an organic electronic sensing device can be tuned according to the environmental needs and restrictions. In 2014, Martinez Hardigree detailed a study in tuning and stabilizing the threshold voltage by intelligently altering the dielectric layer. This includes creating a thinner layer (higher capacitance) with higher permittivity. It is also necessary to ensure complete hydrophobicity such that there is no liquid contamination and leakage through the film [11]. Alley had an additional discussion of dielectric insulators regarding the effect of dielectric constant on the carrier mobility in the OFET geometry[12]. In this section, however, we are primarily concerned with simple devices that do not rely on an organic semiconductor. Rather, many of them will detect changes in capacitance across the film whether due to binding onto the polymer layer, or specifically controlled polymer degradation allowing for water infiltration.

Layered capacitors add in series according to:

Equation 6 Total capacitance addition equation

$$\frac{1}{C1} + \frac{1}{C2} = \frac{1}{C(total)}$$

Therefore, the larger the capacitance of a constant element, the less effect it will have on the overall change. For this reason, it is ideal to have a bulk layer with a relatively high capacitance, so that small capacitive changes will be detected. Conversely, the detection event layer should have relatively low capacitance and will then produce a total larger effect.

B. Concept of degradable polymers

Introduction to Electrochemical Impedance Spectroscopy

Electrochemical impedance spectroscopy (EIS) offers an attractive solution to the development of fast, point-of-care sensors for detecting specific molecules in biological samples[93–96]. The development of a diagnostic system that requires only minutes to complete a sample analysis with an electronic readout could lead to major improvements in prevention and therapy in healthcare settings and increased reliability of food safety.[97–99] We address this latter goal by our choice of a Penicillin-binding protein 2a (PBP2a) as a test analyte for EIS studies as described below. This protein is an indicator of methicillin-resistant Staphylococcus aureus (MRSA), a high priority pathogen for both human health and food safety.[100–103]

Over the past few decades, many researchers have made great strides in increasing the sensitivity of the EIS method of detection through alteration of electrodes, miniaturization and multiplexing, use of different binding materials, and various forms of labeling.[95, 104–107] However, a single molecular binding event would be expected to produce minimal resistive or capacitive change in an impedimetric system, limiting our ability to detect low levels of analyte (pg/ml) in normal human samples that are composed of an extensive mixture of different proteins. Labelling systems, such as the addition of secondary enzymes in a classic enzyme-linked immunosorbent assay (ELISA) geometry, have been shown to drastically increase sensitivity by causing further electronic interactions at the interface, and they could be an ideal solution to diagnostic sensors in environments with trained technical personnel.[108, 109] Unfortunately, the addition of labeling to the EIS system creates extra

steps that both complicate the use of the system and may be a source of increased errors due to improper or insufficient sample washing. With this motivation, for the purposes of creating a sensor that is truly one-step, we focus on designing a more responsive, polymer-based analyte-binding layer, and we avoid any secondary binding steps.

A sensor based on EIS detection of the degradation of a polymer layer is a concept that has already been reported for enzyme-substrate systems, and this phenomenon has been additionally well studied in paint coatings on metals[110–113]. Particularly effective are films composed of enzymatically cleavable bonds that indicate the presence of even a small amount of enzyme in solution. In order to increase the limited signal produced by a single binding interaction of noncatalytic antibody and antigen, we have created and characterized a novel polymer structure with fragile, degradable side chains. The alteration of the polymer dielectric layer upon analyte attachment produces an increased signal compared to the effect of a typical binding event. To the best of the authors' knowledge, this is the first time that EIS has been used to detect polymer degradation based on a label-free antibody-antigen binding event.

The key chemical features in our polymers are trityl-based groups, including unsubstituted trityl, 4-monomethoxytrityl (MMT), and (4,4)-dimethoxytrityl (DMT), which have long been used to protect hydroxyl groups from undesired reactions during chemical transformations of accompanying functional groups. DMT can be very easily removed with weak acid ("deprotected"), making it a favorite protecting group during synthesis. The use of trityl-based groups in polymers has been studied, and their bulkiness compared to the carbon backbone can produce isotropic chains as the monomers are forced into restricted spaces around the steric bulk.[114–116] Due to their fragility, these protecting groups are typically

meant as intermediaries in the synthesis of another compound and are not the final product. Homopolymers of the trityl methacrylate groups are extremely insoluble in standard solvents. Because our group obtained utility from poly(benzyl methacrylate) as a thin film dielectric layer for sensing purposes, we chose to create a series of trityl copolymers incorporating benzyl methacrylate and the various trityl methacrylates.[117]

These previously unreported polymers were extensively characterized using NMR and gel permeation chromatography (GPC), and their thin film layers were tested for their dielectric properties. The free volume around the trityl groups can allow for increased free rotation of polar and polarizable functional groups of the polymer, which would increase the dielectric constant, κ. Additionally, if this volume becomes filled with a polar solvent such as water (κ=~80), there will be a significant change in EIS measurements.[118] A stable dielectric layer for an aqueous EIS system must be impermeable to water since absorption of water into the film would drastically change its capacitive effects. Just as benzyl methacrylate is completely insoluble in water and produces a stable film, out trityl copolymers in their pristine form are similarly hydrophobic. However, as the trityl groups begin to deprotect, water is allowed to enter the film, furnishing an additional mechanism for electronic signaling.

For all analyte sensing measurements in this work, we used a polymer blend of the trityl copolymer and a polymer composed of benzyl methacrylate and methacrylic acid groups. These acid groups were used to covalently bind antibodies to the polymer thin film in very close proximity to the trityl side chains, using standard carbodiimide crosslinking chemistry, which has been well-established as an effective tool for immunosensor fabrication[119–123].

Materials and Methods

Source Materials

Glass slides were purchased from Corning and thoroughly cleaned before use as described below. A 1mL three-probe impedance testing cell was purchased from CH Instruments Inc (Texas). MRSA antibodies corresponding to PBP2a were purchased from Abnova. FITC-tagged glial fibrillary acidic protein (GFAP) antibody was purchased from EMD Millipore. All other chemicals were purchased from Sigma, in anhydrous condition if possible, and were not additionally purified before use. Synthesized monomers and polymers were analyzed using NMR to confirm composition (figures at end of chapter). A PARSTAT 2273 was used to take EIS measurements and controlled with PowerSuite software. An Olympus IX71 was used to take fluorescent images.

Substrate Preparation

Corning glass was cut into 1' squares and cleaned with liquid soap and water, followed by sonication for 15 minutes in both acetone and isopropanol. The glass substrates were dried with nitrogen flow and immediately deposited with Cr/Au (5nm/50nm) at $<6 \times 10^{-6}$ Torr using thermal evaporation. Substrates were kept under vacuum until use.

Trityl-based Monomer synthesis:

Trityl methacrylate (TrM) was synthesized according to Yuki (summarized in Scheme 1), with minor adjustments[115]. Briefly, methacrylic acid was added to a sealed flask of toluene cooled in an ice bath, and triethylamine was added thereto. Trityl chloride was dissolved in a small amount of toluene and injected into the system, while under nitrogen. The mixture was allowed to stir for two hours, and the precipitated salt was filtered away. The mixture

was then held at -5°C overnight, at which point additional salt precipitated and was filtered. The remaining solvent was evaporated, and the monomer was recrystallized from diethyl ether, producing large, white crystals resembling granulated sugar.

Monomethoxytrityl methacrylate (MMTM) was synthesized similarly as above using monomethoxytrityl chloride as the precursor. As this reaction progressed far more slowly due to the additional methoxy group, TLC (DCM:DMF 1:1) was used to confirm that the starting products were converted at various time intervals. The reaction was allowed to continue for three hours, and the precipitated salt was filtered away. The monomer was washed three times with saturated aqueous sodium bicarbonate and dried over sodium sulfate. The remaining organic layer was evaporated away under vacuum, resulting in a viscous, pale yellow oil.

Dimethoxytrityl methacrylate (DMTM) was synthesized in the same manner as MMTM, using dimethoxytrityl chloride as a precursor, resulting in a viscous, yellow oil. Trimethoxytrityl methacrylate (TMTM) was also synthesized as above but was found to be so labile during washing steps that no significant fraction of the desired product was able to survive to polymerization. Trimethoxytrityl is mentioned in the literature as being overly fragile for practical use, so this is not unreasonable.[124]

Polymer Synthesis:

Copolymerization of all monomers and methacrylic acid with benzyl methacrylate (mixed in an equimolar ratio) was accomplished through free-radical polymerization using azobisisobutyronitrile (AIBN) as an initiator under anhydrous conditions in nitrogen, summarized in Scheme 1.2. The polymer was precipitated in hexane cooled below room temperature with an ice bath, and any unreacted monomers were removed in warm toluene.

With the exception of the simple copolymer of methacrylic acid and benzyl methacrylate, these trityl-based polymers did not dissolve fully in most solvents. Only anisole and dimethylformamide (DMF) were found to be suitable candidates [See Table 3]. Polymers were dissolved at a concentration of 50 mg/ml and filtered through a 0.45 um syringe filter. Solutions were deposited through spin casting on prepared substrates at a speed of 1500 rpm for 60 seconds in an inert nitrogen atmosphere. Samples were annealed at 60°C for one hour under nitrogen.

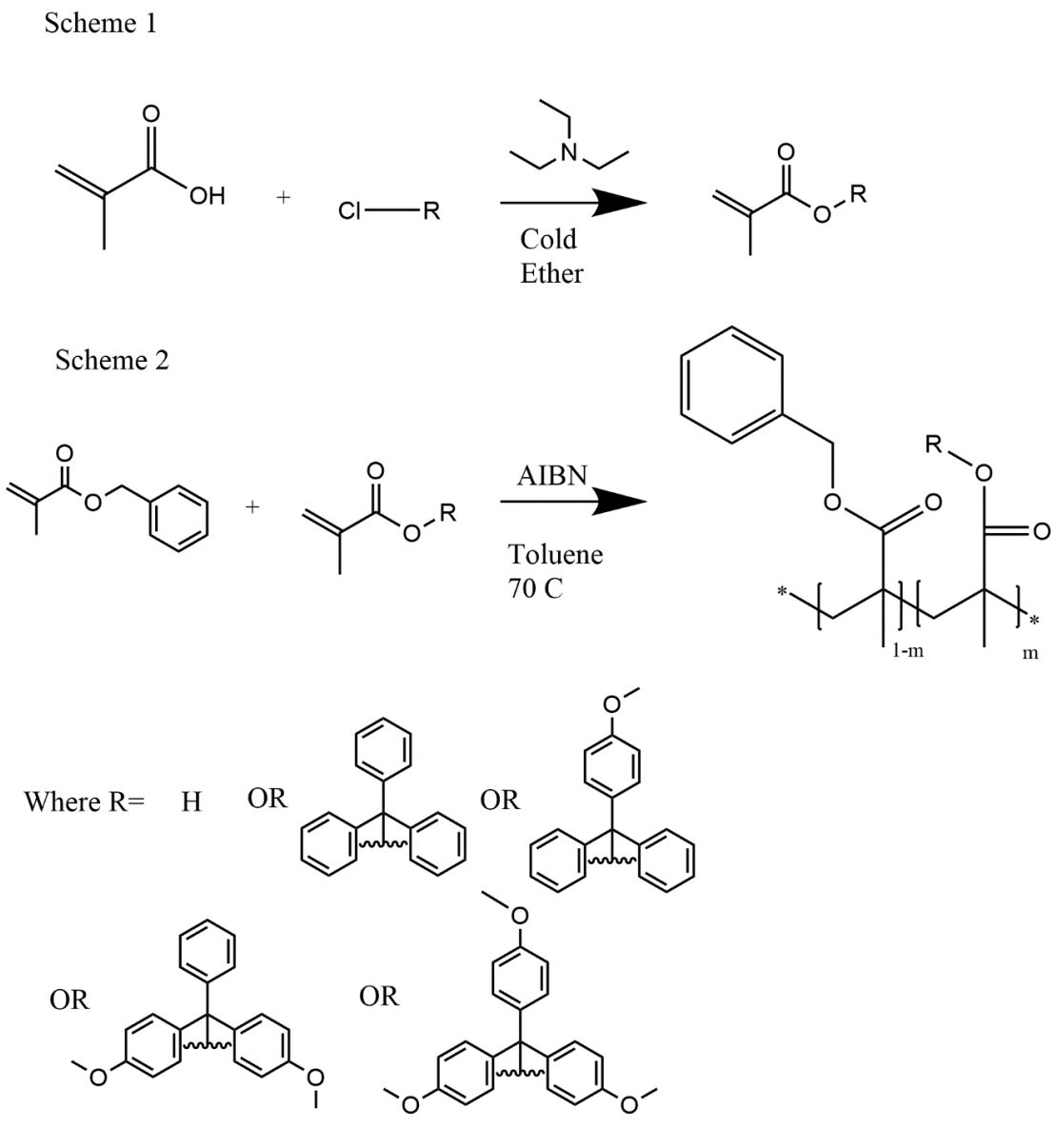

Scheme 1 Polymer design using trityl substituents

Antibody Deposition:

Benzyl methacrylate-co-methacrylic acid polymer (polyBMMA) was activated and attached to MRSA or GFAP antibodies through standard carbodiimide chemistry. The polymer was dissolved in DCM/DMF (1:4) at a concentration of 10 mg/ml. 30 mg/ml 1-ethyl-3-(3-dimethylaminopropyl)carbodiimide hydrochloride (EDC) was added thereto and vortex-

mixed for one hour. 15 mg/ml N-hydroxysuccinimide (NHS) was added thereto and allowed to mix an additional two hours. The EDC/NHS-activated polymer solution was filtered through a 0.45um syringe filter and mixed with polyDTMB (80mg/ml in DCM) at a 1:1 ratio to produce a polymer blend. This was deposited as described previously and subsequently washed with DI water to remove any excess EDC/NHS. MRSA antibody at a concentration of 1 mg/ml was incubated on the film for twelve hours in a humid container to avoid evaporation. Samples were washed three times with DI water. Bovine serum albumin (BSA, 1 mg/ml) was deposited and allowed to react for 1 hour to pacify any remaining activation sites. The substrates were washed three additional times with DI water and promptly measured.

FITC-tagged anti-GFAP (glial fibrillary acidic protein) antibody was also deposited as described above on a clean plain glass substrate covered in activated polymer blend and assayed with a fluorescent microscope to ensure selective antibody attachment. This was compared to a non-EDC/NHS treated polymer blend of the same composition exposed to the fluorescent antibody. This type of fluorescent tagging is commonly used in biological studies and control experiments, since it provides visual evidence of molecule location, but the tag is unlikely to be causing much abnormal interference with the binding we hope to examine.

pH exposure:

PBS buffer was adjusted to various pH using dilute HCl or NaOH as applicable. Buffer was dropped onto prepared films and incubated for one hour in a humid environment to avoid evaporation, then dried under nitrogen flow.

EIS Measurements:

The fabricated sample served as a working electrode and was placed into the cell under an O-ring in the testing cell. Alligator clips were attached to a cleaned gold portion of the glass slide, the top portion of the coil platinum counter electrode, and the Ag/AgCl reference electrode. Measurements were taken at 100 mV and a frequency of 1 Hz to 500 KHz.

Results

Polymer Synthesis

Polymerization stopping time was determined by intermittently taking a few drops from the reaction flask via syringe and observing whether a precipitate formed when dropped into one mL of cold hexane. Once precipitation occurred, the reaction flask was cooled to stop further polymerization and purified to remove unreacted monomer through subsequent precipitation in cold hexane followed by washing in warmed toluene. Percent of active group attachment was determined by NMR and Mn was determined by GPC as shown in Table 3. Both indicate the successful inclusion of the trityl-based protecting groups into the polymer chain. (4,4,4)-trimethoxytrityl (TMT) was briefly studied in this work, but as others have found, its carbocation appeared to form and become substituted so readily that it was unstable in any of our attempted syntheses. Resulting polymers were generally not soluble in most generally used solvents, as has been observed by previous groups. Solvents found to be successful for casting each polymer are listed in Table 3.

Table 3 Characterization of all polymers formed, based on NMR and GPC measurements. % Trityl Monomer successfully polymerized refers to the final polymer percentage, as calculated from NMR, though the original molar concentrations between monomers were 1:1.

Table 3 Polymer blends and resulting solubilities characterized.

Active Group	Monomer/co-Polymer Abbreviation	AIBN added (mol equiv.)	Time (days)	% Trityl Monomer Successfully Polymerized	Mn	Suitable Solvent
Methacrylic acid	MA/pBMMA	.02	1	25	10000	Various
Trityl methacrylate	TrM/pBMTrM	.04	4	25	12500	Anisole
Monomethoxytrityl methacrylate	MTrM/pBMMTrM	.08	7	40	7700	DMF
Dimethoxytrityl methacrylate	DTrM/pBMDTrM	.08	7	10	23000	DMF
Trismethoxytrityl methacrylate	TMTrM/pBMTMTrM	.08	9	N/A	N/A	N/A

NMR data are listed below. This was used to calculate the trityl monomer incorporated in the polymer in Table 1.

a.) Trityl Methacrylate polymer

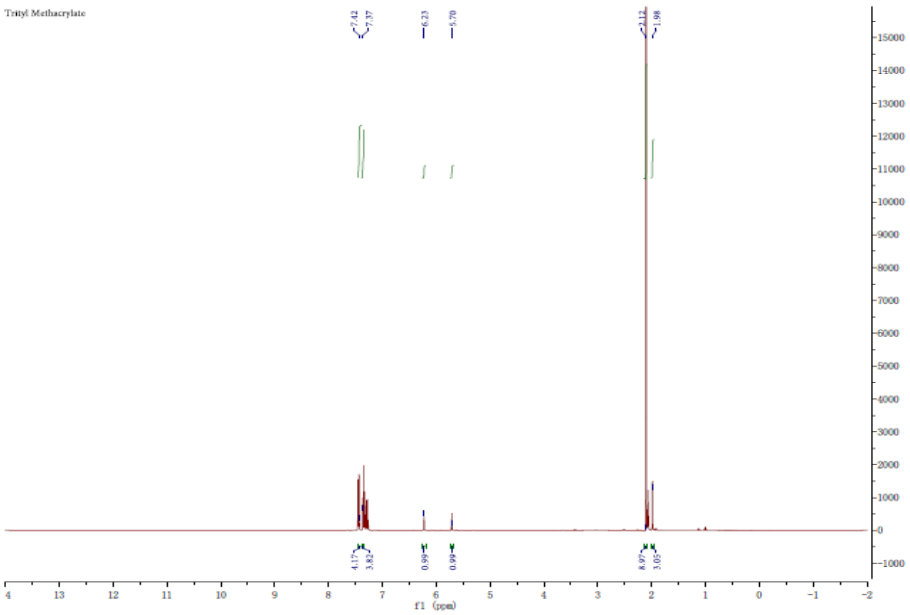

b.) Monomethoxytrityl Methacrylate- We see the methoxy group located near 3.8.

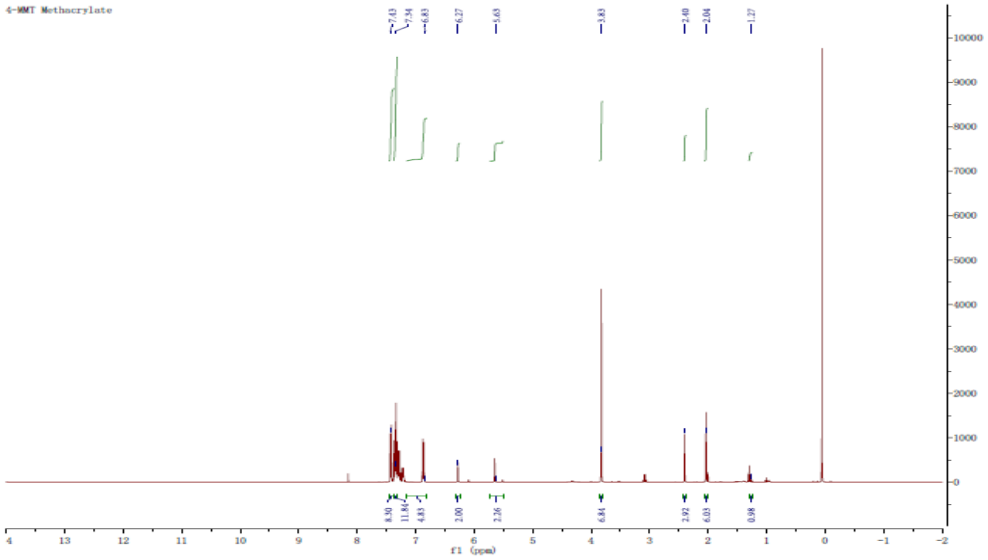

c.) Dimethoxytrityl Methacrylate- The methoxy group at 3.8 doubles due to there being twice as many groups

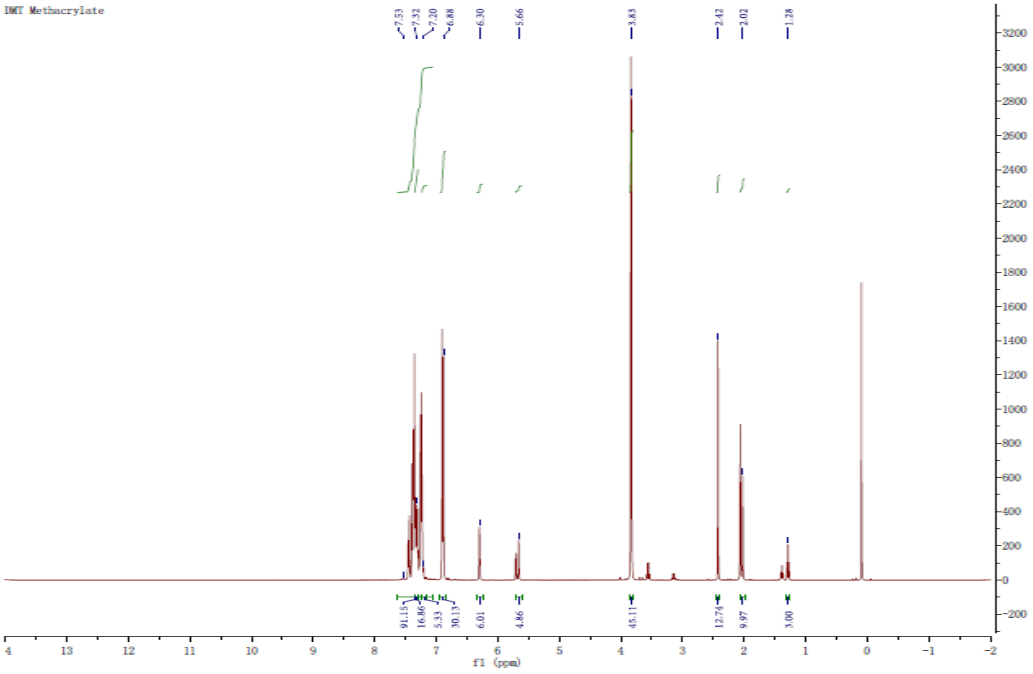

d.) PolyBMTrM- We compare the number of methyl groups to the quantity of trityl so that we can determine the percentage of each monomer.

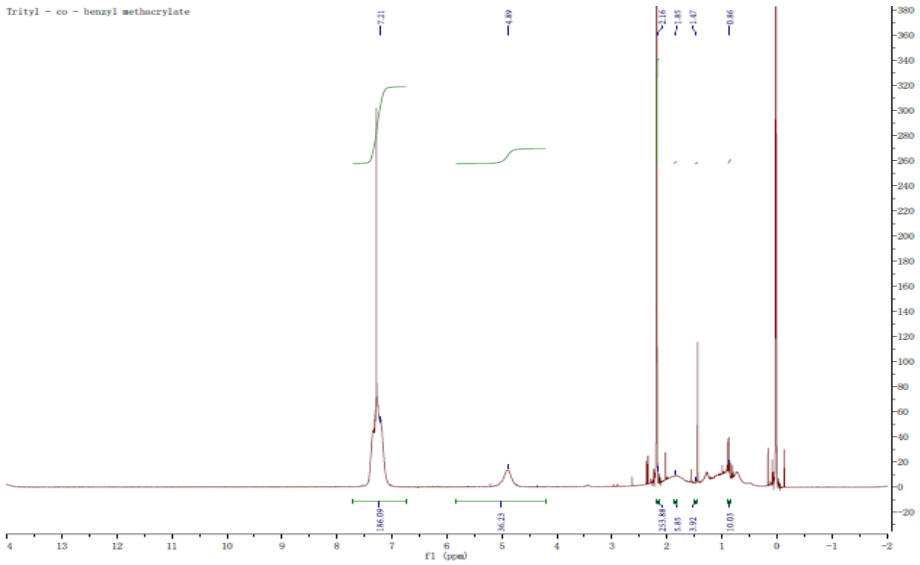

e.) PolyBMMTrM- We can see the small 3.8 peak indicating the methoxy group, its size is correlated to the amount of monomer successfully included in the polymer.

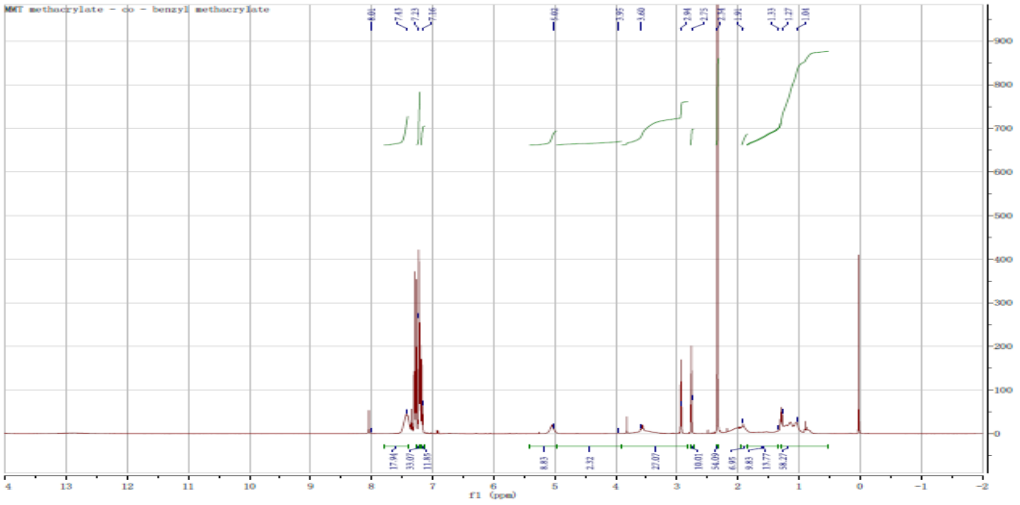

f.) PolyBMDTrM- We can compare the methoxy group peak to the benzyl methacrylate to find the percentage of monomer incorporated.

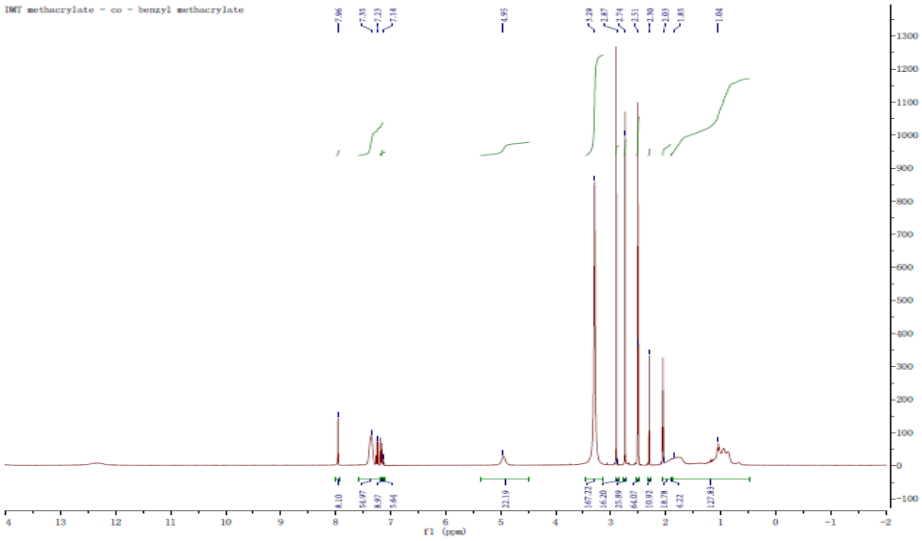

Figure 17 NMR of all monomer and polymers from the above table.

C. Electrical responses of polymers

Dielectric characterization

Polymers were cast into thin films on gold electrodes as described and dielectric constant of each polymer type was measured using a two-probe sandwich capacitor according to the formula:

$$C = \frac{\kappa \varepsilon_0 A}{d}$$

Equation 7 Calculation of parallel plate capacitance.

Where C is our measured capacitance, κ the dielectric constant, ϵ_0 the permittivity of vacuum, A the area covered by our indium-gallium coated top probe tip, and d the height of our thin film measured by laser microscopy and averaged for each sample type. D, the dissipation constant, was also measured. D is a measure of the amount of energy lost as heat

through the system when AC voltage is applied. It is higher in imperfect films containing holes and conductive pathways, and dielectrics considered useful in industry typically have a $D < 0.05$ or lower. Results for each measured benzyl methacrylate copolymer type are shown in Table 4.

Table 4 Average values for each polymer of dielectric constant and dissipation factor

	PolyBMTrM	PolyBMMTrM	PolyBMDTrM
κ:	4.00	4.04	4.31
D:	0.03	0.13	0.05

PMMA has a dielectric constant of 3-5, making these results reasonable for methacrylic polymer thin films. The somewhat higher dielectric constants for the larger side chains are understandable since the methoxy groups are adding bulky side groups to the system and a small amount of polarity, both of which would contribute to the increase in κ, assuming the side groups maintain some degree of rotational freedom.

Film dissolution under acidic pH conditions

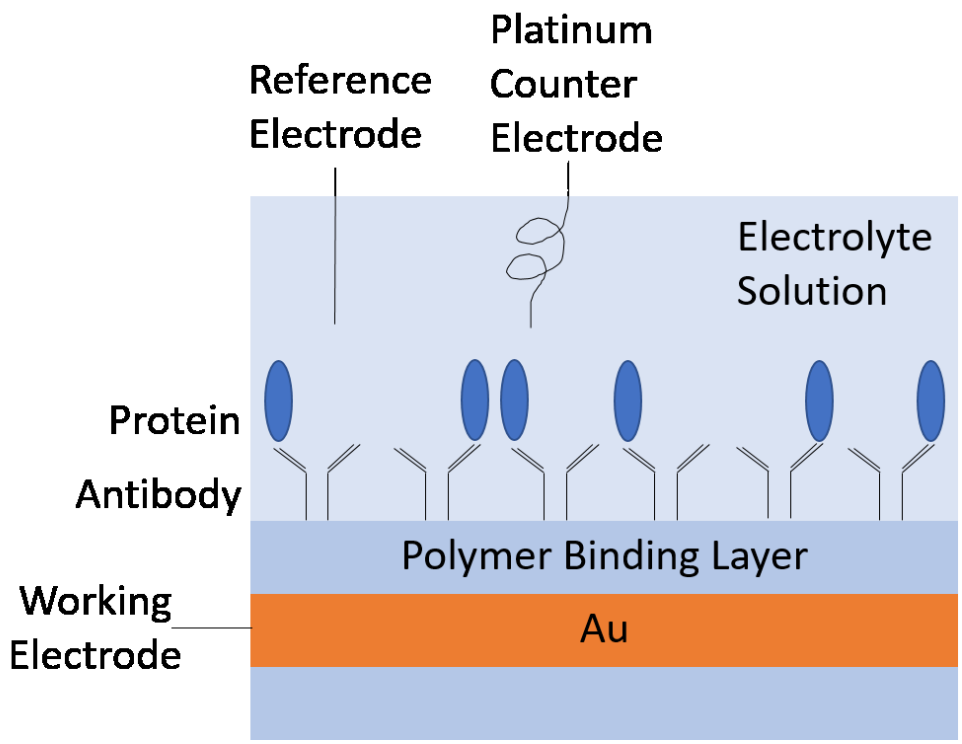

Figure 18 Schematic of standard EIS system using reference, working, and counter electrodes in a PBS electrolyte solution.

A typical three-probe EIS system is composed of working, counter, and reference electrodes. The working electrode supports the dielectric polymer on which the binding sites for our target of interest are located, and the counter electrode is a coiled, inert platinum rod, set to the voltage of the reference electrode, with sufficient surface area so as not to be the limit of charge transfer in the system. The counter and reference electrodes are placed in a solution that covers the totality of the working electrode, and a small AC voltage over a range of frequencies is applied between the working and reference/counter electrodes. Any alteration in working electrode resistance or capacitance will be read on the Nyquist and Bode output graphs as parts of the real and imaginary impedance. Each

measurement takes less than two minutes to run through all frequencies, making each experiment (including a run to check for stability) less than one hour in duration.

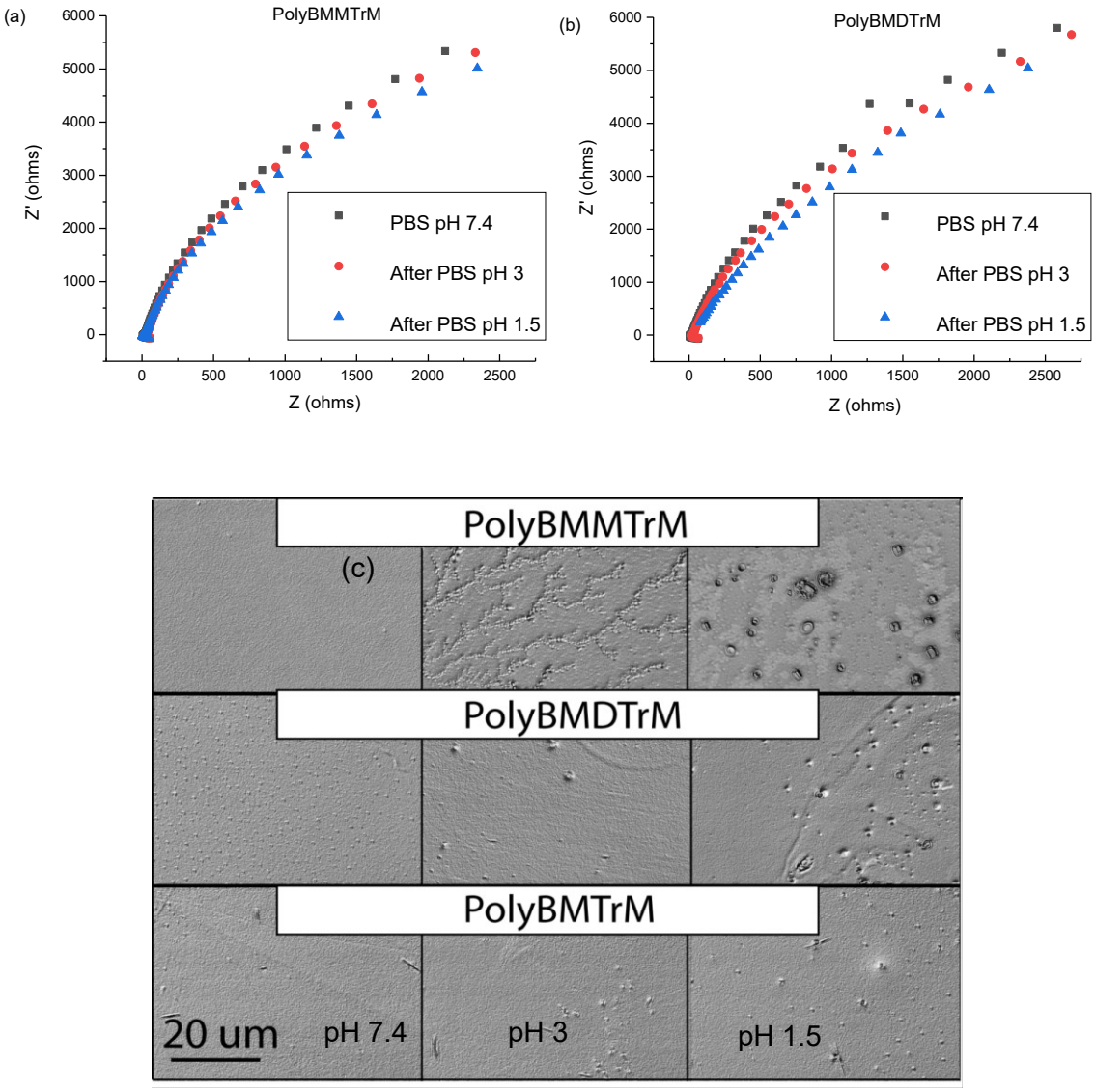

Figure 19 (a) and (b) show the response of each type of polymer film to various acidity levels on standard Nyquist plots. (c) shows DIC images of each type of polymer after it was allowed to react with PBS solutions of different acidities.

Films of each polymer were cast onto cleaned glass substrates and incubated with acidic solutions. Samples were measured qualitatively using differential interference contrast (DIC) microscopy in order to view any large-scale morphological changes in film quality following acid exposure (Figure 20c).

Under optimal spin casting conditions as described in Materials and Methods, the films appear clean and flat under 100X zoom. After incubation with standard PBS (pH 7.4), the films show no visible degradation (left column) and the polymer films remain similar in appearance. Under mildly acidic pH conditions (PBS at pH 3 incubated for one hour, middle column), film degradation becomes somewhat apparent. The monomethoxytrityl-based polymer developed tendril structures that are likely precipitation of the monomethoxytrityl group having cleaved from the polymer chain at this mildly acidic pH. The dimethoxytrityl-based polymer begins to show some larger hills and valleys, and the trityl-based polymer has similar pin-hole features.

Following an hour incubation with more acidic PBS (pH 1.5, right column), larger and more extensive features were noticed in all three polymer films. The monomethoxytrityl and dimethoxy-based polymers both developed much larger holes throughout the film. The trityl-based polymer had more pinholes, but they were not of comparable size compared to what was found in the methoxylated materials. As the monomethoxytrityl group was able to polymerize at a much higher ratio in the polymer, it is presumed that the impact of so many bulky, fragile protecting groups has a very significant impact on the stability of the polymer

in acidic environments. While the dimethoxytrityl group was not as easily incorporated into polymer under similar conditions, the second methoxy group makes this a more fragile protecting group that should deprotect significantly faster than other trityl-based groups, according to the literature. The loss of such bulky side chains would be expected to cause rearrangement of the otherwise stable polymer and result in such apparent film defects. The cleaved dimethoxytrityl group may exist as a more soluble species at this lower pH compared to what was observed at pH 3.

Films were additionally measured by EIS to see the combined resistive and capacitive effect of these morphological changes. To ensure measurement strictly of thin film change and ignore any effects caused by measuring in acidic solution, all measurements were taken in identical PBS (pH 7.4) buffer following incubation with the acidic PBS being measured. Due to the lack of significant morphological change seen with PolyBMTrM, as well as the literature indicating that this protecting group is significantly more stable than the others at anticipated pH's of interest, it was deemed a poor candidate for use in a biosensor system where the pH will rarely deviate drastically.

Both mono- and dimethoxytrityl based polymers have a similar response to acidic pH as seen on the examples of typical Nyquist plots, which corresponds to a small but regular shift in the phase component of the complex impedance, as indicated by the Nyquist plots having a decreased slope near our frequency of interest, 1 kHz for protein interaction studies described in the next Chapter.

For reference, the simple benzyl methacrylate polymer and methacrylic acid –co – benzyl methacrylate polymer, which were fabricated using identical methods as above, were studied and results are shown below.

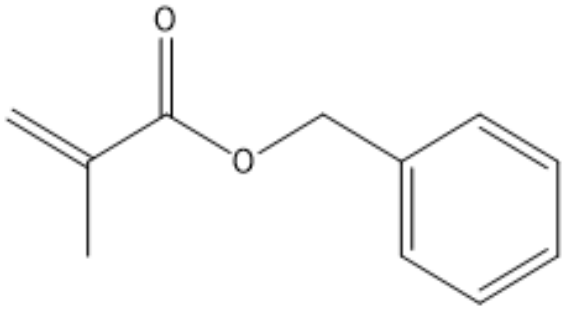

benzyl methacrylate

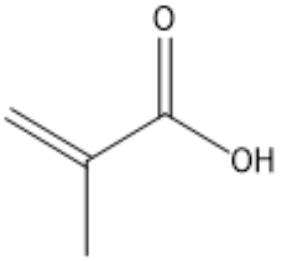

methacrylic acid

Table 5 Calculated dielectric constant and dissipation factor from blended non-trityl containing polymers.

Sample	Capacitance (Farads)	Dielectric Constant	D (tangent loss)
Poly benzyl (20%) methacrylic acid	6.53E-12	4.43	0.014
Poly benzyl methacrylate (PBMA)	5.44E-12	3.69	0.014

IV. Design of Biomolecule Sensors

In Utopia, there would exist a Universal biomolecular sensor that is the least expensive, fastest, and most accurate option available to detect any species of interest. In reality, however, compromises must be made based on what a sensor is intended to accomplish. In some cases, such as scholarly research, speed or price may be far less of a concern than obtaining the most in-depth data. In other instances, there be severe cost or time restrictions on a device which limit many of the more accurate designs. In collaboration with experts from the fields of medicine and public health, we as engineers are able to determine a design approach that will best serve the intended purpose of the desired device, as you will see in this chapter.

A. Requirements of Sensors to Detect Antimicrobial Resistance

For a broader discussion of this issue beyond its applicability to this dissertation, see Silbergeld, Ellen; Aidara-Kane Awa; **Dailey, Jennifer**. 2017. "Agriculture and Food Production as Drivers of the Global Emergence of Antimicrobial Resistance." AMR Control.

See **Appendix A** for further background and literature review regarding the science behind the spread of antimicrobial resistance, which supports the need for a point-of-care detection mechanism.

There is currently an international discussion regarding the possibility that standard antibiotics will lose their ability to treat infections due to bacteria developing antimicrobial resistance (AMR) to all standard pathogens. Briefly, resistance spreads when an antimicrobial kills most of a bacterial population but spares those microbes with some

mutation that prevents susceptibility. These survivors are then able to multiply in the biotic vacuum left by the treatment, and the new population will all have the same resistance mutation. Likely the reader has heard the argument against antibacterial soaps in hospitals, with the assumption that this type of constant hand washing is contributing to the problem of the AMR. Indeed, most of the available data regarding AMR is taken from patients or environmental swabs of medical centers. Those same medical centers have the interest, personnel, and equipment necessary to analyze this data. However, most antibiotics in the United States are used in agriculture. This measurement bias makes it difficult to know the real magnitude of AMR in any location.

The antibiotics used to treat food animals frequently have different brand names, but they are the same molecules using the same mechanisms as seen in human medicine. Thus, if treatment of a herd or flock results methicillin-resistance Staph aureus (MRSA) colonization, these same bacteria can be spread to humans, and vice versa. While humans and hospitals may likely have these types of dangerous infections tracked and contained, the same cannot be said for farms and food production facilities. There is no legal requirement for food suppliers to test every shipment for bacterial contamination, much less for AMR pathogens specifically. This is not unreasonable, as the cost and result waiting period necessary for sending swabs for bacterial culture would be impossible for nearly any company. These conditions, along with poor food handling and preparation practices, may result in consumers developing food-borne infections.

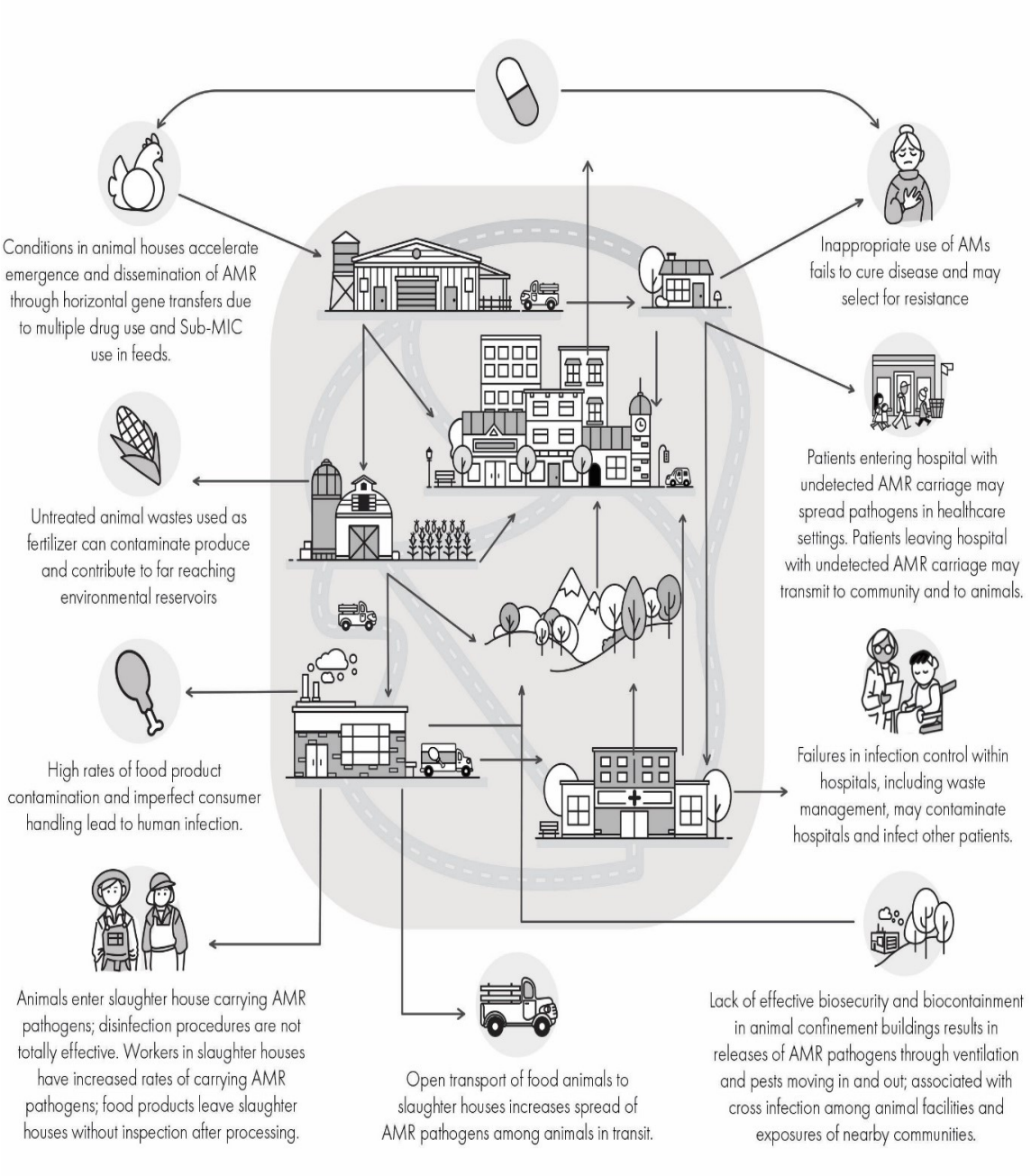

Figure 20 Simplified schematic demonstrating entanglement between medical and agricultural AMR sources.[1]

[1] Diagram created in collaboration with designer Lindsay Evans

As we have determined, there are a significant number of challenges facing the issue of AMR spread in agriculture. There is no question that accurate point-of-care testing would be a boon for both scholarly interests as well as to prevent contamination and consumer outbreaks. Since no company can be forced to use such a product, maintaining a low cost is vital. No successful device can require huge capital investment of lab equipment or trained technical personnel. Additionally, in order to prevent outbreaks from contaminated food, a device operating along the conveyor belt must have an exceptionally fast detection time. This limits the type of sensors we can consider but makes electronic sensors a prime candidate. Specifically, label-free electronic biosensors that require no additional complicated procedures to amplify the signal would be an ideal solution that combines reasonable accuracy[2] with the feasibility of having minimally trained workers perform the necessary measurement and take immediate action before food heads to market.

B. Confirmation of Biocompatibility

1. Regarding Antibodies:

A significant portion of this biological work relies on the use of commercially available antibodies. As there are a wide variety of antibodies available from various sources, it is necessary to understand the underlying terminologies before any purchasing or experimental design decisions can be made.

A typical natural antibody is composed of the heavy chain (constant region) and light chain (variable region). The heavy chain will be constant across all similarly functioning antibodies (immunoglobulin IgG, IgM, etc.) within the species where they are produced. This means

[2] Admittedly, never as sensitive as the most accurate available ELISA.

that were we to examine our blood; we would likely find memory antibodies to mumps and rubella with identical constant regions thanks to previous specific antigen or vaccine exposure. These antibodies would differ in their light chains, with each antibody having a clear attachment site to a particular antigen of interest. Multiple antibodies are produced against any given pathogen and may target many different sites simultaneously[125].

Specific useful attachment compounds, such as the ubiquitous Protein G, have binding affinity to the heavy chains of many different species' antibodies[126]. For example, Protein G will bind strongly to most human IgG, as well as mouse and rabbit. It will not, however, attach to the heavy chain of many rat antibodies. It is therefore vital, when using an attachment mechanism such as Protein G, to be fully aware of the animal source of the purchased antibody as well as its antigen affinity, and to choose hosts appropriately according to experimental design.

Briefly, in a simple inoculation to produce commercial antibodies, a rabbit or mouse may be inoculated with a pathogenic protein of interest. The subject's body, seeing this intruder, will begin producing antibodies to fight it. There will be many different antibodies produced that may bind at the same time to different epitopes of the pathogen. If we extract all of these antibodies at once, we have a polyclonal mixture. This means that, though all of the antibodies will act against the pathogen, they will differ slightly in their attachment locations. If this is purified to a monoclonal antibody (the more expensive version), we are now guaranteed as to the location of the binding event. This is frequently used for forming sandwich structures, where we may have two known monoclonal antibodies that attach to independent epitopes of an antigen of interest. Polyclonal antibodies may be capable of this on some occasions, but the exact binding location is not well known.

All natural antibodies will have a useful amine group at their base, and in most cases this amine can be successfully used to form a chemical linker to carboxylic acid groups without damaging the antibody. Many commercially available antibodies also have useful tags including fluorescent markers, which are an ideal way to determine if binding events have taken place optically. In more advanced cases, microbiology labs can synthetically produce antibodies from bacterial cells and may attach other tags to the antibody depending on the ultimate use (see Lerner et al. [16] for an example orienting the antibody using a histidine tag). Additionally, there is significant interest in developing smaller antibodies (scFv: "single chain variable fragment") that have less bulk and focus primarily on having an active binding variable region. A smaller antibody frequently increases sensing ability by pulling the binding event closer to the detection surface, maximizing the electrical signal[16].

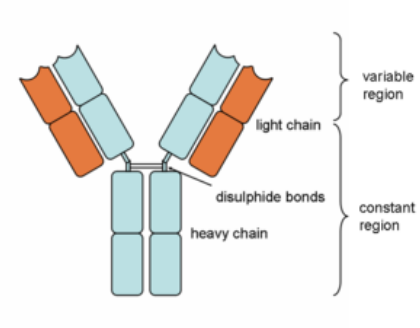

Figure 21 Schematic of an antibody with constant and variable regions

2. Fluorescence Microscopy

The following is a modified excerpt of the work published in Song, Jian; **Dailey, Jennifer;** Li,Hui; Jang, Hyun-June ; Wang, JTH ; Everett, AD ; Katz, Howard. 2017. "Extended Solution Gate OFET-Based Biosensor for Label-Free Glial Fibrillary Acid Protein Detection

with Polyethylene Glycol-Containing Bioreceptor Layer." Advanced Functional Materials. 27(20).

My contribution to the project lay in designing control systems to determining device biocompatibility and confirming antibody viability via fluorescent measurements, which are considered standard in the biological sciences and more trustworthy than electrical measurements for confirmation purposes. For full project methodology and results, see the citation above.

Abstract:

A novel organic field effect transistor (OFET)-based biosensor is described for label-free glial fibrillary acidic protein detection. This study reports the first use of an extended solution gate structure where the sensing area and the organic semiconductor are separated, and a reference electrode is not needed. Different molecular weight polyethylene glycols (PEGs) are mixed into the bioreceptor layer to help extend the Debye screening length. The drain current change is significantly increased with the help of higher molecular weight PEGs, as they are known to reduce the dielectric constant. This study also investigates the sensing performance under different gate voltage (V_g). The sensitivity increases after the V_g is decreased from −5 to −2 V because the lower V_g is much closer to the OFET threshold voltage and the influence of attached negatively charged proteins becomes more apparent. Finally, the selectivity experiments toward different interferents are performed. The stability and selectivity are promising for clinical applications.

Materials and Devices Fabrication:

All the chemical materials were purchased from Sigma-Aldrich without further purification. GFAP from human brain and polyclonal anti-GFAP (ab4674) were purchased from EMD Millipore. The buffer solution was purchased as 10X concentrated PBS for bioreagent, "suitable for cell culture and molecular biology." Highly n-doped 〈100〉 silicon wafers (as gate electrodes) with 70 nm SiO_2 (as dielectric layers) were divided into 1 × 1 in. substrates. After cleaning by piranha solution (DANGER corrosive!), they were sonicated in water, acetone, and isopropanol, and then dried by forced N_2. Substrates were further cleaned by oxygen plasma (100 W, 3 min) and then annealed in a 100 °C vacuum oven with exposure to hexamethyldisilazane (HMDS) for 2 h. Next, pentacene was thermally evaporated on half of each HMDS-treated substrate surface with a thickness of 50 nm at a rate of 0.4 Å s^{-1}. The chamber pressure during deposition was lower than 4×10^{-6} Torr. Then, gold electrodes (50 nm) were thermally evaporated through an interdigitation mask and deposited on the pentacene film with a chamber pressure about 5×10^{-6} Torr. The rate was 0.4 Å s^{-1} and the channel width/length was 28 (W = 7 mm, L = 0.25 mm).

Antibody Immobilization: On the other half of each substrate, we manually etched 8 × 8 mm SiO_2 to expose silicon for the extended solution gate sensing area. The carboxylic acid groups of PS-MA were activated by EDC and NHS. 10 mg PS-MA and 30 mg EDC were first dissolved in 0.5 mL anhydrous dichloromethane and 0.5 mL anhydrous N,N'-dimethylformamide mixed solvent. After stirring at room temperature for 1 h, 15 mg NHS was then added into the mixture with stirring for another 2 h. The resulting mixture was purified through a 0.45 μm filter and then mixed with 5 mg mL^{-1} of one of a series of different molecular weight PEGs (200, 400, 1000, 4000, 6000, and 8000), with continued

stirring at room temperature for half hour. The final mixture was spin-coated on the exposed silicon at a speed of 3000 rpm for 90 s. Then the device surface was carefully washed with DI water to remove excess EDC and NHS and dried at room temperature for antibody modification. Anti-GFAP (1 mg mL^{-1} in 0.05X PBS) was covalently attached to the activated PS-MA surface for 6 h and then gently washed with PBS to remove any noncovalently bound antibodies. To avoid water evaporation and antibody contamination, the samples were maintained in a humid, sealed vessel during the reactions. As control experiments: the devices without anti-GFAP were prepared by putting one drop of 0.05X PBS on the EDC/NHS activated PS-MA film for 6 h; activated PS-MA without PEG was prepared to make devices with the same steps to compare the influence of PEG.

Apparatus:

Electronic analysis of OFETs was conducted on an Agilent 4155C semiconductor parameter analyzer in air. ^{1}H-NMR spectra were recorded on Bruker Avance (300 MHz/400 MHz) spectrometers. The oxygen plasma treatments were done on a Technics West Inc. (PEII-A) plasma system. Fluorescence images were taken by the fluorescence microscope Olympus IX71.

On the extended solution gate, anti-GFAP was immobilized on the (1-ethyl-3-(3-dimethylaminopropyl)carbodiimide) (EDC)/N-hydroxysuccinimide sodium (NHS) treated polystyrene-co-methacrylic acid (PS-MA) layer. The chemical structure of PS-MA is shown in Scheme 1a. EDC is soluble in water and most organic solvents and is widely used in carboxylic group activation for dehydration–condensation reaction.[38] Since the EDC-derivatized compound is unstable, NHS is frequently used with EDC to increase coupling

efficiency. The NHS-activated carboxyl groups of the polymer then react with a given antibody to immobilize it on the PS-MA layer. The ^{1}H-NMR result shows that the styrene:methacrylic acid molar ratio is about 3:1. Before EDC/NHS treatment, the carboxylic acid ^{1}H-NMR peak appears at 11.88 ppm. After EDC/NHS treatment, this peak completely disappears, indicating that 100% yield of carboxyl group activation was achieved. In addition, new proton peaks for NHS at 2.28 ppm and for EDC at 4–4.2 ppm were observed, indicating that the carboxylic acid groups were completely activated by EDC and NHS, desirable for high antibody surface coverage. It can be observed that the PS-MA film provides a smooth surface. After treatment by EDC and NHS, the surface became rough because the concentrations of EDC and NHS are 3 times and 1.5 times higher than PS-MA in solution, respectively. The excess chemicals likely caused some aggregation of polymer and reactant, as visible from some small particulates forming in solution even after filtration through a 0.4 μm filter. These particulates were not observed when EDC and NHS were not added to the solution. After washing the surface with deionized (DI) water, the film surface regained some smoothness, as the DI water removed these unbound particles. Roughness measurements were taken of both substrates with and without 8000 MW PEG using an optical microscope and associated software. The images show no indication of obvious phase separation. Even though the roughness increased from 1.3 to 3.1 μm with the addition of PEG, the PEG-containing sample, if anything, showed more uniform morphology than the non-PEG sample and the feature shapes are similar in both samples. This indicates that there are not likely to be phase-separated regions of predominantly polymer and predominantly PEG on the size scale of micrometers or larger. Also, the UV–vis transmission spectra of the two samples, corrected for thickness, are nearly indentical, indicating similar light-scattering features in both samples.

Furthermore, we placed fluorescein isothiocyanate (FITC)-labeled anti-GFAP on the bioreceptor layer to confirm the binding property between PS-MA and antibody. First, we put 100 μg mL^{-1} FITC labeled anti-GFAP directly on the bare substrate and PS-MA layer before activation by EDC/NHS. After 6 h, the surfaces were washed by PBS 5 times to remove any unbound anti-GFAP. We can see that hardly any antibody was immobilized on the substrate, indicating low nonspecific binding. After FITC-labeled anti-GFAP was applied to the device with the same procedure, visible fluorescence was observed. Comparing these figures, we can see that the antibody was immobilized on the PS-MA surface, indicating that the EDC/NHS activation is effective. The (d) section of the figure shows the substrate with activated PS-MA with the addition of PEG (8000), which was added to the solution prior to spin coating.

Inspired by enzyme-linked immunosorbent assay (ELISA) experiments, we used a "sandwich structure" method to further confirm that the native binding functionality of anti-GFAP antibody to the GFAP protein was not compromised. Herein, we modified the normal anti-GFAP on the PS-MA layer with the same steps described in the Experimental Section, and then put 100 μg mL^{-1} GFAP on the device for 0.5 h to let all the anti-GFAP bind with GFAP as thoroughly as possible. After washing 5 times with 0.05X PBS, we put 100 μg mL^{-1} FITC labeled anti-GFAP on the device for 0.5 h and then again washed 5 times with 0.05X. As a control experiment, we used a readily available penicillin-binding protein 2a (PBP2a) instead of GFAP keeping other steps the same. It is difficult to find any green fluorescence from FITC, indicating that anti-GFAP and GFAP bind together specifically.

In an additional FITC experiment, biotin and FITC-marked streptavidin (known to form a very strong complex together) were used to show the quantity of binding that occurs on

samples with and without the addition of PEG. Biotin was covalently bound to the surface of our substrate and subsequently exposed to FITC-streptavidin (simulating an antibody–protein complex). The presence of PEG had no effect on the overall fluorescence intensity in the streptavidin-exposed samples, indicating that the PEG is not responsible for increasing binding of the protein to antibodies.

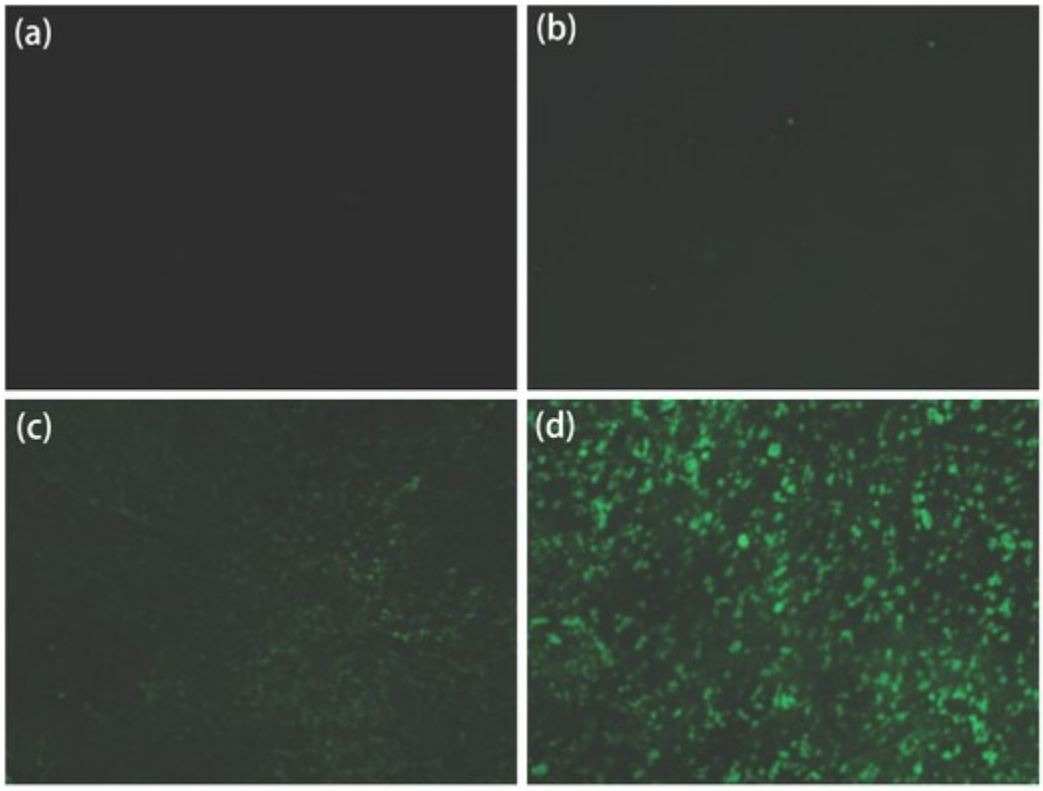

Figure 22 Fluorescence microscope images: a) bare substrate; b) PS-MA layer without activated by EDC/NHS; c) PS-MA layer after activated by EDC/NHS; d) activated PS-MA with PEG (8000) on exposure to 100 μg mL−1 FITC-labeled anti-GFAP.

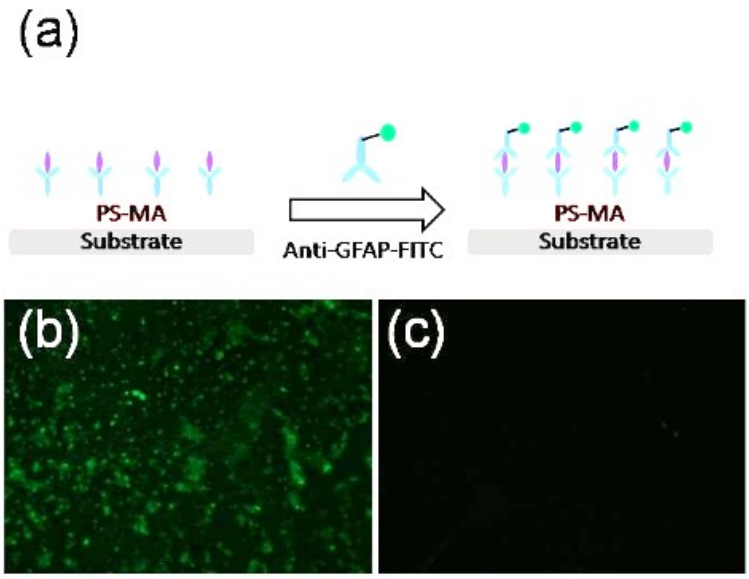

Figure 23 Brightness increased 45% to aid visual. (a) Description of sandwich structure. (b) FITC antibodies with GFAP protein binding. (c) FITC antibodies with PBP2a protein as control, indicating that the high antibody-antigen selectivity has not been compromised by our processing.

Examining antibody surface binding for PBP2a Detection

As an additional test to ensure that our novel trityl-based polymer films are both suitable for integration with biomolecules and will not be overly reactive to interfering species, we performed an antibody fluorescence experiment. Trityl-based co-polymers were blended with EDC-NHS activated polymers containing similar mole fractions of benzyl methacrylate groups to promote homogeneity. A separate film was cast containing the same polymer blend without the EDC-NHS amine crosslinker molecules. Films were washed and incubated with a commercially-available FITC-tagged antibody to GFAP (as GFAP and PBP2a are both proteins with similar charge and size)[127]. FITC-tagged monoclonal antibodies corresponding to the same PBP2a epitope (amino acids 19-348) were not readily

commercially available, but the anti-GFAP- antibody used in this experiment was also IgG1 from murine source, meaning the bulk of the antibody (including the heavy chain and amine group where our crosslinking chemistry of interest is taking place) was nearly identical except for the necessary fluorescent tag, making this product an appropriate substitute to examine antibody-surface interaction. Following several washing steps to remove any unbound antibody, we took fluorescent images of both samples.

In Figure 24 (a), we see a very high amount of fluorescent activity, indicating very good attachment of GFAP antibody in the polymer blend. In (b), we see absolutely no green color, which means that there was no non-specific binding of antibody to our surface without EDC-NHS crosslinking chemistry. This indicates that our antibodies are covalently binding to their substrate as expected, and we do not have unreacted side chains causing unwanted attachment reactions to other moieties.

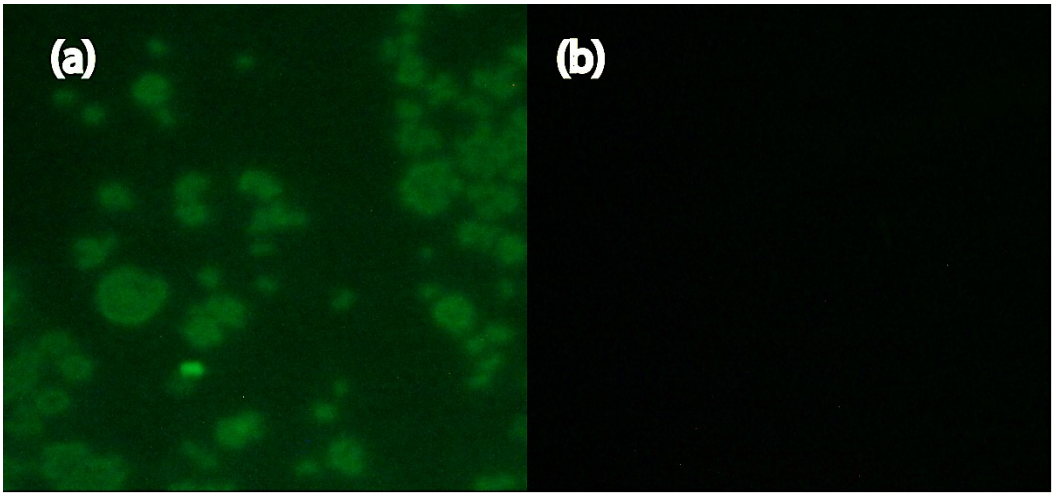

Figure 24 (a) Shows FITC-tagged antibody on EDC-NHS activated polymer blend as shown by fluorescence microscopy. (b) No FITC-tagged antibody is present on unactivated polymer blend, indicating little non-specific binding to the surface. Brightness was increased 25% in both images to better display contrast

C. Amplification schemes

1. Degrading attachment layer

Protein Response Studies

To determine whether antigen binding could result in a complex impedance change related to the acid-induced degradation observed above, we analyzed data taken by EIS with polymer exposure to neutral PBS buffer and added PBP2a antigen or control protein BSA. Data were analyzed for phase shift at 1 kHz, a common frequency for measuring interactions occurring near the electrolyte interface rather than focusing on bulk or electrolyte properties. After sweeping through the frequencies a minimum of three times to ensure stability in PBS, we injected protein solution ranging from 10 ng/ml to 1 ug/ml into the cell and measured the resulting change in complex impedance.

As demonstrated in the examples shown below, for both trityl-based and monomethoxytrityl-based polymers, we note either an increase in phase angle or a small increase in overall resistance of the system following the addition of our protein of interest. This is highly consistent with many impedimetric biosensors that rely on additional coatings on the electrode surface (in this case, the attached protein) to increase charge transfer resistance in the system.[95] PolyBMDTrM, on the other hand, showed consistent results in the opposite direction. In Figure (25d), we show data points indicating the resultant change in phase angle at 1 kHz caused by injection of varying concentrations of PBP2a, along with BSA (at a very concentrated 10 mg/ml). The negative phase shift seen following all PBP2a injections is consistent with an increase in capacitance of the overall film system. No significant change in resistance of the system was found at this frequency.

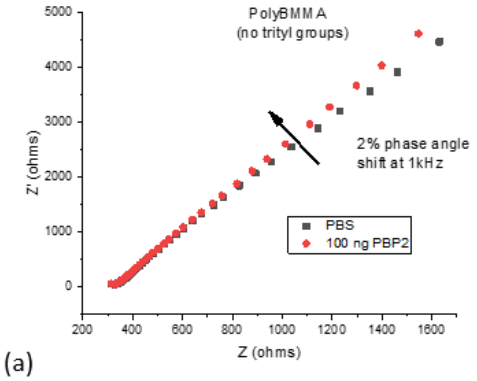
PolyBMMA
(no trityl groups)
2% phase angle
shift at 1kHz
PBS
100 ng PBP2
Z' (ohms)
Z (ohms)

(a)

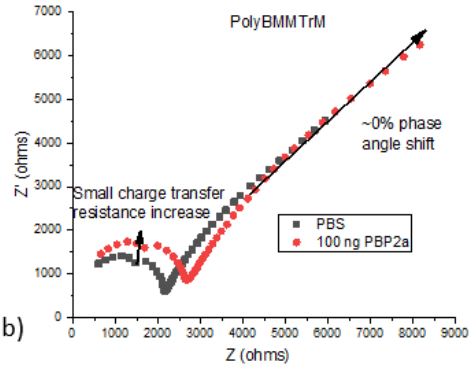
PolyBMMTrM
~0% phase
angle shift
Small charge transfer
resistance increase
PBS
100 ng PBP2a
Z' (ohms)
Z (ohms)

(b)

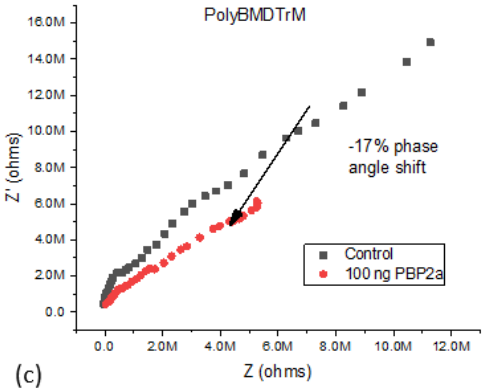
PolyBMDTrM
-17% phase
angle shift
Control
100 ng PBP2a
Z' (ohms)
Z (ohms)

(c)

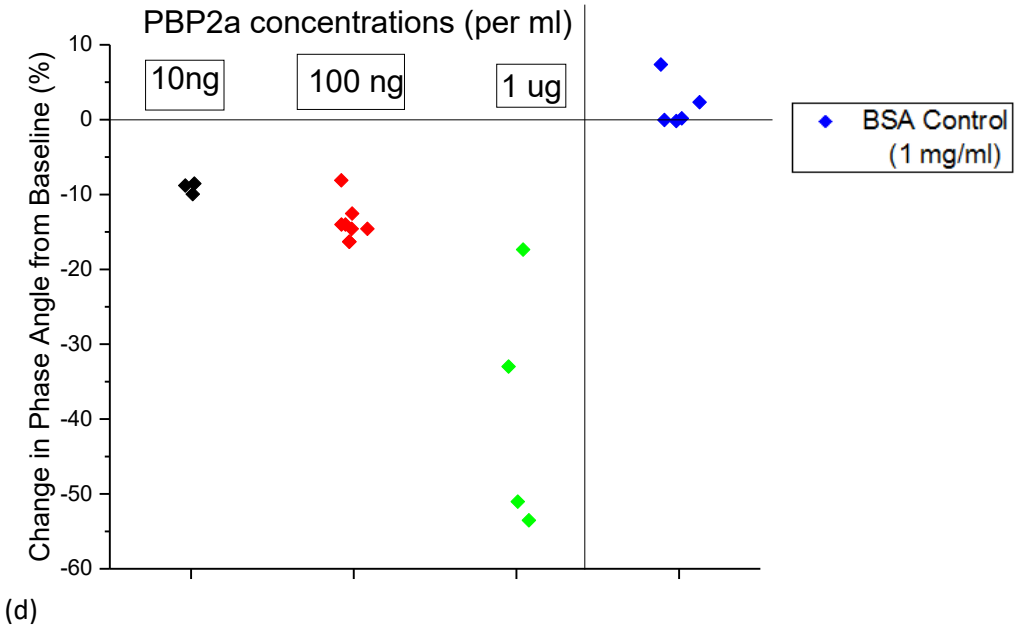

Figure 25 (a)-(c) Demonstrate typical responses of each type of polymer reacting to protein binding. A polymer with no trityl groups (a) shows a small increase in phase angle corresponding to proteins attaching to the surface, (b) with monomethoxytrityl groups has a small increase in resistance as well. (c) Dimethoxytrityl groups result in a decrease in phase angle in response to protein attachment, with (d) displaying all results of PolyBMDTrM and comparing it to bovine serum albumin (BSA) control. The large scatter in (c) is likely due to the cummulative effect of the degradation reactions causing a large difference in pore formation. This 'exponential' effect is difficult to control as the reactions increase due to higher protein concentrations.

Discussion

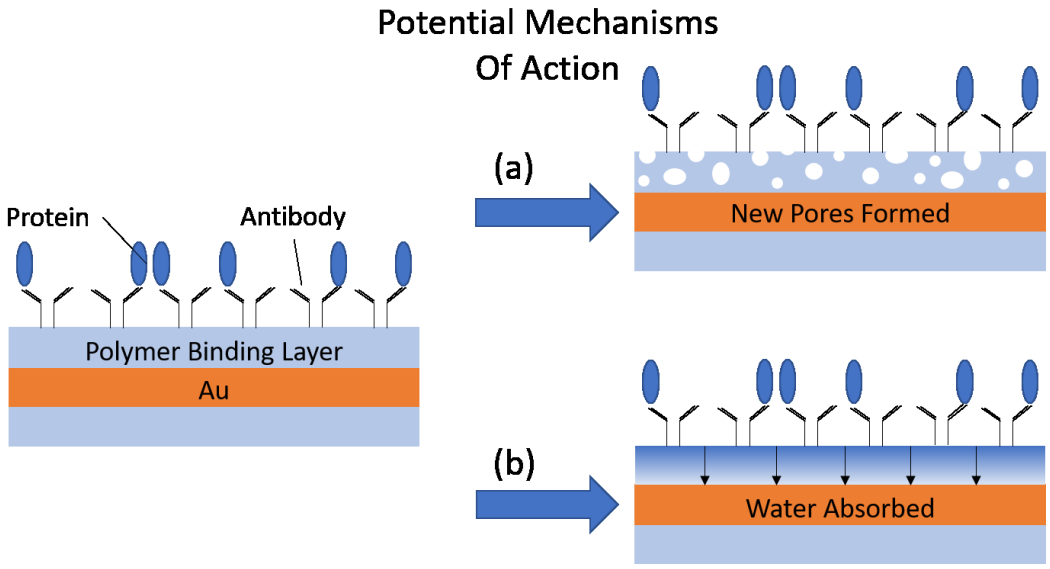

Figure 26 Schematic displaying two potential mechanisms to explain EIS measurements. (a) indicates the formation of large holes through the film as seen in DIC, and (b) indicates gradual water absorption through the film as it becomes increasingly water soluble.

Based on thin film characterizations showing impedimetric shifts upon short time period exposure to acidic pH as well as antigen, we propose two potential mechanisms of action by which this shift may be induced by the antigen, as shown in Figure 26. Shown in the upper picture, as we have purposefully created a film with degradable side chains and have seen large holes forming through DIC measurements when exposed to acidic buffer for longer time periods (1 hour versus several minutes), there is the possibility that pin-holes are forming through the layer in response to protein attachment. As the trityl side chains cleave, areas of the resulting film effectively become poly(methacrylic acid) (PMAA) which is readily soluble in acidic aqueous solutions, compared to its protected counterpart. In the lower picture, we show the possibility of changes in polymer structure allowing for sufficient

molecular movement so as to allow water absorption through the formerly hydrophobic layer, though without visible pore formation.

While DIC measurements do indicate that large pores forming at pH 1.5 in PBS buffer after one hour, we recognize that it is not possible for the small amount of acidic antigen (net charge is -8 at pH 7.5 according to Helassa[127]) to produce similarly acidic local conditions. Additionally, DIC measurements closer to neutral, at pH 3, do not show the same level of pore formation passing through the entire film, though there is some degradation. It is therefore unlikely that the small amounts (10 ng/ml in PBS) of antigen would be able to produce similarly drastic effects.

As our trityl-based side chains are extremely bulky compared to the rest of the film, it is plausible that a limited degree of acid-catalyzed cleavage and removal of the trityl groups will result in sufficient structural alteration so as to allow this film that is relatively stable in neutral pH to still be infiltrated by water through these openings, as shown in the bottom schematic. As the highly hydrated proteins bring additional polar water molecules to the site of the potential trityl cleavage, the reaction is additionally aided by the protonation of the carbonyl groups by COOH groups on the antigen. The resulting deprotected carboxylic acid groups on the polymer will additionally increase the acidity of the system, helping to promote the process further. The areas where cleavage occurred are water soluble and could allow for sufficient polymer flexibility to allow for further water infiltration. The resulting change in dielectric properties caused by the surrounding polar medium should be rapidly observable (within a few minutes) via electronic measurements.

Furthermore, despite the highly regular phase angle shift indicating an antigen sensing response, no similarly consistent decrease in the real portion of the complex impedance was

found in our data. Were there significant pore formation through the bulk of our film, this would resemble an array of conductors in parallel, with weak polymer points being significantly less resistive. In such a case we would expect the overall impedance to decrease significantly. However, as no such shift in resistance was seen in our data, and no visible changes were noted in film quality, we must conclude that there are no large pores acting as conductive pathways through our film. However, the shift in capacitance is consistent with an increase in dielectric constant of our film (measured at a typical 4-5). This is consistent with Brasher and Kingsbury's explanation of water absorption through a polymer coating, where the addition of water with a dielectric constant closer to 80 begins to increase film capacitance before any purely resistive effects are noted.[128] This is due to the speed with which water can enter a film and diffuse, much faster than other electroactive species. Bellucci further noted that, over short timescales such as we have when the polymer film is beginning to react with the antigen of interest (1-5 minutes), resistive changes can be highly variable and are not a reliable measure to determine the change in the polymer thin film.[129] This further supports our decision to examine the phase shift of our EIS data, rather than focusing on overall impedance, as well as supporting our hypothesized mechanism of action.

The fact that only the most labile polymer side chain produced an effective degradation response is consistent with the dimethoxytrityl cation being significantly more stable than monomethoxytrityl or trityl, allowing for faster cleavage. Additionally, the increased number of methoxy groups would attract polar water molecules more strongly, allowing for better conditions for trityl bond cleavage to take place.

As confirmation of these analyses, we performed scanning electron microscopy (SEM) on samples sputter-coated with 5 nm of platinum coating. Organic thin films are not ideal surfaces on which to perform SEM since they are insulating, so the additional metallic coating is necessary to produce sufficient electron scattering signal to obtain any information on the texture of the material. Due to the amount of platinum necessary for coating, objects are assumed to read substantially larger than their true organic size[3].

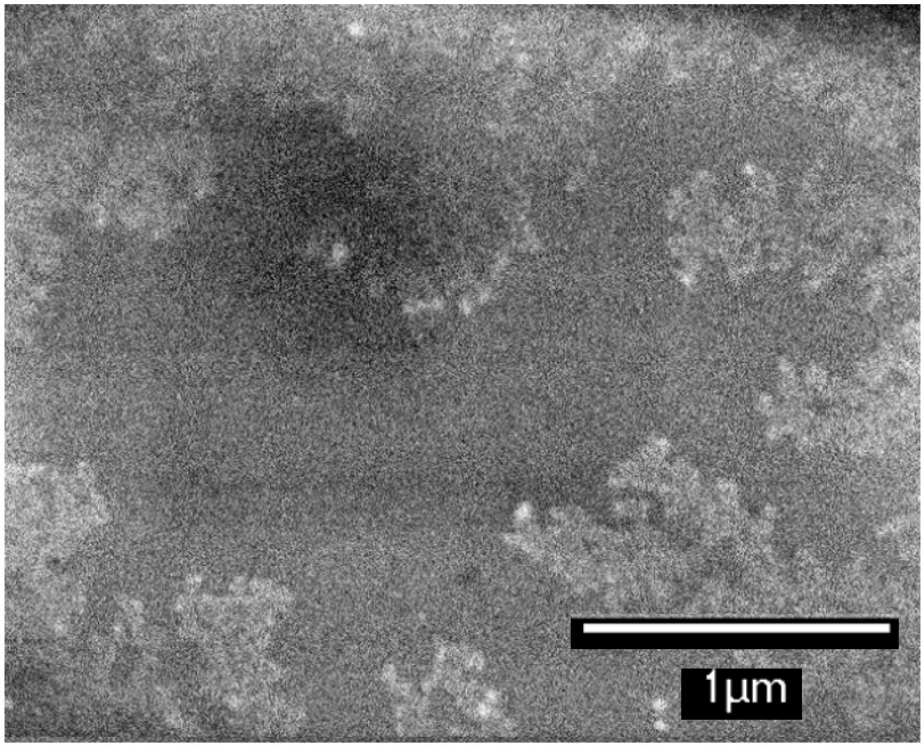

Figure 27 SEM image of polymer blend film (DMT based and activated methacrylic acid) with attached antibodies. Despite good quality film coating to the naked eye, there is normal polymer blend segregation at this extreme magnifications.

[3] We are grateful to Anthony Lewis for his expertise and aid in taking the SEM images.

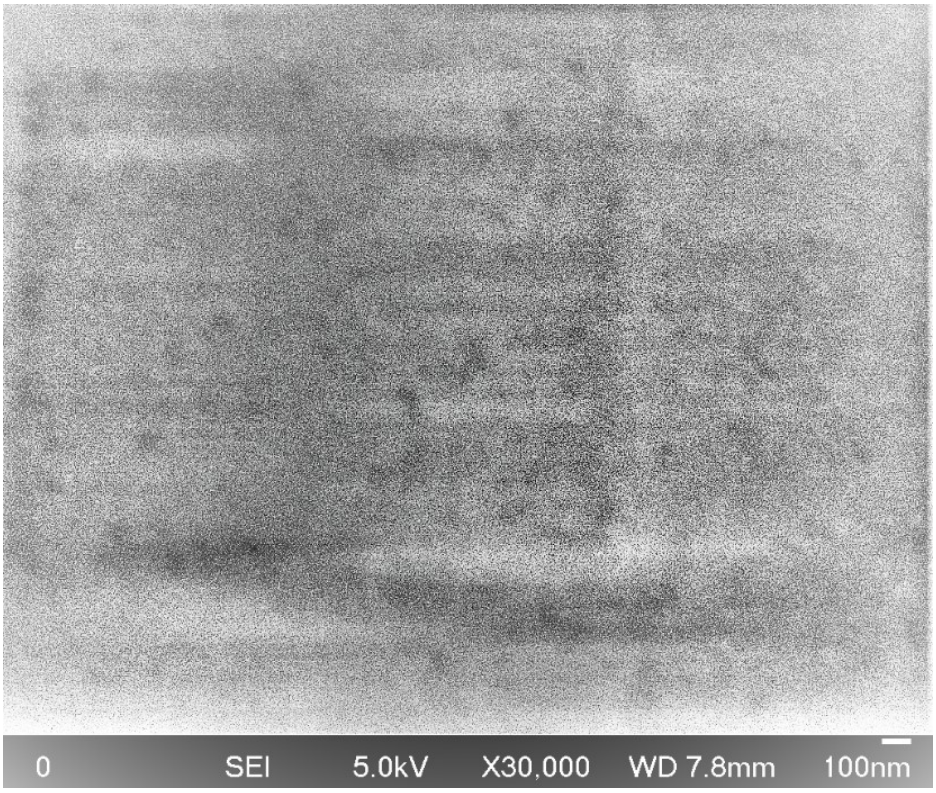

Figure 28 SEM image (same material as the previous figure) post exposure to 10 ug/ml PBP2a protein for two hours. Spotted appearance indicative of nanopore formation, which allows water influx.

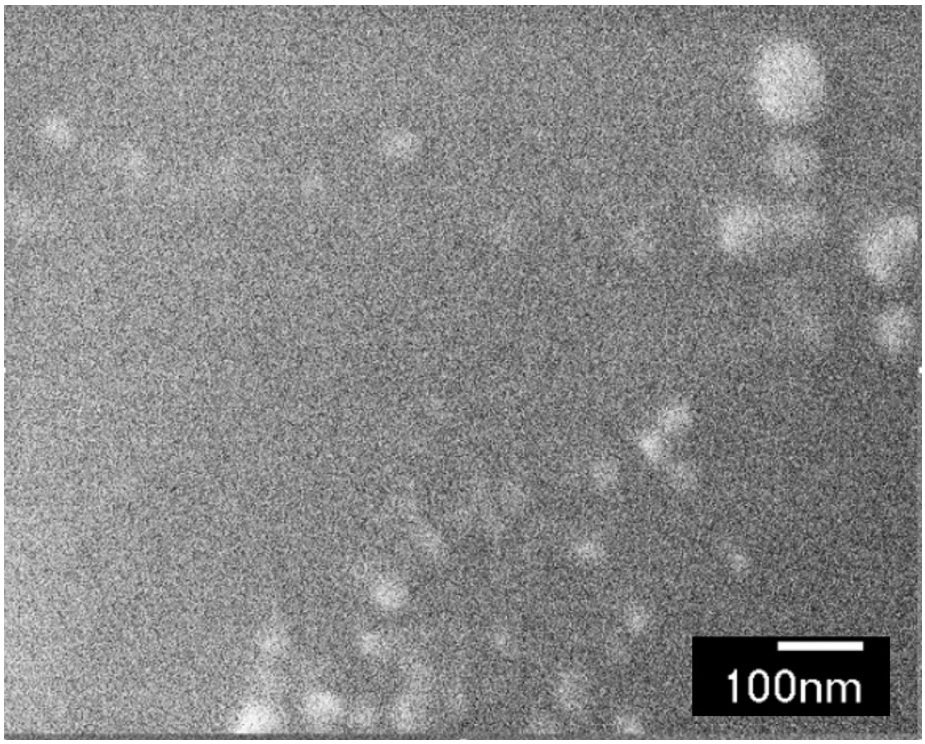

Figure 29 Same material as figures above, treated with myelin basic protein instead of PBP2a, as a selectivity control. There are no visible pores.

Summary

In this work, we have shown a simple method by which to create a series of trityl-based methacrylates and their respective copolymers, which are capable of acting as sufficiently stable dielectric layers for use in electrochemical detection systems. Dimethoxytrityl (as well as the more stable monomethoxytrityl and trityl protecting groups) are sufficiently stable under anhydrous conditions to form copolymers with benzyl methacrylate. Additionally, these polymers show a level of acid-lability caused by their fragile side chains, which leads to a morphological change in the thin film as seen by both DIC and electrochemical impedance spectroscopy.

These polymers can be blended with a related polymer containing carboxylic acid groups capable of being bound to antibodies through carbodiimide attachment chemistry, and the thin films are resistant to non-specific binding as shown by fluorescent microscopy. These polymers are also highly promising binding layers for use in the development of EIS-based sensors due to their apparently consistent capacitive changes following antigen attachment, which does not require any additional label or processing steps to produce a signal. The films are also non-reactive to other proteins such as BSA, even at a very high concentration of 10 mg/ml, and retain their ability to react as expected with our antigen of interest even in the presence of this other protein.

2. Secondary labeling particles

The enzyme-linked immunosorbent assay (ELISA) and related variants of sensing are a remarkable methodology that, for many decades, have been a gold standard for diagnostic testing. Very generally, this type of system involves an analyte-binding entity (typically an antibody or protein) bound to a substrate, the addition of the analyte of interest, many washing steps, which is followed by any of several potential amplifiers that would bind to the free end of the bound analyte and produce a more drastic signal. While highly sensitive and effective, this system can take many hours, use expensive reagents, and require trained technicians in a professional lab setting to successfully complete and read the outcome. However, similar secondary binding and amplification techniques are being used in electronic testing with promising results. Jang et al. had very positive results combining the ELISA system with the typical ISFET, resulting in increased sensitivity compared to unamplified geometries[130]. This method of adding functionalized particles is of great interest in a variety of bioelectronic sensing, for example in the case of electrochemical impedance spectroscopy where Zhu et al. used the sandwich approach to specifically bind a secondary gold nanoparticle to the surface,

significantly altering the impedance more than the original analyte of interest, Clostridium difficile toxin[131].

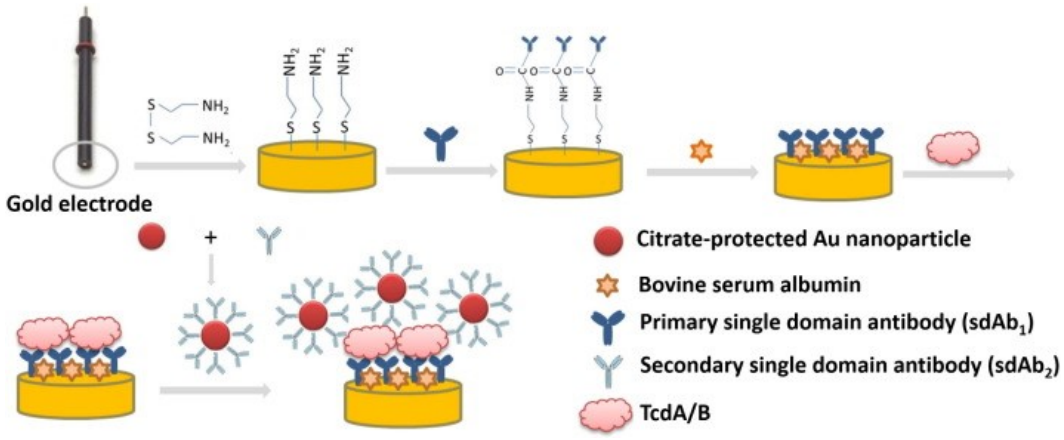

Figure 30 Illustration of the immobilization process of the sandwich-type (ELISA) electrochemical impedance immunosensor.

As an additional study in this EIS work, particle-based secondary markers were designed and compared as potential amplification methods for the PBP2a detection system.

Gold Particle-Antibody Complexing:

50 nm gold nanoparticles already complexed to Protein G were obtained from a commercial source. Protein G is able to bind to the heavy chain (non-sensing portion) of our rabbit-derived antibodies and thus can serve as a simple anchor to the antibodies without the need for any additional chemical modification.

Briefly, 50 ul of gold nanoparticle solution was washed in a 1 ml cuvette with 1 X PBS solution two times, by centrifugation at 1500 G for 30 minutes. Particles were redispersed by vortex mixing for ten seconds. Particles with supernatant removed were incubated with monoclonal anti-PBP2a antibody at a concentration of 1 ug/ml for 1 hour with constant mixing to prevent aggregation. The resulting mixture was washed as described with PBS buffer an additional two times to remove

unbound antibody and supernatant removed to leave approximately 100 ul of suspended particles with a dark pink color. No aggregation is observed with the naked eye following antibody treatment and vortex mixing. 10 ul of this solution is added on top of typical EIS measurements following the incubation with protein of interest and subsequent buffer removal, and it is allowed to sit for 10 minutes, at which point additional PBS buffer is added to bring the device back to its 1 ml operating volume. Measurements were collected with the PARstat as previously described, and compared to unamplified schemes as shown in the following graphs.

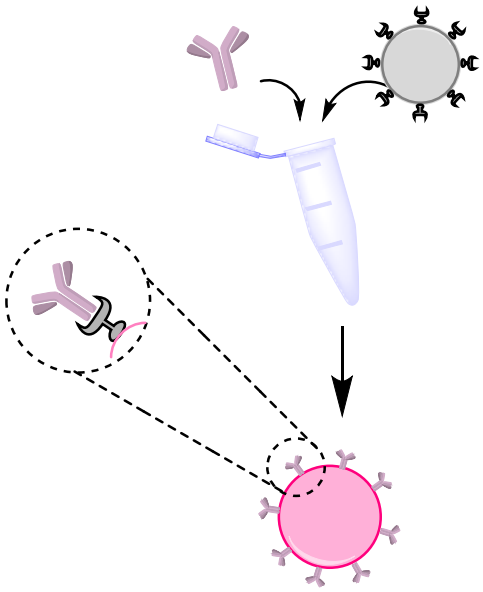

Figure 31 Illustration of Au particle-Protein G (grey) complex binding to anti-PBP2a antibody heavy chain (purple).

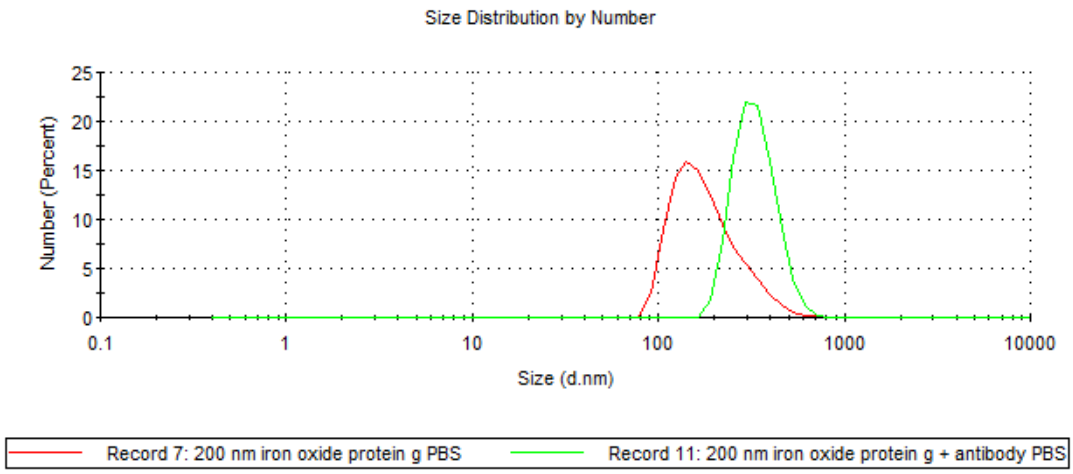

Figure 32 Dynamic light scattering confirming an increase in particle size following antibody attachment to particles.

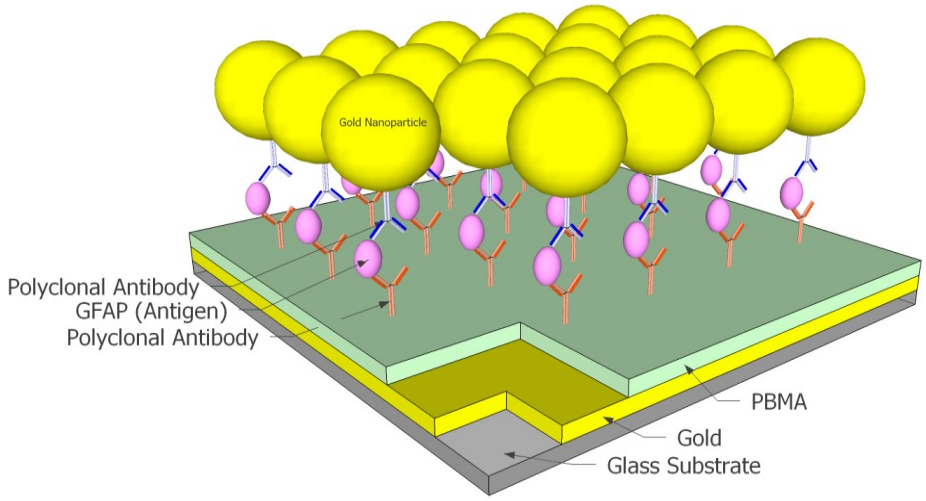

Figure 33 EIS measurement using Au particles as amplification mechanism.

The following Nyquist data shows the testing method to determine selectivity and amplification response of the gold nanoparticle amplification scheme. After a PBS immersion of a surface functionalized with 1702 MRSA epitope antibodies comes to equilibrium and is measured, gold nanoparticles functionalized with the 1704 MRSA epitope antibody are added to the system as a test to check responsiveness. In a selective sensor, there will be little response to this addition, since

there is no analyte to bind the particles specifically to the substrate. Therefore this served as a good control to show that the gold particles bind selectively to our protein of interest. Following this step, the sample is rinsed with buffer and exposed to 1 ug/ml of PBP2a protein in PBS solution. After equilibrium is measured, 1704-labelled gold particles are once again applied and incubated for 5 minutes, and the results are compared.

For additional quantitative data, these plots were fitted using the Zview program and fitting for a double layer capacitance, which is a constant phase element (CPE) and resistor in parallel following some solution resistance of the PBS, shown in Figure 34.

From this fit we obtain many values: Rs, solution resistance, is always small and corresponds simply to the conductivity of the PBS solution, CPE-T is similar to a capacitive value of the constant phase element (admittance, see below), and CPE-P is a quantification of the same element, where 0 would indicate pure resistance and 1 would indicate pure capacitance. Rp is the parallel resistance of this system. As shown in the values below, this system is highly capacitive (as expected, since it is based on a good dielectric material and does not use a redox probe to facilitate charge transfer), with CPE-P values close to 1. From these values, a "true" capacitance may be calculated and compared for each sample.

The capacitance is calculated using the formula:

$$\mathbf{C} = \frac{(\mathbf{Qo} * \mathbf{Rp})^{\frac{\mathbf{1}}{\mathbf{n}}}}{\mathbf{Rp}}$$

Equation 8 Equation comparing capacitance and admittance from the depressed semicircle model of the primarily capacitive dielectric layer (taken from Gamry Instruments tutorial).

Where Qo is the admittance (1/absvalue(Z)) in units of S-s^n at a frequency of 1 radian/s (and CPE-T=Q^n), Rp is the same as in the model described above, and n is CPE-P.

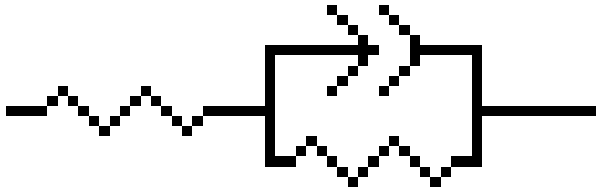

Figure 34 Constant phase element (CPE) schematic fitting circuit of a depressed semicircle on the Nyquist plot.

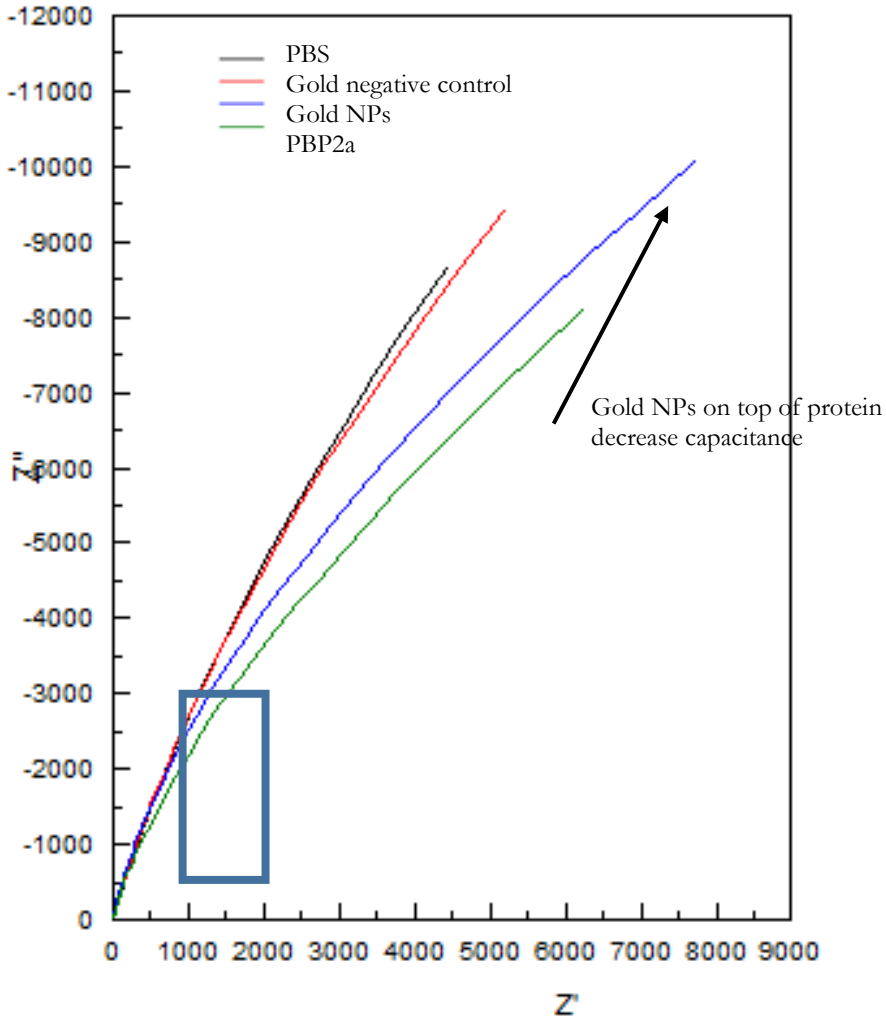

Figure 35 Particle study analyzing amplification scheme of monoclonal antibody labeled gold nanoparticles on benzyl methacrylate – methacrylate acid polymer layer. Rectangle indicates ~1000 Hz frequency data points.

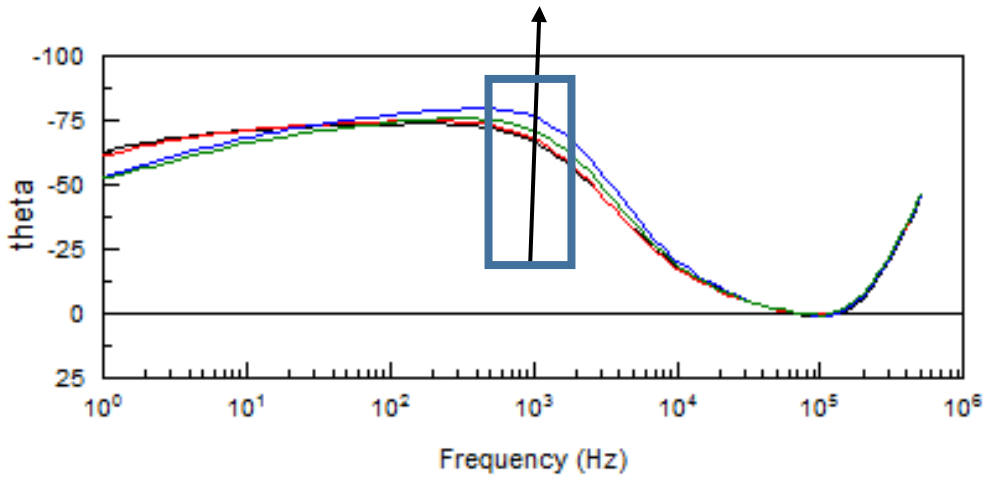

Figure 36 Same data as Figure 35, plotted as frequency versus phase angle. Arrow indicates phase change at 1000 Hz (this was the analysis used in IV.C.1 to determine change). Rectangle indicates ~1000 Hz frequency data points.

Figure 35 and Figure 36 are the Nyquist Plot and Bode plot of the same data, though both are shown to get a better view of the phase angle changes. In Figure 36, marked at 1000 Hz, there is an increase in phase angle magnitude that is small with the addition of protein, but much larger with the addition of the secondary labelling particles. This corresponds to the similar increase seen by the arrow marked in Figure 35, though the scaling makes it difficult to compare purely visually.

Below in Table 6, the fitting algorithm from the ZView Scribner software used the CPE element (Figure 34) to make estimations of the values of all components of the system. A "true" value of capacitance was calculated using Equation 8 and is also shown below on the table.

Looking at Table 6, we see the value of Cpe-T , decrease noticeably with the addition of the secondary labelling particles, indicating a more capacitive system. This pattern was constant

across three samples, as shown in Table 7. After the addition of the protein of interest, the "true" capacitance decreased (corresponding to the height increase from the added protein layer), but after the addition of the gold nanoparticles this value consistently decreased, which may be due to the presence of the gold deforming the local film and allowing for water penetration. While this is not a very useful metric for sensing, it does confirm the selectivity of our gold nanoparticles in attaching to the protein of interest. As shown in Figure 36, the optimum metric for determining sensing response is actually quite simple, and is a measure of the phase angle shift at 1000 Hz. Measuring at a single frequency allows for much faster measurements, and easy data analysis.

Table 6 Values associated with poly benzyl methacrylate polymer sample in particle amplification geometry. This data was gathered using best fit equations of the data in Figure 35 in the ZView program.

Best Fit Values To CPE Model	PBS	Au Control	PBP2a	Au Particles
Rs (ohms)	13.74	14.46	15.33	13.79
Cpe-T*	1.73E-05	1.46E-05	1.20E-05	8.90E-06
Cpe-P ("n")*	0.863	0.872	0.87	0.901
Rp (ohms)	24613	23762	14966	17402
Q (S/s^n)	3.04E-06	2.85E-06	2.21E-06	2.48E-06
Capacitance (uF)	2.01	1.91	1.32	1.755

*Unitless measurement used for fitting to determine capacitance values from Gamry Instruments. Cpe-T refers to a quantity similar to capacitance, Cpe-P refers to a value between 0 and 1 measuring the amount of resistive versus capacitive behavior, with 0 being pure resistive and 1 being pure capacitive. These values above 0.8 are considered somewhat capacitive and are well-modeled by the constant phase element assumptions.

Table 7 Percent change in calculated capacitance following protein and gold particle additions, averaged over three samples.

% Change	Protein Addition	Au Particle Addition
Average	-0.25	0.412
Standard Deviation	0.066	0.084

D. Summary

When designing any biomolecule sensor, it is first vital to determine its purpose and location of use. In the case of MRSA detection, public health threat analysis indicates that the ideal sensor would be one capable of being used in both hospital and agricultural settings. Only an extremely fast detection mechanism, one that does not require sending out to a lab for measurement, will be useful to preventing bacterial outbreaks in food.

The degradable polymer dielectric layer offers an embedded amplification scheme to an EIS-based sensor. This simplicity allows for this sensor to be used by a minimally trained user without excess washing or amplification steps, which is ideal for point-of-care use. We have demonstrated that dimethoxytrityl-based polymers are sensitive enough to small environmental changes that they will significantly alter the capacitance of the bulk film. Additionally, this measurement shows good selectivity in the presence of a high concentration of bovine serum albumin. SEM images confirm antibody attachment as well as the creation of pores after incubation with the analyte of interest.

As a potential additional amplification mechanism, for use when a sensor is not required to be point-of-care, we also explored the use of secondary labeling particles. These act by providing an additional capacitive layer between the bulk film and an electrolyte solution, as well as providing other charge transfer opportunities. Gold nanoparticles coated with a monoclonal antibody provide a consistent change in the form of an increasing capacitance following attachment. These sorts of secondary particles are frequently used in the design of novel EIS sensors, but the additional steps required to incubate them make them less than ideal.

V. Conclusion

Chapter 1 offered an overview of general electronic sensor design and motivation for various applications. Organic electronic semiconductors and insulating polymers were also introduced. Organic materials are readily modified with functional groups, making them ideal for many purposes.

Chapter 2 showed some of these modifications to the OSC layers. For the ethylene sensor, physical components were added to a P3HT layer in the form of pores and metal particles. Both of these contributed to the increased sensitivity of the device. The ammonia sensor was composed of two separate polymers, one n-type and one p-type, which react oppositely to ammonia gas. The NO2 sensor similarly relied on multiple individual devices for increased sensitivity but also used chemical modification to the alkylthio-thiophene polymer which added increased sensitivity to the analyte of interest by comparing the differing responses between the two polymers.

Chapters 3 and 4 focused on meeting the needs of biomolecule sensors. In Chapter 3, novel polymers were developed that offer a high level of pH sensitivity but can still act as a dielectric layer in an EIS experiment. In Chapter 4, these polymers were tested for biocompatibility by using a polymer blend activated with antibodies. Fluorescent microscopy confirmed antibody attachment and protein selectivity on these films. The trityl-based polymer film has a higher electrical response to the analyte of interest, PBP2a, an antigen of MRSA. The small amount of degradation allows for microscopic pore formation that allows for water infiltration into this normally hydrophobic film, drastically increasing the dielectric constant and increasing the capacitance. This self-amplifying layer can produce large electrical responses without needing the addition of washing steps or additional labels,

which makes it ideal for point-of-care detection. Secondary labels in the form of gold nanoparticles coated with monoclonal complementary antibodies were also measured to detect EIS response. While this can increase the response of the system reliably, it still does increase the time and materials necessary to produce a sensing response, which is not ideal outside of a medical lab.

Organic electronic-based sensors are readily modified through both physical and chemical means. With the advent of new polymer semiconductors that have increased stability compared to the originals, many of these technologies will continue quickly developing and going to market. Their clear outputs and ease of use make them especially ideal in factory or home settings, where traditional medical lab technology is too cumbersome to be practical. Many of the modification methods introduced in this dissertation are applicable to a variety of systems and can be easily incorporated as further semiconductors are developed.

VI. End Matter

A. Appendix A

Evaluating biological plausibility in supporting evidence for action through systematic reviews in public health

Jennifer Dailey
Johns Hopkins University
Whiting School of Engineering
Department of Materials Science
jdailey4@jhu.edu

Lori Rosman
Johns Hopkins University
Johns Hopkins School of Medicine
Welch Medical Library
Lrosman1@jhmi.edu

Ellen Kovner Silbergeld*
Johns Hopkins University
Bloomberg School of Public Health
Department of Environmental Health and Engineering
esilber2@jhu.edu

*Corresponding author

Abstract:

Background: Information on the biological plausibility of observed associations between exposures or interventions and outcomes has been recognized as an important component of evidence-based decision making in medicine and other disciplines for over 70 years. Despite this, there has been little in the way of developing, validating, and using normalized methods for systematic approaches to this topic. This paper presents an exercise in applying transparent methods to access information related to biological plausibility in support of public health interventions. Our research topic was to develop evidence for action to control uses of antimicrobials in food animal production in order to reduce the risks of exposure to and infection by antimicrobial-resistant pathogens in humans. Two recently published systematic reviews on this topic drew upon observational studies for evidence on this subject. The gold standard in quality of medically-relevant data is a randomized control study. However, there are obvious ethical and practical reasons why these designs are impossible for most public health concerns and interventions. Because of the inherent limitations of such studies, there is an important need for mechanistic information to support evidence from studies using these designs.

Methods: We identified two detailed methods relevant to assessing evidence for biological plausibility. We used their recommendations, which included expert consultation, to identify mechanisms relevant to biological plausibility of the association we selected to test.

Results: Expert consultation with both researchers and a public health informationist yielded sources that assisted us in identifying structures evaluating biological plausibility based on mechanistic understanding of the events linking antimicrobial use in food animals

and increased risks of human exposures to antimicrobial resistant pathogens of zoonotic origin.

Conclusions: This analysis of biological plausibility used transparent methods to assess the evidence used in systematic reviews based on observational studies accessed through searches of the scientific literature. Given the importance of this topic in systematic reviews and evidence-based decision making, further research is needed to define and test methodological approaches to access and properly evaluate information from the scientific literature.

Keywords: biological plausibility, systematic reviews, mechanisms, antimicrobial resistance, foodborne infections

Background

Evidence-based methods in medicine and other health-related fields have emphasized biological plausibility as an important element in assessing the strength of evidence since the work of Bradford Hill[132, 133]. As noted in a recent review of cancer risks, information on biological plausibility is particularly important as a complement to associations observed in epidemiological studies[134]. For observational studies, the quality of evidence is often judged weaker than evidence based on randomized controlled studies. These study designs, which are necessary given the ethical ramifications of interventions in public health, are considered to be less able to eliminate the effects of residual bias. As a consequence, evaluating biological plausibility or mechanisms may be of particular value in assessing the strength of evidence from this literature. This has been recognized by several regulatory agencies, including the US Environmental Protection Agency and the European Food Safety Agency, as well as by the WHO and CODEX[135, 136].

However, despite the importance of the topic, there are no generally accepted methods for evaluating biological plausibility, and many reviews discussing these mechanisms include only general statements on relatively nonspecific physiological events or target organs with no supporting references.

Our research question concerned the biological plausibility of observed associations between antimicrobial use in agriculture and increased risks of human exposures to drug-resistant zoonotic pathogens. There are many reviews of this topic, including two recent systematic

reviews. One of these systematic reviews was undertaken by a WHO Guidelines Development Group to support its task to develop evidence-based recommendations and guidelines to reduce antimicrobial resistance related to agricultural use[136]. An additional systematic review was published independently[137]. The WHO systematic review utilized the GRADE methodology to assess the quality of the evidence, and following GRADE criteria, the evidence was rated of low confidence[138]. The other systematic review[137] used a modified GRADE approach for evaluating evidence in which the "sufficient component" causal model proposed by Rothman was incorporated[139].

Assessments utilizing GRADE can cause confusion among users of guidance based on these reviews. A statement issued by the USDA shortly after publication of the WHO guideline referred to this "low-quality evidence" as effectively disqualifying any WHO recommendations, despite the surrounding analyses and expert opinion[140]. To provide additional support for this evidence, we undertook an assessment of the biological plausibility of the observed associations between antimicrobial use in food animal production and increased risks of human exposures to and infections by antimicrobial-resistant zoonotic pathogens[141].

Methods: Primarily through expert consultation, we identified papers with general discussions of methods related to biological plausibility [142, 143]. From these papers, we identified papers from the biomedical literature with more detailed methods for defining causal pathways in terms of molecular and genetic mechanisms[134, 144, 145]. We further accessed papers from the toxicology and ecology literature that defined causal pathways in terms of adverse outcome analytic methods[146–148].

These two approaches are shown below:

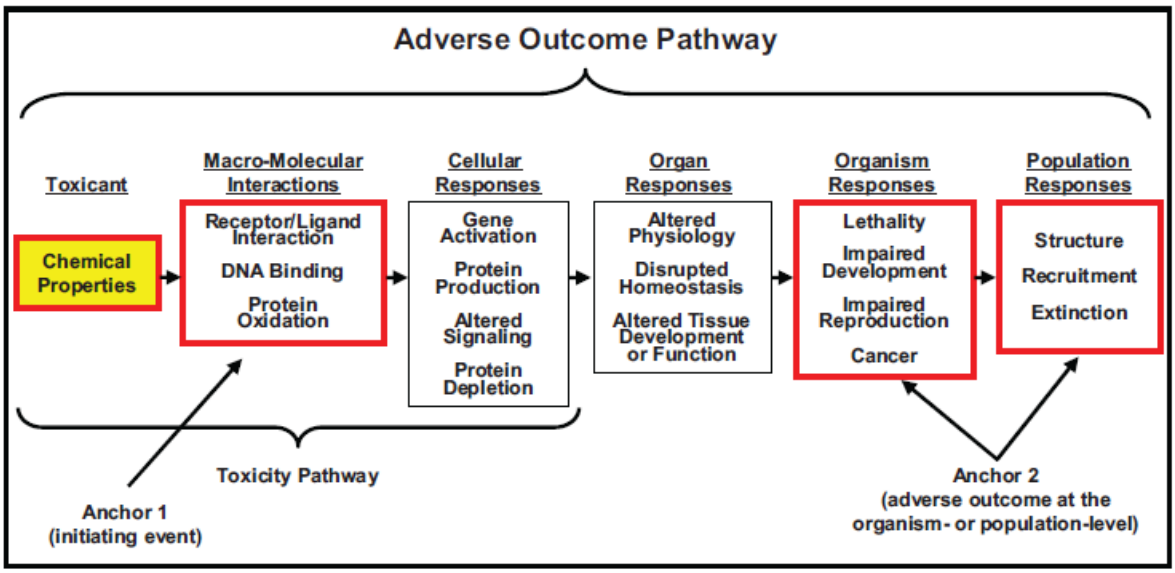

Figure 1. An adverse outcome pathway as used in toxicology to define events in a causal sequence connecting exposures to outcomes at the population level [146].

We utilized the adverse outcome pathway model, as it more closely represents the research question we sought to investigate, that is, a series of discrete mechanistic events not as strictly limited to one molecular pathway as in Lewis et al. [134]. In order to assess the biological plausibility of observed associations between antimicrobial use in agriculture and increased risks of human exposure to and infection by antimicrobial resistant pathogens from food animals, we developed and populated a similar structure for this review based on a conceptual structure that represents a sequence of mechanisms involved in the emergence and dissemination of antimicrobial resistance[149–152]To this model we added the routes that connect these events in agriculture to human exposure. Consistent with WHO practice in guideline development, we sought a global sampling of papers.

Our conceptual model is shown below (Figure 2).

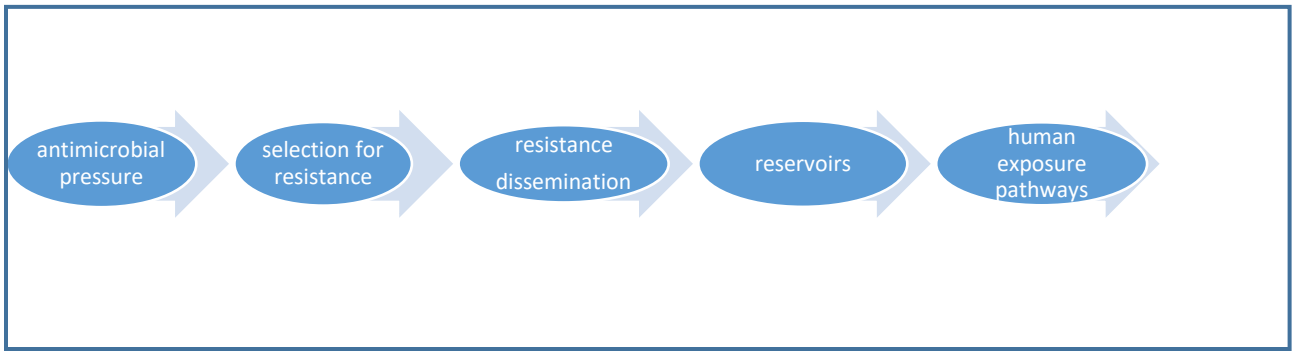

Fig. 2. A conceptual model of the mechanisms by which use of antimicrobials in food animal production increases risks of antimicrobial resistance as well as exposure of human populations to pathogenic bacteria.

In this model, antimicrobial pressure includes several variables: volume of antimicrobial use, concentrations of antimicrobials encountered by pathogens in animal guts, duration of antimicrobial use, and use of >1 antimicrobial at a time. Selection for resistance includes both natural selection through evolutionary mechanisms and horizontal gene transfer of one or multiple resistance genes. Resistance dissemination includes clonal expansion of resistant organisms as well as gene flow among organisms through horizontal gene transfer involving mobile genetic elements, conjugation, and other mechanisms. Reservoirs include the resistome (defined as microbial resources of resistance genes) and the mobilome (defined as microbial resources for enabling intercellular transfers of resistance genes) that are available within microbiomes in hosts and the external environment[153]. We defined human exposure pathways to include direct and indirect animal:human contact; releases from animal confinement houses; waste disposal; and consumption of food products derived from animals[154][155].

Antimicrobial Pressure
Volume of AM use in agriculture exceeds use in medicine in many countries
Conditions of use
Low concentration of drugs in feeds expose gut microbes to sub MIC concentrations
Multiple drugs and extended uses of drug cocktails for growth promotion

Drivers of resistance
Mutation and HGT are both stimulated by conditions of use;
Housing conditions expose herds and flocks to resistant strains and to antimicrobials in waste

Resistance dissemination
Conditions of use fail to kill microbes; these conditions activate intercellular signaling and plasmid mediated HGT of multigene cassettes encoding resistance to multiple drugs

Reservoirs
Conditions expand reservoirs of resistance genes and mobile genetic elements in host and environmental microbiome

Exposure pathways
Human exposure involves food consumption, animal and farm contact, wastes, environmental sources

ribe the biological plausibility between agricultural AM

Summary review of evidence

STEP 1 Antimicrobial pressure → selection for resistance

Fundamental to our understanding of mechanisms involved in the emergence of antimicrobial resistance is the fact that antimicrobial resistance is inherent within microbial populations. For billions of years, microbes have produced almost all currently used antimicrobial molecules in response to intense competition for resources and survival within the microbiome[156]. In this context, AMR evolved as an evolutionary mechanism by which microbes survived through natural selection by random gene mutation that encoded traits that conferred resistance to these natural biotoxins.

In contrast, human uses of antimicrobials are very recent, beginning in the early 1940s. Yet due to this prehistory, resistance mechanisms were already present within bacterial populations[97]. During the first years of experimentation by Fleming and others, resistance was recognized as a consequence of exposure. Evolutionary theory explained the emergence of antimicrobial resistance as a process of random genetic mutations that conferred biological resistance to drugs[157] . This theory also supported the assumption that each instance of resistance required either vertical transmission from the replication of a resistant organism or a separate evolutionary event. At first, little was known of the specific mutations or molecular mechanisms of AMR, but with the rapid development of molecular genetics, these altered proteins were identified[158] .

Evolutionary theory also supported the assumption that there was a cost of resistance involving a trade-off between resistance and growth rate (the *r*K selection theory). Without this cost, bacteria would be equally likely to be resistant or susceptible in the absence of AM

pressure and with the removal of AM pressure the prevalence of resistant strains would decrease. However, experimental observations contradicted theory, which was amended to include more complex evolutionary responses, such as "bet-hedging," by which microbial populations under AM pressure could acquire additional mutations to compensate for the cost of resistance[159].

Over the past 50 years, a substantial revolution has occurred in our understanding of the mechanisms by which AMR emerges and is disseminated. Current research now supports the hypothesis that horizontal gene transfer (HGT), rather than mutation, is the major mode by which bacteria (and other microbes) respond to antimicrobial pressure[160]. Horizontal or lateral gene transfer among live cells was observed, although not understood mechanistically, as early as 1928[161]. Bacteria utilize several mechanisms to share resistance genes, including conjugation or exchange through direct cell:cell contact, transformation or incorporation of naked DNA from disrupted organisms in the extracellular environment, and transduction involving transfer of genetic material by transposable genetic elements[157, 162]. Later experiments demonstrated mechanisms by which donor cells initiate plasmid-mediated gene transfer and how antimicrobials stimulate intercellular signaling between susceptible and resistant bacterial strains to initiate events including gene transcription that facilitate horizontal gene transfer from chromosomal DNA within the donor cell and responses such as swarming within the susceptible recipient organisms[162–164]. The mechanisms by which resistance genes that are transferred among cells can be incorporated into the chromosomal genome of the recipient cell and expressed are also understood[165].

Concentrations of antimicrobials The conditions of AM use also affect resistance emergence as well as dissemination. The most significant overall risk factor driving AMR

emergence in any setting is the volume of drug use. Associations between overall drug use and prevalence of AMR has been shown by cross-sectional comparisons of national drug use data[36] and longitudinally after bans on use of certain drugs in agriculture [37]. In addition, the concentrations of AMs to which microbes are exposed is also significant. Exposures to subtherapeutic concentrations of AMs (defined by bioassay at concentrations below the minimum inhibitory concentration, or MIC) are particularly effective as drivers of selection for AMR. This seemingly paradoxical observation reflects the Nietzschean aspects of bacteria: that which does not kill them makes them strong. Higher concentrations of AMs (greater than or equal to the MIC) *kill* bacteria whereas sublethal exposures *stress but spare* bacteria. As a consequence, these stressful but nonlethal conditions are particularly effective as drivers of selection for AMR through two mechanisms: increased growth and mutation rates and enhanced transfer of resistance plasmids and conjugative transposons[168].The survivors acquire resistance through these mechanisms as well as increased incorporation of resistance genes into chromosomal DNA. Continuous or prolonged low level AM use also expands the resistome and enhances the role of mobile genetic elements (MGEs), including plasmids, in mediating the dissemination of resistance within hosts and the environment within the microbiome[153, 169] .

Use of multiple drugs Repeated exposure to multiple AMs affects the emergence and dissemination of multidrug resistance through HGT of mobile genetic elements containing multiple resistance genes encoding resistance to several drugs. This results in both cross resistance and co-selection. These mechanisms were first demonstrated in 1989, with experiments showing that cross resistance among antimicrobials can be selected by one drug represented in the multi-drug resistant cassette[170]. Through HGT, bacteria not only exchange individual resistance genes but also cassettes of multiple resistance genes, which

encode for co-resistance to multiple antimicrobials. In other words, both pathogenic and nonpathogenic bacteria can easily share an entire cookbook of avoidance tactics rather than a single recipe. In response to repeated exposures to multiple AMs, bacteria acquire "genetic capital" in the form of sequential acquisition of resistance genes that can be transferred as a package through transposons within the mobilome[171]. These cassettes may be highly complex. A salmonella strain resistant to 13 antimicrobials was isolated from a child living on a farm who presented with ceftriazone resistance; all but one of the genes encoding multidrug resistance were on the same plasmid[172]. These multigene cassettes can include metal resistance genes such that co-selection and cross resistance can) also be driven by metals such as copper, cadmium, nickel. mercury, arsenic, and zinc[173, 174].

These conditions -- use of concentrations of antimicrobials that result in subtherapeutic microbial exposures and use of multiple drugs in feeds – are common in the use of antimicrobials in poultry and livestock production. Another agricultural use is the long duration of repeated exposures for so-called prophylaxis or metaphylaxis (preventive treatment in the expectation of but absence of diagnosed disease). This may also involve sublethal concentrations of antimicrobials[175]. These low dose and extended exposures to single or multiple antimicrobials condition networks of gene flow within the microbiome such that HGT is facilitated and role of mobile genetic elements in mediating resistance gene flow is enhanced within the gut microbiomes in animal hosts as well as in the environment[176].

STEP 2 Selection → Dissemination of resistance

HGT enables the rapid and efficient dissemination of resistance among bacteria (and other microbes) through highly efficient community signaling within the microbiome. This is in

contrast to evolutionary mechanisms dependent upon random mutation or clonal expansion. At low concentrations, horizontal transfers of resistance genes among microbes rather than vertical transmission or *de novo* mutations are now recognized as the most important mechanism and explanation for the rapid and far-ranging dissemination of resistance within and among microbial populations within hosts and the environment[177]. These mechanisms support highly efficient mobilization of community resources of resistance. As a consequence, these resources are available to microbial networks that can be geographically distant as well as phylogenetically distinct.

Within and among microbial communities, HGT moves individual resistance genes as well as cassettes of multiple genes that encode for co-resistance and co-selection of resistance[153, 160]. These mechanisms underlie the complexities and underscore the facility with which bacteria respond to antimicrobial pressure with both emergence and dissemination. Once a new resistance trait and gene emerges, it spreads rapidly among microbial communities. This dissemination is further facilitated by movement of bacteria through air and water, changes in methods of food animal production, and human behavior including food consumption patterns, global travel, and international trade in animals and food.

These mechanisms of dissemination are exemplified by the rapidity and global range of resistance of β-lactams as evidenced in the emergence of extended β-lactamases in response to the introduction of new cephalosporins [178, 179]. Since the isolation of the first of these drugs in 1948, there are now five generations of cephalosporins. Bacteria have rapidly responded to each generation of new cephalosporins with increasing numbers of distinct β-lactamase genes, now exceeding 1000[178]. Both resistant bacteria and resistance genes

encoding extended spectrum β-lactamase (ESBL) have spread rapidly and globally[180]. Moreover, ESBL resistance genes are frequently bundled with other resistance determinants in transposable gene cassettes[181]. Co-selection has been suggested as the mechanisms for the rapidity of selection for resistance to novel cephalosporins such as carbapenem as well as colistin[182] .

STEP 3 Dissemination → Reservoirs of resistance

Resistance reservoirs include the resistome (defined as the biological resources for responding to antimicrobial pressure) and the mobilome (defined as all the biological resources for transferring genes in response to pressure) [153].

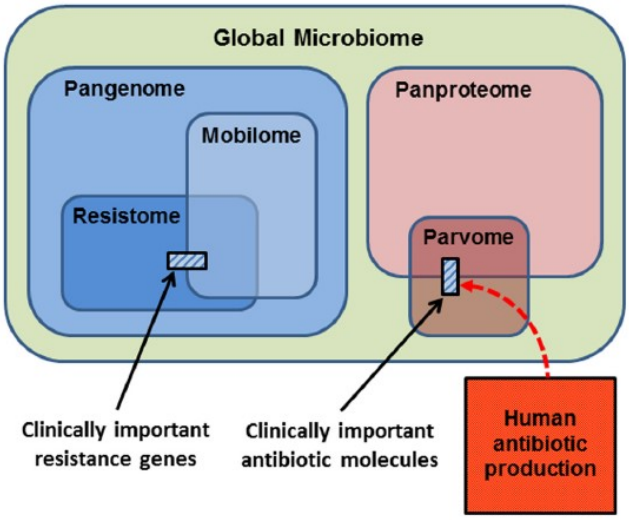

Fig 4. The relationships within the global microbiome and its pangenome including the resistome and the mobilome that support horizontal gene transfer in response to antimicrobial pressure including those genes encoding resistance to clinically important antimicrobials. The panproteome includes the gene products of the microbiome, including the parvome which includes clinically important antimicrobial molecules produced by humans[153]**.**

These reservoirs exist within microbes and as naked DNA within physiological niches such as the gut and ecological niches in the external environment. The increasing use of antimicrobials has enlarged the resistome and increased the activity of the mobilome [153, 183]. Increases in antimicrobial resistance genes and class 1 integrons have been reported in animals fed antimicrobials and have been documented in studies of soils treated with animal wastes or veterinary antimicrobials[177, 184, 185].

The environmental reservoirs of resistance may constitute the largest resources of these functions and are of specific concern in the context of agricultural uses through the release of untreated animal wastes containing resistance genes and antimicrobials that augment selection pressures within environmental microbiomes[169].

The environmental resistome has been a source of resistance in pathogenic bacteria isolated from humans[156]. Since agriculture is situated directly within the physical and biotic environment, with numerous porosities from farm to fork, gene flow within and from food animal production contributes significantly to the environmental resistome[186]. This involves both release of antimicrobials as well as resistance genes. Several studies have reported concentrations of antimicrobials in sediments impacted by aquaculture that are many fold greater than the minimal inhibitory concentrations for many drugs and pathogens[187]. In addition, multiple mobile genetic elements have also been measured in soils and sediments[184]. Empirical assessments of gene flow from agriculture into environmental microbiomes in soils and sediments have been published[188].

STEP 4 Reservoirs → Exposure pathways

To evaluate the last step in this conceptual sequence, exposure of human populations to drug resistant pathogens from food animal production, we considered the role of the

mechanisms discussed above within the conditions and context of food animal production. Many of the conditions in food animal production resemble those risk factors that are conducive to the mechanisms of AMR emergence and dissemination first identified in healthcare settings, and for which interventions and guidance programs have been developed and implemented in many countries[189]. They are exacerbated by animal stress and crowding during growth stages and transport[190, 191] .

In Figure 2, we summarize the evidence for the role of mechanisms listed in Figure 1 within the context of antimicrobial use in food animal production. We also indicate evidence supporting routes of exposure to these zoonotic pathogens from food animal production to human populations.

The food supply is the most significant pathway for human exposure to AMR pathogens from agriculture in terms of numbers of persons exposed, followed by multiple pathways of release to the environment. These two pathways operate both separately and in combination. In addition to consumption of food products from animals, there is an underappreciated and overlooked pathway of food-borne dissemination from the environment to crops consumed by humans. This is of particular risk when crops are grown with animal wastes (as in organic production) or with irrigation by surface water sources contaminated by run off from land disposal of animal[192, 193].

The food and environmental pathways of exposure blur distinctions between healthcare and agriculture. Common sources of food are eaten inside and outside of healthcare facilities, and hospitals are located in environments where ambient air and water that may be contaminated by agricultural releases. Moreover, people – patients, visitors, and healthcare personnel -- move in and out of healthcare settings[194]. For this reason, there are no real

barriers between the presence of AMR in agriculture and the entrance of these same AMR pathogens into healthcare settings. These factors make it impossible to identify sources of resistance or to allocate burdens of disease between clinical and agricultural uses. This circularity is shown in Figure 20 of the main text.

Regardless of the original source of AMR, in most cases it is not possible to separate agricultural and clinical sources of genetic determinants of resistance in pathogens isolated from human populations, since genes and pathogens originating in agriculture quickly become sources of exposures and infections in human communities and eventually move into healthcare settings, and strains in humans can be transferred to animal populations. This gene flow goes both ways. There is a well annotated history of the cross transmission of so-called "livestock" strains of MRSA (ST398) from humans to animals and from animals to humans[102]. Some studies of ESBL+ genes in *E coli* isolates from animals, including carbapenemase, suggest that this may represent contamination of the agricultural environment by human wastes[195].

Discussion We undertook this study to improve the evaluation of evidence related to biological plausibility of associations observed in non RCT studies relevant to public health. The development of a transparent method for assessing the quality of these types of associations in observational studies is of high importance. Current assessment methods based on GRADE are not appropriate because of the inherent limitations of public health studies. Moreover, the use of GRADE, as in the systematic reviews conducted by WHO, may lead to underestimation of important findings. The USDA issued a statement shortly after publication of the WHO guideline, which referred to this "low-quality evidence" as effectively disqualifying any WHO recommendations despite the surrounding analyses and

expert opinion[140]. We selected the adverse outcome pathway approach based on our interest in the application of these methods for supporting the evidence derived from observational studies on the contribution of agricultural antimicrobial use to the global burden of infectious diseases caused by antimicrobial resistant (AMR) pathogens.

With expert consultation, we accessed papers describing methods in detail for organizing structural models representing biological plausibility through mechanisms that link exposures to health outcomes. One of these uses a comprehensive information set based on the molecular biology of cancer (Lewis et al), and the other utilizes the more generalizable concept of adverse outcome pathways (Ankley et al) [134, 146]. The former is novel and, as discussed by the authors, includes some steps in evidence evaluation that have not been validated. In contrast, the adverse outcomes pathway methodology has a substantial record of use in toxicology and ecology to support evidence based decisions related to risk assessment[135, 196, 197]. For that reason, we adopted the conceptual framework of adverse outcomes pathway analysis, which enabled us to utilize the literature on mechanisms of antimicrobial resistance within which we assigned mechanistic evidence to a sequential pathway linking antimicrobial exposure of microbial communities to human exposure to drug resistant pathogens.

Using the adverse outcomes pathway approach, we focused on mechanisms that drive microbial response to antimicrobial stress through the emergence and dissemination of resistance as well as accumulation of resistance genes and organisms in reservoirs. To this model, we added evidence on the major pathways of human exposure to AMR pathogens from agricultural sources. The conditions of agricultural use facilitate many of the mechanisms in AMR emergence and transmission, such as horizontal gene transmission and

the frequency of multidrug resistant phenotypes. By including a further focus on agricultural use, this mechanism-based assessment of the evidence also supported the importance of the microbiome perspective. Moreover, it illuminated the role of agricultural use in expanding environmental repositories or resistomes through the direct contribution of agriculture to multiple pathways of release, and from which AMR genes can be transferred to bacteria in human populations.

Conclusions: lt is recognized that all uses of antimicrobials contribute to the emergence and dissemination of resistance[198] . In the context of increasing global threats of antimicrobial resistance, we need evidence to support effective interventions to control uses of antimicrobials in both healthcare and agriculture. The evidence has been summarized in recent systematic reviews[136, 137, 199], both of which reported associations observed between agricultural use of antimicrobials for all purposes and increased risks of AMR exposure of human populations. This paper adds an analysis in support of the biological plausibility of these observations, using published methods based on a mechanistic approach. We conclude that this approach may be applicable to evaluating the evidence for biological plausibility as part of an overall assessment of evidence for action based systematic reviews on topics in which associations have been observed based on observational studies. This first application requires validation by application to other systematic reviews where the criterion of biological plausibility is of value.

List of Abbreviations:

AMR: Antimicrobial resistance

ESBL: Extended spectrum beta lactamase

GRADE: Grades of Recommendation Assessment, Development and Evaluation

HGT: Horizontal Gene Transfer

MGE: Mobile genetic elements

RCT: Randomized control trial

WHO: World Health Organization

Funding: Silbergeld received funding from the World Health Organization to support her participation as a member of the Guidelines Development Group on antimicrobial use in food animal production; Dailey was supported by graduate fellowships from the Johns Hopkins Universiy (Center for a Livable Future) and the National Science Foundation. LR received funding from the US Cochrane Center and the Hopkins Population Center.

Authors' contributions: Both authors contributed equally to the conceptualization of this paper and writing this manuscript. Silbergeld conducted literature searches and Dailey produced the original figures in the paper

Acknowledgements: We thank our collaborating designer Lindsay Evans for her work in creating Figure 5. This review started as a background paper commissioned by the World Health Organization as part of the development of evidence supporting guidelines for reducing use of antimicrobials in food animal production. WHO also provided support to EKS for participating in the guidelines development group. JLD was supported by the National Science Foundation through a Graduate Research Fellowship and the Center for a Livable Future through a CLF-Lerner Fellowship. We acknowledge the important comments and suggestions made by our colleagues in the WHO guidelines development group. The authors also acknowledge the contributions of the following colleagues Kay Dickersin and Roberta Scherer of the US Cochrane Center, Daniele Mandrioli of the Ramazzini Institute, and our colleagues at Johns Hopkins Stefan Baral, Lori Rosman, and Alan Goldber

B. References

1. Lin P, Yan F. Organic thin-film transistors for chemical and biological sensing. Adv Mater. 2012;24:34–51. doi:10.1002/adma.201103334.

2. Mehrabani S, Maker AJ, Armani AM. Hybrid integrated label-free chemical and biological sensors. Sensors (Switzerland). 2014;14:5890–928.

3. Timmer B, Olthuis W, Berg A van den. Ammonia sensors and their applications—a review. Sensors Actuators B Chem. 2005;107:666–77. doi:10.1016/j.snb.2004.11.054.

4. Torsi L, Magliulo M, Manoli K, Palazzo G. Organic field-effect transistor sensors: a tutorial review. Chem Soc Rev. 2013;42:8612–28. doi:10.1039/c3cs60127g.

5. Leeflang MMG, Ang CW, Berkhout J, Bijlmer HA, Van Bortel W, Brandenburg AH, et al. The diagnostic accuracy of serological tests for Lyme borreliosis in Europe: a systematic review and meta-analysis. BMC Infect Dis. 2016;16:140. doi:10.1186/s12879-016-1468-4.

6. Liang Y-R, Zhang Z-M, Liu Z-J, Wang K, Wu X-Y, Zeng K, et al. A highly sensitive signal-amplified gold nanoparticle-based electrochemical immunosensor for dibutyl phthalate detection. 2017. doi:10.1016/j.bios.2016.12.007.

7. Lu J, Liu D, Zhou J, Chu Y, Chen Y, Wu X, et al. Porous Organic Field-Effect Transistors for Enhanced Chemical Sensing Performances. Adv Funct Mater. 2017;27:1700018. doi:10.1002/adfm.201700018.

8. Adhyam M, Gupta AK. A Review on the Clinical Utility of PSA in Cancer Prostate. Indian J Surg Oncol. 2012;3:120–9. doi:10.1007/s13193-012-0142-6.

9. Silbergeld E, Aidara-Kane A, Dailey J. Agriculture and Food Production as Drivers of the Global Emergence and Dissemination of Antimicrobial Resistance | AMR Control. AMR Control. 2016. http://resistancecontrol.info/2017/agriculture-and-food-production-as-drivers-of-the-global-emergence-and-dissemination-of-antimicrobial-resistance/. Accessed 16 Dec 2017.

10. Zhao W, Li S, Yao H, Zhang S, Zhang Y, Yang B, et al. Molecular Optimization Enables over

13% Efficiency in Organic Solar Cells. J Am Chem Soc. 2017;139:7148–51. doi:10.1021/jacs.7b02677.

11. Martínez Hardigree JF, Katz HE. Through Thick and Thin: Tuning the Threshold Voltage in Organic Field-Effect Transistors. Acc Chem Res. 2014;47:1369–77. doi:10.1021/ar5000049.

12. Alley O. CHARGE TRAPPING IN POLYMER DIELECTRICS AND POTENTIALS AT ORGANIC DONOR-ACCEPTOR JUNCTIONS—THE ROLE OF INTERFACE AND BULK CONTRIBUTIONS. 2016. https://jscholarship.library.jhu.edu/bitstream/handle/1774.2/40257/ALLEY-DISSERTATION-2016.pdf?sequence=1&isAllowed=y. Accessed 8 Nov 2017.

13. Yi M, Shu J, Wang Y, Ling H, Song C, Li W, et al. The effect of porous structure of PMMA tunneling dielectric layer on the performance of nonvolatile floating-gate organic field-effect transistor memory devices. Org Electron physics, Mater Appl. 2016;33:95–101. doi:10.1016/j.orgel.2016.02.034.

14. Jaffrezic-Renault N. Label-Free Af fi nity Biosensors Based on Electrochemical Impedance Spectroscopy. 80. doi:10.1007/978-1-62703-370-1_14.

15. Song J, Dailey J, Li H, Jang H-J, Zhang P, Wang J, et al. Extended Solution Gate OFET-based Biosensor for Label-free Glial Fibrillary Acidic Protein Detection with Polyethylene Glycol-Containing Bio-Receptor Layer. Adv Funct Mater. 2017.

16. Lerner MB, D'Souza J, Pazina T, Dailey J, Goldsmith BR, Robinson MK, et al. Hybrids of a genetically engineered antibody and a carbon nanotube transistor for detection of prostate cancer biomarkers. ACS Nano. 2012;6:5143–9.

17. Al-Hardan N, Abdul Hamid M, Ahmed N, Jalar A, Shamsudin R, Othman N, et al. High Sensitivity pH Sensor Based on Porous Silicon (PSi) Extended Gate Field-Effect Transistor. Sensors. 2016;16:839. doi:10.3390/s16060839.

18. Wu S, Wang G, Xue Z, Ge F, Zhang G, Lu H, et al. Organic Field-Effect Transistors with Macroporous Semiconductor Films as High-Performance Humidity Sensors. ACS Appl Mater

Interfaces. 2017;9:14974–82. doi:10.1021/acsami.7b01865.

19. Kang B, Jang M, Chung Y, Kim H, Kwak SK, Oh JH, et al. Enhancing 2D growth of organic semiconductor thin films with macroporous structures via a small-molecule heterointerface. Nat Commun. 2014;5.

20. Yu SH, Cho J, Sim KM, Ha JU, Chung DS. Morphology-Driven High-Performance Polymer Transistor-based Ammonia Gas Sensor. ACS Appl Mater Interfaces. 2016;8:6570–6. doi:10.1021/acsami.6b00471.

21. Surya SG, Ashwath BSN, Mishra S, A.R.B. K, Sastry AB, B.L.V. P, et al. H2S detection using low-cost SnO2 nano-particle Bi-layer OFETs. Sensors Actuators B Chem. 2016;235:378–85. doi:10.1016/J.SNB.2016.05.096.

22. Zheng H, Ramalingam B, Korampally V, Gangopadhyay S. Large sensitivity enhancement in semiconducting organic field effect transistor sensors through incorporation of ultra-fine platinum nanoparticles. Cit Appl Phys Lett. 2013;103. doi:10.1063/1.4829145.

23. Han S, Cheng J, Fan H, Yu J, Li L. Achievement of High-Response Organic Field-Effect Transistor NO2 Sensor by Using the Synergistic Effect of ZnO/PMMA Hybrid Dielectric and CuPc/Pentacene Heterojunction. Sensors. 2016;16:1763. doi:10.3390/s16101763.

24. Besar K, Dailey J, Katz HE. Ethylene Detection Based on Organic Field-Effect Transistors With Porogen and Palladium Particle Receptor Enhancements. ACS Appl Mater Interfaces. 2017;9:1173–7. doi:10.1021/acsami.6b12887.

25. Abeles, FB, Page W.Morgan MES. Ethylene in plant biology. Academic Press, San Diego; 1973.

26. Kepczynski J, Kepczynska E. Ethylene in seed dormancy and germination. Physiol Plant. 1997;101:720–6.

27. Jackson MB, Osborne DJ. Ethylene, the natural regulator of leaf abscission. Nature. 1970;225:1019–22.

28. Burg SP. Ethylene in plant growth. Proc Natl Acad Sci U S A. 1973;70:591–7.

29. Cooke AR. 2-Haloethanephosphonic acids as ethylene releasing agents for the induction of

flowering in pineapples. Nature. 1968;218:974–5.

30. Guo H, Ecker JR. The ethylene signaling pathway: New insights. Curr Opin Plant Biol. 2004;7:40–9.

31. Binder BM. The ethylene receptors: Complex perception for a simple gas. Plant Sci. 2008;175:8–17.

32. Stepanova AN, Alonso JM. Ethylene signaling and response: where different regulatory modules meet. Curr Opin Plant Biol. 2009;12:548–55.

33. Galotto M, Ulloa P. Effect of high-pressure food processing on the mass transfer properties of selected packaging materials. Packag Technol Sci. 2010;23 May:253–66.

34. Ivanov P, Llobet E, Vergara a., Stankova M, Vilanova X, Hubalek J, et al. Towards a micro-system for monitoring ethylene in warehouses. Sensors Actuators, B Chem. 2005;111–112 SUPPL.:63–70.

35. Santiago Cintrón M, Green O, Burstyn JN. Ethylene sensing by silver(I) salt-impregnated luminescent films. Inorg Chem. 2012;51:2737–46.

36. Giberti a., Carotta MC, Guidi V, Malag?? C, Martinelli G, Piga M, et al. Monitoring of ethylene for agro-alimentary applications and compensation of humidity effects. Sensors Actuators, B Chem. 2004;103:272–6.

37. Janssen S, Schmitt K, Blanke M, Bauersfeld ML, Wöllenstein J, Lang W. Ethylene detection in fruit supply chains. Philos Trans R Soc A. 2014;372:20130311,.

38. Esser B, Schnorr JM, Swager TM. Selective detection of ethylene gas using carbon nanotube-based devices: Utility in determination of fruit ripeness. Angew Chemie - Int Ed. 2012;51:5752–6.

39. Kathirvelan J, Vijayaraghavan R. Development of prototype laboratory setup for selective detection of ethylene based on multiwalled carbon nanotubes. J Sensors. 2014;2014:1–6.

40. Krupke R, Hennrich F. Separation Techniques for Carbon Nanotubes. Adv Eng Mater. 2005;7:111–6. doi:10.1002/adem.200400170.

41. Charitidis C a., Georgiou P, Koklioti M a., Trompeta A-F, Markakis V. Manufacturing

nanomaterials: from research to industry. Manuf Rev. 2014;1:11. doi:10.1051/mfreview/2014009.

42. Khim D, Ryu G, Park W, Kim H, Lee M. Precisely Controlled Ultrathin Conjugated Polymer Films for Large Area Transparent Transistors and Highly Sensitive Chemical Sensors. 2016;:2752–9.

43. Durgun E, Ciraci S, Zhou W, Yildirim T. Transition-Metal-Ethylene Complexes as High-Capacity Hydrogen-Storage Media. Phys Rev Lett. 2006;97:226102. doi:10.1103/PhysRevLett.97.226102.

44. Ma LJ, Jia J, Wu HS, Ren Y. Ti-η2-(C2H2) and HCC-TiH as high capacity hydrogen storage media. Int J Hydrogen Energy. 2013;38:16185–92.

45. Ma L-J, Jia J, Wu H-S. Computational investigation of hydrogen storage on scandium–acetylene system. Int J Hydrogen Energy. 2015;40:420–8.

46. Valencia H, Gil A, Frapper G. Trends in the hydrogen activation and storage by adsorbed 3d transition metal atoms onto graphene and nanotube surfaces: A dft study and molecular orbital analysis. J Phys Chem C. 2015;119:5506–22.

47. Dong H, Hou T, Lee S-T, Li Y. New Ti-decorated B40 fullerene as a promising hydrogen storage material. Sci Rep. 2015;5:9952.

48. Meng Y, Han Y, Zhu H, Yang Z, Shen K, Suo B, et al. Two dimetallocenes with vanadium and chromium: Electronic structures and their promising application in hydrogen storage. Int J Hydrogen Energy. 2015;40:12047–56.

49. Han S, Zhuang X, Shi W, Yang X, Li L, Yu J. Poly(3-hexylthiophene)/polystyrene (P3HT/PS) blends based organic field-effect transistor ammonia gas sensor. Sensors Actuators, B Chem. 2016;225:10–5.

50. Tiwari S, Singh AK, Joshi L, Chakrabarti P, Takashima W, Kaneto K, et al. Poly-3-hexylthiophene based organic field-effect transistor: Detection of low concentration of ammonia. Sensors Actuators, B Chem. 2012;171–172:962–8.

51. Besar K, Yang S, Guo X, Huang W, Rule AM, Breysse PN, et al. Printable ammonia sensor based on organic field effect transistor. Org Electron. 2014;15:3221–30.

52. Kalita A, Hussain S, Malik AH, Subbarao NV V., Iyer PK. Vapor phase sensing of ammonia at

the sub-ppm level using a perylene diimide thin film device. J Mater Chem C. 2015;3:10767–74. doi:10.1039/C5TC02521D.

53. Yu X, Zhou N, Han S, Lin H, Buchholz DB, Yu J, et al. Flexible spray-coated TIPS-pentacene organic thin-film transistors as ammonia gas sensors. J Mater Chem C. 2013;1:6532. doi:10.1039/c3tc31412j.

54. Stadler J, Aswal DK, Gupta SK, Mater J, Chem C. Simple and low-temperature polyaniline-based flexible ammonia sensor: A step towards laboratory synthesis to economical model design. 2015. doi:10.1039/C5TC01483B.

55. Garg K, Singh A, Majumder C, Nayak SK, Aswal DK, Gupta SK, et al. Room temperature ammonia sensor based on jaw like bis-porphyrin molecules. Org Electron. 2013;14:1189–96. doi:10.1016/j.orgel.2013.01.033.

56. Li L, Gao P, Baumgarten M, Müllen K, Lu N, Fuchs H, et al. High Performance Field-Effect Ammonia Sensors Based on a Structured Ultrathin Organic Semiconductor Film. Adv Mater. 2013;25:3419–25. doi:10.1002/adma.201301138.

57. López de Mishima BA, Mishima HT. Ammonia sensor based on propylene carbonate. Sensors Actuators B Chem. 2008;131:236–40. doi:10.1016/j.snb.2007.11.012.

58. Markovics Á, Kovács B. Fabrication of optical chemical ammonia sensors using anodized alumina supports and sol–gel method. Talanta. 2013;109:101–6. doi:10.1016/j.talanta.2013.01.054.

59. Zhang Y, Kim JJ, Chen D, Tuller HL, Rutledge GC. Electrospun Polyaniline Fibers as Highly Sensitive Room Temperature Chemiresistive Sensors for Ammonia and Nitrogen Dioxide Gases. Adv Funct Mater. 2014;24:4005–14. doi:10.1002/adfm.201400185.

60. de la Hoz RE, Schlueter DP, Rom WN. Chronic lung disease secondary to ammonia inhalation injury: A report on three cases. Am J Ind Med. 1996;29:209–14. doi:10.1002/(SICI)1097-0274(199602)29:2<209::AID-AJIM12>3.0.CO;2-7.

61. Brautbar N, Wu MP, Richter ED. Chronic Ammonia Inhalation and Interstitial Pulmonary Fibrosis: A Case Report and Review of the Literature. Arch Environ Heal An Int J. 2003;58:592–6.

doi:10.3200/AEOH.58.9.592-596.

62. International Program on Chemical Safety., International Labour Organisation., World Health Organization., United Nations Environment Programme. Ammonia health and safety guide. World Health Organization; 1990.

63. Usepa, Ord, Iris. Toxicological Review of Ammonia (Noncancer Inhalation): Executive Summary. 2016. https://cfpub.epa.gov/ncea/iris/iris_documents/documents/subst/0422_summary.pdf. Accessed 29 Mar 2017.

64. Besar K, Yang S, Guo X, Huang W, Rule AM, Breysse PN, et al. Printable ammonia sensor based on organic field effect transistor. Org Electron. 2014;15:3221–30. doi:10.1016/j.orgel.2014.08.023.

65. Tremblay NJ, Jung BJ, Breysse P, Katz HE. Digital Inverter Amine Sensing via Synergistic Responses by n and p Organic Semiconductors. Adv Funct Mater. 2011;21:4314–9. doi:10.1002/adfm.201101324.

66. Huang W, Yu J, Yu X, Shi W. Polymer dielectric layer functionality in organic field-effect transistor based ammonia gas sensor. Org Electron. 2013;14:3453–9. doi:10.1016/j.orgel.2013.09.018.

67. Jeong JW, Lee YD, Kim YM, Park YW, Choi JH, Park TH, et al. The response characteristics of a gas sensor based on poly-3-hexylithiophene thin-film transistors. Sensors Actuators B Chem. 2010;146:40–5. doi:10.1016/j.snb.2010.02.019.

68. Braga D, Horowitz G. High-Performance Organic Field-Effect Transistors. Adv Mater. 2009;21:1473–86. doi:10.1002/adma.200802733.

69. Deshmukh KD, Reuter K, Kempa H, West JE, Katz HE. Tuning of threshold voltage in organic field-effect transistors with hydrophobic gate dielectric using monoenergetic low-energy electron beams and triode corona. Appl Phys Lett. 2009;95:113307. doi:10.1063/1.3222854.

70. Kaltenbrunner M, Sekitani T, Reeder J, Yokota T, Kuribara K, Tokuhara T, et al. An ultra-lightweight design for imperceptible plastic electronics. Nature. 2013;499:458–63.

doi:10.1038/nature12314.

71. Mirza M, Wang J, Li D, Arabi SA, Jiang C. Novel Top-Contact Monolayer Pentacene-Based Thin-Film Transistor for Ammonia Gas Detection. ACS Appl Mater Interfaces. 2014;6:5679–84. doi:10.1021/am5001954.

72. Fukuda K, Takeda Y, Mizukami M, Kumaki D, Tokito S. Fully Solution-Processed Flexible Organic Thin Film Transistor Arrays with High Mobility and Exceptional Uniformity. Sci Rep. 2014;4. doi:10.1038/srep03947.

73. Kola S, Sinha J, Katz HE. Organic transistors in the new decade: Toward n-channel, printed, and stabilized devices. J Polym Sci Part B Polym Phys. 2012;50:1090–120. doi:10.1002/polb.23054.

74. Pecora A, Zampetti E, Pantalei S, Valletta A, Minotti A, Maiolo L, et al. Interdigitated sensorial system on flexible substrate. In: 2008 IEEE Sensors. IEEE; 2008. p. 21–4. doi:10.1109/ICSENS.2008.4716373.

75. Zhong H, Smith J, Rossbauer S, White AJP, Anthopoulos TD, Heeney M. Air-Stable and High-Mobility n-Channel Organic Transistors Based on Small-Molecule/Polymer Semiconducting Blends. Adv Mater. 2012;24:3205–11. doi:10.1002/adma.201200859.

76. Wang C, Qin Y, Sun Y, Guan YS, Xu W, Zhu D. Thiophene-Diketopyrrolopyrrole-Based Quinoidal Small Molecules as Solution-Processable and Air-Stable Organic Semiconductors: Tuning of the Length and Branching Position of the Alkyl Side Chain toward a High-Performance n-Channel Organic Field-Effect Tran. ACS Appl Mater Interfaces. 2015;7:15978–87.

77. Hall P, Selinger B. Statistical Significance: Balancing Evidence Against Doubt. Aust J Stat. 1986;28:354–70. doi:10.1111/j.1467-842X.1986.tb00708.x.

78. Randall Munroe. xkcd: Significant. https://xkcd.com/882/. Accessed 9 Feb 2018.

79. Sun J, Jung B-J, Lee T, Berger L, Huang J, Liu Y, et al. Tunability of Mobility and Conductivity over Large Ranges in Poly(3,3‴-didodecylquaterthiophene)/Insulating Polymer Composites. ACS Appl Mater Interfaces. 2009;1:412–9. doi:10.1021/am8001132.

80. Chen J, Chen Z, Yang D, Ye F, Wang S, Yang X. Improved Electrical Performance of Poly(3-

hexylthiophene) Induced by Stable Doping with Polymer Dopants. Macromol Chem Phys. 2015;216:1008–13. doi:10.1002/macp.201500045.

81. Yang H, Zhang G, Zhu J, He W, Lan S, Liao L, et al. Improving Charge Mobility of Polymer Transistors by Judicious Choice of the Molecular Weight of Insulating Polymer Additive. J Phys Chem C. 2016;120:17282–9. doi:10.1021/acs.jpcc.6b07000.

82. Chen L, Wang H, Liu J, Xing R, Yu X, Han Y. Tuning the π-π stacking distance and J-aggregation of DPP-based conjugated polymer via introducing insulating polymer. J Polym Sci Part B Polym Physics, vol 54, issue 8, pp 838-847. 2016;54:838–47. doi:10.1002/POLB.23984.

83. Ford MJ, Wang M, Patel SN, Phan H, Segalman RA, Nguyen T-Q, et al. High Mobility Organic Field-Effect Transistors from Majority Insulator Blends. Chem Mater. 2016;28:1256–60. doi:10.1021/acs.chemmater.5b04774.

84. Han S, Yu X, Shi W, Zhuang X, Yu J. Solvent-dependent electrical properties improvement of organic field-effect transistor based on disordered conjugated polymer/insulator blends. Org Electron. 2015;27:160–6. doi:10.1016/j.orgel.2015.09.003.

85. Herous L, Nemamcha M, Remadnia M, Dascalescu L. Factors that influence the surface potential decay on a thin film of polyethylene terephthalate (PET). J Electrostat. 2009;67:198–202. doi:10.1016/j.elstat.2009.01.028.

86. Armbruster DA, Pry T, Armbruster D. Limit of Blank, Limit of Detection and Limit of Quantitation. Clin Biochem Rev. 2008;29 i. https://www.ncbi.nlm.nih.gov/pmc/articles/PMC2556583/pdf/cbr29_s_pgs49.pdf. Accessed 21 Mar 2017.

87. Dubois S, Eng S, Bhattacharya R, Rulyak S, Hubbard T, Putnam D, et al. Breath Ammonia Testing for Diagnosis of Hepatic Encephalopathy. Dig Dis Sci. 2005;50:1780–4. doi:10.1007/s10620-005-2937-6.

88. Timmer B, Olthuis W, Berg A van den. Ammonia sensors and their applications—a review. Sensors Actuators B Chem. 2005;107:666–77. doi:10.1016/j.snb.2004.11.054.

89. Verploegen E, Miller CE, Schmidt K, Bao Z, Toney MF. Manipulating the morphology of P3HT-PCBM bulk heterojunction blends with solvent vapor annealing. Chem Mater. 2012;24:3923–31.

90. He M, Han W, Ge J, Yu W, Yang Y, Qiu F, et al. Annealing effects on the photovoltaic performance of all-conjugated poly(3-alkylthiophene) diblock copolymer-based bulk heterojunction solar cells. Nanoscale. 2011;3:3159. doi:10.1039/c1nr10293a.

91. Huang W, Sinha J, Yeh ML, Hardigree JFM, LeCover R, Besar K, et al. Diverse organic field-effect transistor sensor responses from two functionalized naphthalenetetracarboxylic diimides and copper phthalocyanine semiconductors distinguishable over a wide analyte range. Adv Funct Mater. 2013;23:4094–104.

92. Huang W., Besar K., Lecover R., Rule AM., Breysse PN., Katz HE. Highly sensitive NH 3 detection based on organic field-effect transistors with tris(pentafluorophenyl)borane as receptor. J Am Chem Soc. 2012;134:14650–3. doi:10.1021/ja305287p.

93. Varshney M, Li Y. Interdigitated array microelectrodes based impedance biosensors for detection of bacterial cells. Biosens Bioelectron. 2009;24:2951–60. doi:10.1016/j.bios.2008.10.001.

94. Varshney M, Li Y. Interdigitated array microelectrode based impedance biosensor coupled with magnetic nanoparticle–antibody conjugates for detection of Escherichia coli O157:H7 in food samples. Biosens Bioelectron. 2007;22:2408–14. doi:10.1016/j.bios.2006.08.030.

95. Lisdat F, Schäfer D. The use of electrochemical impedance spectroscopy for biosensing. Anal Bioanal Chem. 2008;391:1555–67. doi:10.1007/s00216-008-1970-7.

96. Hang TC, Guiseppi-Elie A. Frequency dependent and surface characterization of DNA immobilization and hybridization. Biosens Bioelectron. 2004;19:1537–48. doi:10.1016/j.bios.2003.12.014.

97. Silbergeld E. Chickenizing Farms and Food. Johns Hopkins Press; 2016.

98. Scientific Advisory Group on Antimi, Scientific Advisory Group on Antimicrobials of the Committee for Medicinal Products for Veterinary Use. Reflection paper on the use of third and

fourth generation cephalosporins in food producing animals in the European Union: development of resistance and impact on human and animal health. 2009;32. doi:10.1111/j.1365-2885.2009.01075.x.

99. Angulo FJ, Baker NL, Olsen SJ, Anderson A, Barrett TJ. Antimicrobial use in agriculture: Controlling the transfer of antimicrobial resistance to humans. Seminars in Pediatric Infectious Diseases. 2004;15:78–85.

100. Neyra RC, Frisancho J, Rinsky J, Resnick C, Carroll K, Rule A, et al. Multidrug-resistant and methicillin-resistant Staphylococcus aureus (MRSA) in hog slaughter and processing plant workers and their community in North Carolina (USA). Environ Health Perspect. 2014. http://hsrc.himmelfarb.gwu.edu/sphhs_enviro_facpubs/98. Accessed 10 Nov 2016.

101. Cuny C, Wieler L, Witte W. Livestock-Associated MRSA: The Impact on Humans. Antibiotics. 2015;4:521–43. doi:10.3390/antibiotics4040521.

102. Price LB, Stegger M, Hasman H, Aziz M, Larsen J, Andersen PS, et al. Staphylococcus aureus CC398: Host adaptation and emergence of methicillin resistance in livestock. MBio. 2012;3:1–6.

103. Rinsky JL, Nadimpalli M, Wing S, Hall D, Baron D, Price LB, et al. Livestock-Associated Methicillin and Multidrug Resistant Staphylococcus aureus Is Present among Industrial, Not Antibiotic-Free Livestock Operation Workers in North Carolina. PLoS One. 2013;8:1–11.

104. Pejcic B, De Marco R. Impedance spectroscopy: Over 35 years of electrochemical sensor optimization. Electrochim Acta. 2006;51:6217–29. doi:10.1016/j.electacta.2006.04.025.

105. Ramanavicius A, Finkelsteinas A, Cesiulis H, Ramanaviciene A. Electrochemical impedance spectroscopy of polypyrrole based electrochemical immunosensor. Bioelectrochemistry. 2010;79:11–6. doi:10.1016/j.bioelechem.2009.09.013.

106. Han Y. Label-free detection of biomolecules by a f ield-effect transistor microarray biosensor with bio-functionalized gate surfaces Yinhua Han. 2006.

107. Ahmed R, Reifsnider K. Study of Influence of Electrode Geometry on Impedance Spectroscopy. Int J Electrochem Sci. 2011;6:1159–74.

108. Sadik OA, Aluoch AO, Zhou A. Status of biomolecular recognition using electrochemical

techniques. Biosens Bioelectron. 2009;24:2749–65. doi:10.1016/j.bios.2008.10.003.

109. Zhou Y, Chiu C-W, Liang H. Interfacial structures and properties of organic materials for biosensors: an overview. Sensors (Basel). 2012;12:15036–62. doi:10.3390/s121115036.

110. Amirudin A, Thierry D. Application of electrochemical impedance spectroscopy to study the degradation of polymer-coated metals. Prog Org Coatings. 1995;26:1–28.

111. Amor Y Ben, Sutter EMM, Takenouti H, Orazem ME, Tribollet B. Interpretation of Electrochemical Impedance for Corrosion of a Coated Silver Film in Terms of a Pore-in-Pore Model. J Electrochem Soc. 2014;161:573–9.

112. Sumner C, Krause S, McNeil C. Biosensor based on enzyme-catalysed degradation of thin polymer films. Biosens Bioelectron. 2001;16:709–14.

113. McNeil CJ, Athey D, Ball M, Ho WO, Krause S, Armstrong RD, et al. Electrochemical Sensors Based on Impedance Measurement of Enzyme-Catalyzed Polymer Dissolution: Theory and Applications. Anal Chem. 1995;67:3928–35. doi:10.1021/ac00117a018.

114. Yuki H, Hatada K, Niinomi T, Kikuchi Y. Stereospecific Polymerization of Trityl, Diphenylmethyl and Benzyl Methacrylates. Polym J. 1970;1:36–45. doi:10.1295/polymj.1.36.

115. Okamoto Y, Suzuki K, Ohta K, Hatada K, Yuki H. Optically active poly(triphenylmethyl methacrylate) with one-handed helical conformation. J Am Chem Soc. 1979;101:4763–5. doi:10.1021/ja00510a072.

116. Okamoto Y, Nakashima S, Ohta K, Hatada K, Yuki H. Microstructure of methyl methacrylate-trityl methacrylate copolymer obtained by n-BuLi in THF. J Polym Sci Polym Lett Ed. 1975;13:273–7. doi:10.1002/pol.1975.130130505.

117. Alley OJ, Plunkett E, Kale TS, Guo X, McClintock G, Bhupathiraju M, et al. Synthesis, Fabrication, and Heterostructure of Charged, Substituted Polystyrene Multilayer Dielectrics and Their Effects in Pentacene Transistors. Macromolecules. 2016;49:3478–89. doi:10.1021/acs.macromol.6b00253.

118. Popov B, Alwohaibi M, White R. Using Electrochemical Impedance Spectroscopy as a Tool for

Organic Coating Solume Saturation Monitoring. J Electrochem Soc. 1993;:947–51.

119. Huang W, Besar K, LeCover R, Dulloor P, Sinha J, Martínez Hardigree JF, et al. Label-free brain injury biomarker detection based on highly sensitive large area organic thin film transistor with hybrid coupling layer. Chem Sci. 2014;5:416. doi:10.1039/c3sc52638k.

120. Buth F, Donner A, Sachsenhauser M, Stutzmann M, Garrido J a. Biofunctional electrolyte-gated organic field-effect transistors. Adv Mater. 2012;24:4511–7. doi:10.1002/adma.201201841.

121. Kharitonov AB, Zayats M, Lichtenstein A, Katz E, Willner I. Enzyme monolayer-functionalized field-effect transistors for biosensor applications. Sensors Actuators, B Chem. 2000;70:222–31.

122. Khan HU, Roberts ME, Johnson O, Förch R, Knoll W, Bao Z. In situ, label-free DNA detection using organic transistor sensors. Adv Mater. 2010;22:4452–6. doi:10.1002/adma.201000790.

123. Zaccari I, Davies AG, Walti C, Laurenson SX. Label-free electrochemical biosensors for clinical diagnostic. Proc 7th Cairo Int Biomed Eng Conf. 2015. http://eprints.whiterose.ac.uk/84302/1/Zaccari et al CIBEC paper - accepted version.pdf. Accessed 14 Sep 2017.

124. Fraser-Reid BO, Tatsuta K, Thiem J (Joachim). Glycoscience : chemistry and chemical biology I-III. Springer; 2001. https://books.google.com/books?id=1CEncSLzHUMC&dq=%2522trimethoxytrityl%2522&source=gbs_navlinks_s. Accessed 25 Oct 2017.

125. Serafini AN. From monoclonal antibodies to peptides and molecular recognition units: an overview. J Nucl Med. 1993;34 3 Suppl:533–6. http://www.ncbi.nlm.nih.gov/pubmed/8441052. Accessed 8 Feb 2018.

126. Björck L, Kronvall G, Bjorck2 L, Kronvall G. reagent. streptococcal protein G, a novel IgG-binding Purification and some properties of PURIFICATION AND SOME PROPERTIES OF STREPTOCOCCAL PROTEIN G, A NOVEL IgG-BINDING REAGENT'. J Immunol J Immunol by guest Febr. 1984;133:969–74. http://www.jimmunol.org/content/133/2/969. Accessed

8 Feb 2018.

127. Helassa N, Vollmer W, Breukink E, Vernet T, Zapun A. The membrane anchor of penicillin-binding protein PBP2a from Streptococcus pneumoniae influences peptidoglycan chain length. FEBS J. 2012;279:2071–81. doi:10.1111/j.1742-4658.2012.08592.x.

128. Brasher DM, Kingsbury AH. Electrical measurements in the study of immersed paint coatings on metal. I. Comparison between capacitance and gravimetric methods of estimating water-uptake. J Appl Chem. 2007;4:62–72. doi:10.1002/jctb.5010040202.

129. Bellucci F, Valentino M, Monetta T, Nicodemo L, Kenny J, Nicolais L, et al. Impedance spectroscopy of reactive polymers. 1. J Polym Sci Part B Polym Phys. 1994;32:2519–27. doi:10.1002/polb.1994.090321509.

130. Jang H-J, Ahn J, Kim M-G, Shin Y-B, Jeun M, Cho W-J, et al. Electrical signaling of enzyme-linked immunosorbent assays with an ion-sensitive field-effect transistor. Biosens Bioelectron. 2015;64:318–23. doi:10.1016/J.BIOS.2014.09.020.

131. Zhu Z, Shi L, Feng H, Zhou HS. Single domain antibody coated gold nanoparticles as enhancer for Clostridium difficile toxin detection by electrochemical impedance immunosensors. Bioelectrochemistry. 2015;101:153–8. doi:10.1016/j.bioelechem.2014.10.003.

132. Hill AB. The environment and disease: association or causation? Proc R Soc Med. 1965;58:295–300.

133. Baral SD, Wirtz A, Sifakis F, Johns B, Walker D, Beyrer C. The Highest Attainable Standard of Evidence (HASTE) for HIV/AIDS Interventions: Toward a Public Health Approach to Defining Evidence. Public Health Reports (1974-). 127:572–84. doi:10.2307/23646640.

134. Lewis SJ, Gardner M, Higgins JPT, Holly JMP, Gaunt TR, Perks CM, et al. Developing the WCRF International/University of Bristol methodology for identifying and carrying out systematic reviews of mechanisms of exposure-cancer associations. Cancer Epidemiol Biomarkers Prev. 2017;:1667–76.

135. Becker RA, Dellarco V, Seed J, Kronenberg JM, Meek B, Foreman J, et al. Quantitative weight

of evidence to assess confidence in potential modes of action. Regul Toxicol Pharmacol. 2017;86:205–20. doi:10.1016/j.yrtph.2017.02.017.

136. Tang KL, Caffrey NP, Nóbrega DB, Cork SC, Ronksley PE, Barkema HW, et al. Restricting the use of antibiotics in food-producing animals and its associations with antibiotic resistance in food-producing animals and human beings: a systematic review and meta-analysis. Lancet Planet Heal. 2017;1:e316–27. doi:10.1016/S2542-5196(17)30141-9.

137. Hoelzer K, Wong N, Thomas J, Talkington K, Jungman E, Coukell A. Antimicrobial drug use in food-producing animals and associated human health risks: what, and how strong, is the evidence? BMC Vet Res. 2017;13:211. doi:10.1186/s12917-017-1131-3.

138. Norris SL, Bero L. GRADE methods for guideline development: Time to evolve? Ann Intern Med. 2016;165:810–1.

139. Rothman KJ, Greenland S. Causation and causal inference in epidemiology. American Journal of Public Health. 2005;95 SUPPL. 1.

140. USDA Chief Scientist Statement on WHO Guidelines on Antibiotics | USDA. https://www.usda.gov/media/press-releases/2017/11/07/usda-chief-scientist-statement-who-guidelines-antibiotics. Accessed 16 Dec 2017.

141. WHO | WHO guidelines on use of medically important antimicrobials in food-producing animals. WHO. 2017. http://who.int/foodsafety/publications/cia_guidelines/en/. Accessed 16 Dec 2017.

142. Khan KS, Ball E, Fox CE, Meads C. Systematic reviews to evaluate causation: an overview of methods and application. Evid Based Med. 2012;17:137–41. doi:10.1136/ebmed-2011-100287.

143. Zaza S, Wright-De Agüero LK, Briss PA, Truman BI, Hopkins DP, Hennessy MH, et al. Data collection instrument and procedure for systematic reviews in the Guide to Community Preventive Services. Am J Prev Med. 2000;18 1 SUPPL. 1:44–74.

144. Ertaylan G, Le Cornet C, van Roekel EH, Jung AY, Bours MJL, Damms-Machado A, et al. A Comparative Study on the WCRF International/University of Bristol Methodology for Systematic

Reviews of Mechanisms Underpinning Exposure–Cancer Associations. Cancer Epidemiol Biomarkers Prev. 2017. doi:10.1158/1055-9965.EPI-17-0230.

145. Smith MT, Guyton KZ, Gibbons CF, Fritz JM, Portier CJ, Rusyn I, et al. Key characteristics of carcinogens as a basis for organizing data on mechanisms of carcinogenesis. Environmental Health Perspectives. 2016;124:713–21.

146. Ankley GT, Bennett RS, Erickson RJ, Hoff DJ, Hornung MW, Johnson RD, et al. Adverse outcome pathways: A conceptual framework to support ecotoxicology research and risk assessment. Environ Toxicol Chem. 2010;29:730–41.

147. Galbraith D, Levy PE, Sitch S, Huntingford C, Cox P, Williams M, et al. Multiple mechanisms of Amazonian forest biomass losses in three dynamic global vegetation models under climate change. New Phytol. 2010;187:647–65.

148. Leist M, Ghallab A, Graepel R, Marchan R, Hassan R, Bennekou SH, et al. Adverse outcome pathways: opportunities, limitations and open questions. Archives of Toxicology. 2017;:1–29.

149. D'Agata EMC, Dupont-Rouzeyrol M, Magal P, Olivier D, Ruan S. The impact of different antibiotic regimens on the emergence of antimicrobial-resistant bacteria. PLoS One. 2008;3:4–12.

150. Alban L, Ellis-Iversen J, Andreasen M, Dahl J, Sønksen UW. Assessment of the risk to public health due to use of antimicrobials in pigs – an example of pleuromutilins in Denmark. Front Vet Sci. 2017;4 May:74. doi:10.3389/FVETS.2017.00074.

151. Ashbolt NJ, Amézquita A, Backhaus T, Borriello P, Brandt KK, Collignon P, et al. Human health risk assessment (HHRA) for environmental development and transfer of antibiotic resistance. Environ Health Perspect. 2013;121:993–1001.

152. MacLean RC, Hall AR, Perron GG, Buckling A. The population genetics of antibiotic resistance: Integrating molecular mechanisms and treatment contexts. Nat Rev Genet. 2010;11:405–14. doi:10.1038/nrg2778.

153. Gillings MR. Evolutionary consequences of antibiotic use for the resistome, mobilome, and microbial pangenome. Frontiers in Microbiology. 2013;4 JAN.

154. Graham JP, Nachman KE. Managing waste from confined animal feeding operations in the United States: The need for sanitary reform. J Water Health. 2010;8:646–70.

155. Silbergeld EK, Davis M, Leibler JH, Peterson AE. One Reservoir: Redefining the Community Origins of Antimicrobial-resistant Infections. Med Clin North Am. 2008;92:1391–407.

156. Perry JA, Wright GD. Forces shaping the antibiotic resistome. BioEssays. 2014;36:1179–84. doi:10.1002/bies.201400128.

157. Barbosa TM, Levy SB. The impact of antibiotic use on resistance development and persistence. Drug Resist Updat. 2000;3:303–11. doi:10.1054/drup.2000.0167.

158. Arber W. Horizontal Gene Transfer among Bacteria and Its Role in Biological Evolution. Life (Basel, Switzerland). 2014;4:217–24. doi:10.3390/life4020217.

159. Hernando-Amado S, Sanz-García F, Blanco P, Martínez JL. Fitness costs associated with the acquisition of antibiotic resistance. Essays Biochem. 2017;61 October 2016:37–48. doi:10.1042/EBC20160057.

160. Von Wintersdorff CJH, Penders J, van Niekerk JM, Mills ND, Majumder S, van Alphen LB, et al. Dissemination of antimicrobial resistance in microbial ecosystems through horizontal gene transfer. 2016. doi:10.3389/fmicb.2016.00173.

161. Fleming A. Nobel Lecture: Penicillin. Nobel Lect Physiol or Med 1942-1962. 1945;:83–93.

162. Hanahan D. Studies on transformation of Escherichia coli with plasmids. J Mol Biol. 1983;166:557–80.

163. Yim G, Huimi Wang H, Davies FRS J. Antibiotics as signalling molecules. Philos Trans R Soc B Biol Sci. 2007;362:1195–200. doi:10.1098/rstb.2007.2044.

164. Overhage J, Bains M, Brazas MD, Hancock REW. Swarming of Pseudomonas aeruginosa is a complex adaptation leading to increased production of virulence factors and antibiotic resistance. J Bacteriol. 2008;190:2671–9.

165. Boucher Y, Labbate M, Koenig JE, Stokes HW. Integrons: mobilizable platforms that promote genetic diversity in bacteria. Trends Microbiol. 2007;15:301–9.

166. Aarestrup FM, Seyfarth AM, Emborg HD, Pedersen K, Hendriksen RS, Bager F. Effect of Abolishment of the Use of Antimicrobial Agents for Growth Promotion on Occurence of Antimicrobial Resistance in Fecal Entercocci from Food Animals in Denmark. Antimicrob Agents Chemother Agents Chemother. 2001;45:2054–9.

167. Cheng AC, Turnidge J, Collignon P, Looke D, Barton M, Gottlieb T. Control of fluoroquinolone resistance through successful regulation, Australia. Emerg Infect Dis. 2012;18:1453–60.

168. ter Kuile BH, Kraupner N, Brul S. The risk of low concentrations of antibiotics in agriculture for resistance in human health care. 2016;363:fnw210. doi:10.1093/femsle/fnw210.

169. Martinez JL. Antibiotics and Antibiotic Resistance Genes in Natural Environments. Science (80-). 2008;321:365–7. doi:10.1126/science.1159483.

170. Cohen SP, McMurry LM, Hooper DC, Wolfson JS, Levy SB. Cross-resistance to fluoroquinolones in multiple-antibiotic-resistant (Mar) Escherichia coli selected by tetracycline or chloramphenicol: decreased drug accumulation associated with membrane changes in addition to OmpF reduction. Antimicrob Agents Chemother. 1989;33:1318–25. http://www.ncbi.nlm.nih.gov/pubmed/2679373. Accessed 18 May 2017.

171. Cantón R, Morosini MI. Emergence and spread of antibiotic resistance following exposure to antibiotics. FEMS Microbiol Rev. 2011;35:977–91.

172. Fey PD, Safranek TJ, Rupp ME, Dunne EF, Ribot E, Iwen PC, et al. Ceftriaxone-Resistant Salmonella Infection Acquired by a Child from Cattle. N Engl J Med. 2000;342:1242–9. doi:10.1056/NEJM200004273421703.

173. Argudín MA, Lauzat B, Kraushaar B, Alba P, Agerso Y, Cavaco L, et al. Heavy metal and disinfectant resistance genes among livestock-associated methicillin-resistant Staphylococcus aureus isolates. Vet Microbiol. 2016;191:88–95. doi:10.1016/j.vetmic.2016.06.004.

174. Yu Z, Gunn L, Wall P, Fanning S. Antimicrobial resistance and its association with tolerance to heavy metals in agriculture production. Food Microbiol. 2017;64:23–32.

175. You Y, Hilpert M, Ward MJ. Detection of a common and persistent tet(L)-carrying plasmid in chicken-waste-impacted farm soil. Appl Environ Microbiol. 2012;78:3203–13. doi:10.1128/AEM.07763-11.

176. Cantón R, Ruiz-Garbajosa P. Co-resistance: An opportunity for the bacteria and resistance genes. Curr Opin Pharmacol. 2011;11:477–85. doi:10.1016/j.coph.2011.07.007.

177. Graham DW, Knapp CW, Christensen BT, McCluskey S, Dolfing J. Appearance of β-lactam Resistance Genes in Agricultural Soils and Clinical Isolates over the 20th Century. Sci Rep. 2016;6:21550. doi:10.1038/srep21550.

178. Davies J, Davies D. Origins and Evolution of Antibiotic Resistance. Microbiol Mol Biol Rev. 2010;74:417–33. doi:10.1128/mmbr.00016-10.

179. Shigemura K, Tanaka K, Adachi M, Yamashita M, Arakawa S, Fujisawa M. Chronological change of antibiotic use and antibiotic resistance in Escherichia coli causing urinary tract infections. J Infect Chemother. 2011;17:646–51. doi:10.1007/s10156-011-0241-2.

180. Molton JS, Tambyah PA, Ang BSP, Ling ML, Fisher DA. The global spread of healthcare-associated multidrug-resistant bacteria: A perspective from Asia. Clin Infect Dis. 2013;56:1310–8. doi:10.1093/cid/cit020.

181. Skurnik D, Clermont O, Guillard T, Launay A, Danilchanka O, Pons S, et al. Emergence of Antimicrobial-Resistant *Escherichia coli* of Animal Origin Spreading in Humans. Mol Biol Evol. 2016;33:898–914. doi:10.1093/molbev/msv280.

182. Mollenkopf DF, Stull JW, Mathys DA, Bowman AS, Feicht SM, Grooters S V, et al. Carbapenemase-Producing Enterobacteriaceae Recovered from the Environment of a Swine Farrow-to-Finish Operation in the United States. Antimicrob Agents Chemother. 2017;61:AAC.01298-16. doi:10.1128/AAC.01298-16.

183. Ravi A, Avershina E, Foley SL, Ludvigsen J, Storrø O, Øien T, et al. The commensal infant gut meta-mobilome as a potential reservoir for persistent multidrug resistance integrons. 2015;5:15317. doi:10.1038/srep15317.

184. Muurinen J, Stedtfeld R, Karkman A, Pärnänen K, Tiedje J, Virta M. Influence of Manure Application on the Environmental Resistome under Finnish Agricultural Practice with Restricted Antibiotic Use. Environ Sci Technol. 2017;51:5989–99.

185. Cleary DW, Bishop AH, Zhang L, Topp E, Wellington EMH, Gaze WH. Long-term antibiotic exposure in soil is associated with changes in microbial community structure and prevalence of class 1 integrons. FEMS Microbiol Ecol. 2016;92.

186. Davis MF, Price LB, Liu CM-HH, Silbergeld EK. An ecological perspective on U.S. industrial poultry production: The role of anthropogenic ecosystems on the emergence of drug-resistant bacteria from agricultural environments. 2011. doi:10.1016/j.mib.2011.04.003.

187. Cabello FC, Godfrey HP, Tomova A, Ivanova L, Dölz H, Millanao A, et al. Antimicrobial use in aquaculture re-examined: Its relevance to antimicrobial resistance and to animal and human health. Environ Microbiol. 2013;15:1917–42.

188. Zhu YG, Zhao Y, Li B, Huang CL, Zhang SY, Yu S, et al. Continental-scale pollution of estuaries with antibiotic resistance genes. Nat Microbiol. 2017;2.

189. You Y, Silbergeld EK. Learning from agriculture: Understanding low-dose antimicrobials as drivers of resistome expansion. Frontiers in Microbiology. 2014;5 JUN.

190. Hayes JR, English LL, Carr LE, Wagner DD, Joseph SW. Multiple-Antibiotic Resistance of Enterococcus spp. Isolated from Comemercial Poultry Production Environments. Apllied Environ Microbiol. 2004;70:6005–11.

191. Berriman ADC, Clancy D, Clough HE, Armstrong D, Christley RM. Effectiveness of Simulated Interventions in Reducing the Estimated Prevalence of Salmonella in UK Pig Herds. PLoS One. 2013;8.

192. van Hoek AHAM, Veenman C, van Overbeek WM, Lynch G, de Roda Husman AM, Blaak H. Prevalence and characterization of ESBL- and AmpC-producing Enterobacteriaceae on retail vegetables. Int J Food Microbiol. 2015;204:1–8. doi:10.1016/j.ijfoodmicro.2015.03.014.

193. Ben Said L, Jouini A, Klibi N, Dziri R, Alonso CA, Boudabous A, et al. Detection of extended-

spectrum beta-lactamase (ESBL)-producing Enterobacteriaceae in vegetables, soil and water of the farm environment in Tunisia. Int J Food Microbiol. 2015;203:86–92. doi:10.1016/j.ijfoodmicro.2015.02.023.

194. Leibler, J. H., Dalton, K., Pekosz, A., Gray, G. C. and Silbergeld EK. Epizootics in Industrial Livestock Production: Preventable Gaps in Biosecurity and Biocontainment. Zoonoses Public Heal. 2017;64:137–145.

195. Agersø Y, Wulff G, Vaclavik E, Halling-Sørensen B, Jensen LB. Effect of tetracycline residues in pig manure slurry on tetracycline-resistant bacteria and resistance gene tet(M) in soil microcosms. Environ Int. 2006;32:876–82.

196. Villeneuve DL, Crump D, Garcia-Reyero N, Hecker M, Hutchinson TH, LaLone CA, et al. Adverse outcome pathway (AOP) development I: Strategies and principles. Toxicol Sci. 2014;142:312–20.

197. Patlewicz G, Simon TW, Rowlands JC, Budinsky RA, Becker RA. Proposing a scientific confidence framework to help support the application of adverse outcome pathways for regulatory purposes. Regul Toxicol Pharmacol. 2015;71:463–77. doi:10.1016/j.yrtph.2015.02.011.

198. O'Brien TF. The global epidemic nature of antimicrobial resistance and the need to monitor and manage it locally. Clin Infect Dis. 1997;24 Suppl 1:S2-8. http://www.ncbi.nlm.nih.gov/pubmed/8994775. Accessed 18 May 2017.

199. Hoelzer K, Wong N, Thomas J, Talkington K, Jungman E, Coukell A. Antimicrobial drug use in food-producing animals and associated human health risks: what, and how strong, is the evidence? BMC Vet Res. 2017;13:211. doi:10.1186/s12917-017-1131-3.

C. Bibliography

Refereed journal articles

Dailey, Jennifer; Fichera, Michelangelo; Silbergeld, Ellen; Katz, Howard. Under Review. "Impedance Spectroscopic Detection of Binding and Reactions in Acid-Labile Dielectric Polymers for Biosensor Applications". Journal of Materials Chemistry B.

Dailey, Jennifer; Rosman, Lori; Silbergeld, Ellen. Under Review. "Evaluating biological plausibility in supporting evidence for action through systematic reviews in public health". Antimicrobial Resistance and Infection Control.

Dailey, Jennifer. 2018. "Learning Outcomes and Insights from a Chocolate-based Undergraduate Materials Science Course and Other Topical Outreach Activities". MRS Advances. *1-7.*

Li, Hui; **Dailey, Jennifer**; Kale, Teju; Besar, Kalpana; Koehler, K; Katz, Howard. 2017. "Sensitive and Selective NO2 Sensing Based on Alkyl- and Alkylthio-Thiophene Polymer Conductance and Conductance Ratio Changes from Differential Chemical Doping." ACS Applied Materials & Interfaces. 9 (24), pp 20501–20507

Song, Jian; **Dailey, Jennifer;** Li,Hui; Jang, Hyun-June ; Wang, JTH ; Everett, AD ; Katz, Howard. 2017. "Extended Solution Gate OFET-Based Biosensor for Label-Free Glial Fibrillary Acid Protein Detection with Polyethylene Glycol-Containing Bioreceptor Layer." Advanced Functional Materials. 27(20).

Besar, Kalpana; **Dailey, Jennifer**; Katz, Howard. 2017. "Ethylene Detection Based on Organic Field-Effect Transistors with Porogen and Palladium Particle Receptor Enhancements." ACS Applied Materials & Interfaces. 9(2), pp. 1173-1177

Silbergeld, Ellen; Aidara-Kane Awa; **Dailey, Jennifer**. 2017. "Agriculture and Food Production as Drivers of the Global Emergence of Antimicrobial Resistance." AMR Control.

Besar, Kalpana*; **Dailey, Jennifer***; Zhao, Xingang; Katz, Howard. 2017. "Flexible Organic Inverter Made from Printable Materials with Synergistic Ammonia Sensing." Journal of Materials Chemistry C. 26(5) pp 6506-6511
***Equal Contribution**

Huang, Weiguo; Diallo, AK; **Dailey, Jennifer**; Besar, Kalpana; Katz, Howard. 2015. "Electrochemical processes and mechanistic aspects of field-effect sensors to biomolecules." Journal of Materials Chemistry C. 3(25) pp 6445-6470.

Lerner, MB*; **Dailey, Jennifer***; Goldsmith, Brett; Brisson, Dustin; Johnson, ATC. 2013. "Detecting Lyme Disease using antibody-functionalized single-walled carbon nanotube transistors." Biosensors and Bioelectronics. 45, pp 163-167.
***Equal Contribution**

Published proceedings

Dailey, Jennifer; Liu, Baoying; Jaward, Shayma; Nussenblatt, Robert; Sen, HN. 2013. "Immune Market Changes in Patients with Non-Paraneoplastic Autoimmune Retinopathy." Investigative Ophthalmology & Visual Science 54 (15) p2513.

Patents

Johnson, AT; Lerner, Mitchell; Robinson, Michael; Pazina, Tatiana; Brisson, Dustin; **Dailey, Jennifer**. "Carbon Nanotube Biosensors and Related Methods." US Patent App 14/241,671

Selected Presentations

Jennifer Dailey*, Michelangelo Fichera, Ellen Silbergeld, Howard Katz. "Impedance Spectroscopic Detection of Binding and Reactions in Acid-Labile Dielectric Polymers for Biosensor Application." 2017 MRS Fall Meeting. Session BM03. ***Poster presenter**

Jennifer Dailey*, Kalpana Besar, Xingang Zhao, Howard Katz. "A Flexible Ammonia Sensor based Organic Inverter Structure". MAMNA Conference, April 2017, APL, Maryland. ***Invited Speaker**

Jennifer Dailey*, Kalpana Besar, Xingang Zhao, Howard Katz. "A Flexible Ammonia Sensor based Organic Inverter Structure". E2SHI Poster Presentation, March 2017

Jennifer Dailey*, Jean Fan. "The Materials Science of Chocolate: Analyzing the Educational Benefits of a Topical Approach". 2016 MRS Fall Meeting. Session BI1.7.03. ***Presenting Author**

Jennifer L. Dailey, Daniele Mandrioli, Michelangelo Fichera, Ellen Silbergeld, Howard E. Katz. "Rapid Culture-Free Optoelectronic Signaling for Detection of Methicillin-Resistant Antigen-Staphylococcus Aureus (MRSA) by Multidentate Nanoparticle Aggregation". 2015 MRS Fall Meeting. Session L6.10.
Also presented at the Johns Hopkins INBT poster session and received third place out of over sixty

D. About the Author

Jennifer Dailey was born in Delaware County, Pennsylvania, on August 30, 1990. She graduated from the University of Pennsylvania in Philadelphia, PA, in 2008 with a BA in Physics with a concentration in Chemical Principles and a minor in Chemistry. Her accolades included the Rose Award for undergraduate research as well as being peer-voted to speak at the College commencement. From 2012-2013 Dailey worked as a Post-Baccalaureate Intramural Research Trainee in Bethesda, MD at the National Eye Institute within the National Institutes of Health studying immunology of the eye in a clinical setting. Dailey began her graduate training at Johns Hopkins University in the Department of Materials Science and Engineering in 2013 and received independent funding as a National Science Foundation Graduate Fellow. She received her Master's degree from Hopkins in 2015, and this dissertation concludes her Ph.D. Besides the research work discussed in this dissertation, Dailey has been a strong proponent of lab safety and learning to rebuild and customize high vacuum deposition systems.

While at Hopkins, Dailey has been funded through a variety of grants, including the NIH, E2SHI, and the Center for a Livable Future-Lerner Fellowship through the JHU School of Public Health. A passionate teacher thanks to her father's example, Dailey also completed the Preparing Future Faculty Teaching Academy program and completed a capstone project for Teaching as Research, using popular topical subjects to teach materials science to undergraduate students. She designed and instructed two classes as a primary lecturer, acted as a teaching assistant for two other courses, and was extremely involved in the mentoring of many elementary school and high school students, as well as mentoring two undergraduate engineering students through their senior projects. Her educational research work was

published in MRS Advances in 2018, and all materials are freely available for use by any other instructors who would like to use these class and lab plans.

Dailey will serve as the 2018-2019 American Physical Society Congressional Science Fellow.